Numerical Investigation of Model Combustors for Efficiency Improvement and Miniature Applications

Miguel Alejandro Gutiérrez Contreras

A Thesis

in

The Department

of

Mechanical and Industrial Engineering

Presented in Partial Fulfillment of the Requirements

for the Degree of Master of Applied Science (Mechanical Engineering) at

Concordia University

Montréal, Québec, Canada

March 2010

Your file Votre référence
ISBN: 978-0-494-67218-1
Our file Notre référence
ISBN: 978-0-494-67218-1

ABSTRACT

Numerical Investigation of Model Combustors for Efficiency Improvement and Miniature Applications

Miguel Alejandro Gutiérrez Contreras

Non-premixed combustion process is an important subject in most applications of combustion. Understanding of this phenomenon is crucial in the design of reliable, efficient, economical power generation systems. Microfabrication technologies in the development of power micro electro-mechanical systems is also becoming an increasing trend nowadays and the complete understanding of microfluid dynamics and non-premixed micro-combustion phenomena will lead the success in this field. In recent years numerical simulations have become an essential tool to understand combustion process to overcome experimental problems without losing accuracy.

In this study, two numerical simulations were performed on the analysis of the effect of injection on the turbulent mixing quality in a simple combustor and on the dynamics non-premixed flame street in a mesoscale channel using the commercial software Fluent®.

The effect of inlet geometries were first investigated for a Lockwood-type combustor in terms of combustion and energy efficiency and an efficient design configuration is deduced. The effect of wall temperature and flow velocities on the dynamics of non-premixed flame in a scaled combustion channel was investigated in the second part of this study. The results suggest that the two main parameters affecting the development of a non-premixed flame street in a mesoscale channel are the heat transfer to and from the wall and the diffusion time of the flow. The analysis of numerical details such as grid resolution, turbulent and chemistry models is emphasized throughout the study to understand the influence of these numerical parameters on the simulated phenomenon by comparing with experimental observations.

ACKNOWLEDGMENTS AND DEDICATIONS

First of all I would like to thank God for giving me the joy of being able to study and for giving me the opportunity to accomplish the childhood dream of study a Masters Degree and for giving me all the necessary wisdom to overcome every challenge.

I want to thank Dr. Hoi Dick Ng, for all his support and dedication to my research work, without his constant advice and commitment the result of this research wouldn't be the same. I would like to thank him for all the extra hours that he had to spend to support me and my research, I will always be very grateful for all his support. I also want to thank Dr. Ali Dolatabadi for all his support during my research.

De igual manera el agradecimiento es inmenso a mis padres por darme la oportunidad de venir a Canadá a estudiar una Maestría y sacrificar tiempo, dinero y esfuerzo para otorgarme las armas necesarias para tener un desarrollo profesional integral. Siempre estaré muy agradecido con los consejos que me dio mi padre para nunca perder la concentración necesaria para cumplir mis objetivos y no desviar la atención de mi meta última. Igualmente a mi madre le agradezco el esfuerzo que realizó para afrontar mi separación del seno familiar todo para cumplir mi sueño. No tengo palabras para agradecerles a los dos todo el cariño y amor que me demuestran día con día.

Mi agradecimiento es también grande para mis abuelos ya finados, para mis abuelas por su eterno cariño y a toda mi familia que siempre me ha apoyado.

Finally, I want to thank Sheena for being by my side in all the journeys of study times where the only thing that I was able to do was to continue with my research.

TABLE OF CONTENTS

LIST OF FIGURES

LIST OF TABLES

NOMENCLATURE

VARIABLE	DESCRIPTION
$\vec{r}$	Displacement vector
ε	Dissipation rate
Γ	Effective diffusivity
K_{eff}	Effective thermal conductivity
t_{r}	Flow residence time
G	Generation of kinetic energy
g	Gravity
H	Instantaneous enthalpy
k	Kinetic energy
Y_{i}	Local mass fraction of species i
Z_{i}	Mass fraction for element i
f	Mixture fraction
$\overline{f'^2}$	Mixture fraction variance
S	Source term
ω	Specific dissipation rate
L_{s}	Subgrid length scale
T	Time
S_{i}	Rate of creation by addition from the dispersed phase
R_{i}	Rate of production of species i

E	Total energy
μ_t	Turbulent viscosity
ACRONYM	**DESCRIPTION**
CFD	Computational Fluid Dynamics
DNS	Direct Numerical Simulation
EDC	Eddy-Dissipation Concept
LES	Large Eddy Simulation
LFL	Lean Flammability Limit
MEMS	Micro-Electro-Mechanical Systems
MMF	Mean Mixture Fraction
PDF	Probability Density Function
PRESTO	Pressure Staggering Option
RANS	Reynolds-Averaged Navier-Stokes
RFL	Rich Flammability Limit
DIMENSIONLESS NUMBER	**DESCRIPTION**
Pe	Peclet Number
Pr	Prandatl Number
Re	Reynolds Number
Sc	Schmidt Number

Chapter 1

INTRODUCTION

1.1 Overview and Significance

When it comes to achieve both environmental sustainability and operating efficiency demands, power engineering has to face two major concerns, the optimization of combustion efficiency and the environmental problem. To accomplish these matters, a precise prediction of the fundamental physical and chemical properties of the reacting flows is essential. In the case of industrial furnaces (enclosed structures used to facilitate a wide range of chemical reactions) the design process includes currently careful and deliberate compromises between often conflicting design requirements. These consist of high operating pressure and temperature, and low emission requirements, as well as low operating costs. This goal cannot be achieved by using empirical design experience only. Today, almost every single industry uses advanced design engineering tools such as Computational Fluid Dynamics (CFD) to predict and optimize flow processes.

Turbulent combustion systems involve many phenomena and processes, such as turbulence, mixing, mass and heat transfer, multiphase flow and radiation, which strongly interact. Also, combustion chamber analysis typically comprises the areas of fluid mechanics, turbulence, heat transfer, thermodynamics, and chemical kinetics. It is then, easy to understand that combustor design and turbulent mixing are one of the most challenging topics in engineering guided by empirical methods, and largely algebraic correlations. As a consequence the design of most combustion systems is far from the

optimum and, even though the needs of industry may be diverse, they are not as extensive as the enormous variety of present day combustors would suggest.

The ultimate goal is a general prediction procedure enabling the performance of a proposed combustor to be determined accurately in the absence of a costly experimental program. Its realization demands the adoption by the designer of a more fundamental approach. At the basic level the problem is two-fold. First, it is necessary to solve (in an economical and accurate way) the partial differential equations of hydrodynamics and the convective heat and mass transfer as well as the thermal radiation. Second, good physical models must be available for the turbulence, chemistry and thermodynamic properties.

With the increasing progress in micro-fabrication techniques, there is an increasing inclination towards miniaturization of mechanical and electro-mechanical engineering devices (MEMS). Nevertheless, these miniature devices are limited by the current available power systems by their size, weight, and durability. The need to reduce weight, increase operational lifetime and reduce costs has created a significant challenge in the combustion research [1-2]. The sizes of combustors providing the majority of energy around the world are usually much larger than the smallest length scale of a self-sustainable flame. However, recent developments of many small scale systems, such as portable electronic devices, unmanned aerial vehicles, and small spacecrafts that present size constraints on power components have driven the research interest in meso- and micro- scale combustors. These microcombustors are aimed to address the needs for high energy density power sources for miniature devices. Length scales of the reaction

chamber in these microcombustors are often on the same order as the characteristic dimension of the reaction zones.

Utilizing combustion for power generation in micro systems is motivated by the fact that the stored energy densities of hydrocarbon fuels are two orders of magnitude greater than the current battery technology. With the large energy densities of liquid hydrocarbon fuels (~45 MJ/kg), combustion based micro power devices remain surpassingly competitive with contemporary lithium batteries (~ 0.6 MJ/kg), even if the overall efficiency is as low as 10% [3]. Besides, chemically-driven power generation modes may also complement the use of batteries, when high power output or power peaking is desired. Therefore, combustion based power generators remain a promising solution to meet the need for a compact high energy density source [4]. Nevertheless, in order to develop and realize this technology there is still a significant need in the fundamental studies of flame propagation and extinction in small scale channels. More specifically, understanding the thermal, chemical and transport phenomena in small scale combustion/reaction system is critical for developing microscale power systems and any fuel reforming and catalytic conversion systems.

1.2 Combustion Efficiency and the Effect on the Environment

Energy represents the ability to do work. Nowadays engineering and technology recognize that the earth is a finite eco-sphere having limited terrestrial resources and a delicately balanced environment. In order to present the main developments in energy demand, it is important to identify the principal purposes for which energy is used. Four major energy-related services [6] have been identified: electrical services, mobility,

stationary, and fuel used in power generation. The physical and chemical properties of solid, liquid and gaseous fossil fuels vary over a wide range and these variations have an important influence on flame characteristics. Because of the critical energy balances that are developing between conservation, fuel economy, and restriction of emissions, the role of fuel properties is becoming much more important. The combustion of fossil fuels is the main source of energy supplied to our modern society; the knowledge of the limited supply of fuels has triggered an important effort to search for other means of energy sources. It is a natural idea therefore to avoid as much as possible the wastage of fuels and the overall energy efficiency will become the most important criterion in the design of energy systems.

The vast amount of money invested in the combustion of fossil fuels in industrial furnaces has for many years stimulated efforts to optimize furnace performance. Many studies have been held in order to achieve better combustion efficiency. The study performed by Michel et al. [7] on prediction procedures for the calculation of furnace performance illustrates in a very complete fashion these efforts to get more efficient systems. The concept of low-excess-air firing is nowadays being accepted as a way to achieve better energy efficiency; Kouprianov et al. [8] studied two different approaches to achieve better efficiencies by using this concept. An additional new trend to achieve most efficient systems is through the preheating of the incoming air, Hatsuki and Hasegawa [9] studied the effect and technology of this new approach. A novel method of studying and achieving more efficient systems is trough plasma aided combustion, Kim et al. [10], Lou et al. [11], and Lin et al. [12] are very fine examples of this new technique. Another concepts being developed to get most efficient systems are

atomization of fuel, fuel moisture content and ash content [13-15]. In despite of all of the efforts that are being made in order to achieve better energy efficiency the design of combustion systems is still the main area of research and study.

Several fluid dynamics approaches have been researched in order to optimize combustion systems during the past years. Important efforts have been undertaken regarding the effect of swirl in order to achieve better efficiencies. Swirl is one of the most important parameters that affect mixing and flow pattern in furnaces. In the field of applied combustion, special attention is paid on studies of swirl due to its big effect on flame stabilization, dimensions and efficiency. Studies made by El-Mahallawy and Habib [16], Moneib et al. [17] and Khalil [18] prove the intensive research done in flows with swirl. Some other studies have been conducted to analyze the geometry of the combustion systems. Ibrahim and El-Mahallawy [19] investigated experimentally and computationally the structure and height of a turbulent free diffusion flame issued from a vertical burner, analyzing thus, the effect of relative angle between fuel and air jets. El-Mahallawy and Hassan [20] studied the effect of the exit section geometry and the furnace length on mixing and flow patterns in a cold model industrial furnace. El-Mahallawy and Ghali [21] investigated the effect of burner geometry on the aerodynamic mixing pattern in a cold model furnace. All these efforts to improve energy efficiency through design is what triggers this thesis research in order to get a better understanding of the factors involved in the combustion process and design techniques to improve efficiency to meet the modern industries demands.

In a general way, the three T's of good combustion (time, temperature and turbulence) are qualitative descriptions of burner's behavior. Nevertheless, more quantitative criteria are needed in order to define performance in a better way. The most used quantitative criterion nowadays to describe combustion systems behavior is the combustion efficiency - that is completeness of combustion. For many years it has been customary to think in terms of the time that the combustion gases spend in the furnace (residence time) as an important criterion for good combustion. When residence time was not specified, it was often given as an equivalent of furnace heat release rate. This identified the first of the three T's of combustion: time. It has become more evident that residence times can vary by a factor of a thousand between a good and a bad burner. Since the best burners usually have the highest rates of heat release, it is unwise to specify a long residence time as a criterion for achieving a complete combustion. High swirl (a way to describe turbulence, the third T of combustion) numbers can reduce residence time requirements. While the size of a furnace may be dictated by the arrangement and size of the heat transfer surface, rigid adherence to obsolete residence-time criteria may result in costly oversized furnace designs.

Energy conservation requires achievement of maximum combustion efficiencies. It is obvious that burning of stoichiometric mixtures with long residence times leads to complete combustion and elimination of emission of CO, HC, and carbon particulates. However, burning at stoichiometric mixture ratios occurs close to the maximum theoretically attainable (adiabatic) temperatures. Formation of NOx is directly related to temperature, so that attempts to reduce emissions of NOx must involve reduction in flame temperatures, for example the use of excess air, and this leads to reductions in the overall

thermodynamic and energy efficiency of systems. Hence, there is a basic conflict between attempts to increase energy conservation by increasing combustion efficiency and the requirement to restrict emission of NOx. Because of the high activation energy of the thermal NO_x mechanism any scheme that suppresses peak temperatures will lower the NO_x output.

1.3 Reactive Flow Modeling Approaches

Validation is the testing of the model with data from the situation of interest. All models must be validated. Theoretical models require validation to define their applicable range. For example, the ideal gas law is wrong at high pressures and low temperatures. Newton's second law of motion is wrong at high speeds approaching the velocity of light. But in their spheres of applicability they are highly accurate. Simulations require validation because there may be errors in the computer code, improper convergence, etc. Semi empirical models require some data to determine values of the adjustable parameters. Therefore, regardless of the model type, validation is always a good practice and one should be carefully assessed whether or not the results represent extrapolation.

Non-premixed (diffusion) combustion occurs in all systems where fuel and oxidizer are not perfectly premixed before entering the combustion chamber. Because many practical combustion devices operate with non-premixed flames in the presence of turbulent flow, modeling of non-premixed turbulent combustion has always been a central issue in understanding combustion systems.

Turbulent flows and combustion chemistry are characterized by a large spectrum of time and length scales. The largest scales of the turbulence are directly linked to the physical size of the combustion chamber, while the smallest scales represent the dissipation of turbulence energy by viscosity. When the reactants are supplied in separate streams, the entrainment of fuel and oxidizer by large scales leads to incomplete mixing. Then micromixing mechanisms, acting at smaller scales, bring fuel and oxidizer into contact in the reaction zone where products are formed. The elementary chemical reactions also have a broad spectrum of time scales. Depending on the overlap between turbulence time scales and chemical times, strong or weak interactions between chemistry and turbulence may appear [22]. Because of the description of non-premixed turbulent combustion needs the understanding of simultaneous turbulent mixing and combustion process, the modeling of these flames is challenging and there has been numerous studies on the subject [23-24].

A full numerical solution of a non-premixed turbulent flame should solve from the smallest to the largest characteristics scales. Because it is not possible to develop such a complete solution for most practical devices, averaging techniques must be introduced. Much of the research on turbulent diffusion flames is directed at improving the modeling of the many component phenomena in these calculation methods. Chemical reaction rates are highly nonlinear functions of species concentrations and temperature, and severe problems are faced in evaluating mean reaction rates for inclusion in averaged species and energy balances. Much of the progress that has been made is for the case of "fast chemistry", that is, where chemical reaction rates are large compared with the rates of molecular mixing of the reactants. As illustrated by Hawthorne et al. [25], reaction rates

are limited by the rate of turbulent mixing, and the correct mean concentration of reactants and products can be obtained by allowing for the fluctuations in the local instantaneous mixture ratio, with the instantaneous mixture being fully reacted. Toor [26] and Spalding [27] further developed this approach, and Bilger [28] derived an expression relation the mean reaction rate to the dissipation rate of a conserved scalar.

Numerical models are capable of providing the necessary information of the flow and scalar fields must be able to predict the highly unsteady behavior, in particular that associated with turbulence-chemistry interactions. The final goal of these models must be a reliable prediction of combustion systems of practical and technical importance.

In recent years a large increase in numerical modeling of real combustion phenomena has been observed. These techniques, if reliable and correctly developed, should be able to avoid a large part of the experimental work necessary to develop a new combustor giving information otherwise obtainable only by means of troublesome and costly experiments. Nonlinear partial differential equations must be solved in numerical modeling; this leads to numerical problems like convergence and stability and computer storage capacity.

In general two distinct lines of approaching the combustor modeling problem can be seen. Some authors have tried to model the furnace by dividing it into several separate sections, each representing a simple system [29]. Although such methods are useful for the prediction of the trends in furnace behavior of pollutants formation, additional model assumptions and empirical data are often required for particular calculations. On the other hand methods have been developed that simulate the furnace performance in more detail,

generally by solving the conservation equations in finite difference form [30-31].These methods lead to a fair prediction of the influence of furnace geometry and configuration dependent phenomena.

Direct numerical simulations (DNS) resolve all scale structure of scalar and velocity fluctuations. Although recent DNS of laboratory-jet flame experiments have been reported with reduced or realistic chemical kinetics [32], they are computationally expensive and remain limited to low Reynolds number flow. For complex turbulent flows of practical importance, unsteady Reynolds averaging-based numerical simulations (RANS) and large eddy simulation (LES) have emerged as realistic alternatives.

RANS-based turbulence models represent all scales of motion, so that more modeling effort is required. The determination of model coefficients is often a problem, when new configurations are studied. It is worth mentioning that numerical schemes are also frequently too dissipative. Recent innovative concepts have been studied in [33-34].

In LES, the large energy-containing scales of motion are simulated numerically, while the small unresolved subgrid scales and their interactions with the large scales are modeled. The application of LES to combustion systems has been facilitated by the availability of comprehensive experimental data for confined coaxial jets with and without chemical reactions, due to the classic experiments that were conducted by Akselvoll and Moin [35] and Johnson and Bennett [36].

1.4 Combustion Systems Scales

There are three characteristics lengths in combustion systems. Depending on the ratio of flame thickness and burner scale, combustion problems can be divided into three regimes: macroscale combustion, mesoscale combustion, and microscale combustion. Depending on the ratio of mean free path and burner scale, the problem can be divided into another three regimes: continuum regime, slip regime, and free-molecule regime. The properties of gases can be described by the Boltzmann transport equation. If the system has a characteristic length, the molecule will introduce another characteristic length called "mean free path". The mean free path defines the average distance a molecule travels between each collision. When the mean free path is larger than the characteristic length of the system, molecules will directly reach the boundary before colliding with any other molecules and the gas phase collision can be neglected, this is called the free molecule regime. When the mean free path is much smaller than the characteristic length of the system, each molecule will have sufficient collisions before colliding with the boundary. The whole gas phase can be considered as continuous media and the Boltzmann equation reduces to the Navier-Stokes equations and the flow falls into the continuum regime. When the mean free path is close to zero, all the diffusion terms reduce to zero and the Navier-Stokes equations reduce to the Euler equations. Even though the mean free path is much smaller than the characteristic length of the system, the molecule collision with the boundary is comparably smaller than the gas phase collision, from the macroscopic point of view the properties on the boundary is not continuous, this is called the slip regime.

In the mesoscale combustion regime, the combustion length scales is close to the quenching diameter, defined by the flame thickness (~15 δ). When the characteristic length of the combustion chamber is much larger than the flame thickness, the combustion phenomena can be described without considering the wall effect, this is considered to be the macro combustion regime. With the decrease of the combustion chamber, the wall effect on the combustion process and flame dynamics is not negligible anymore, thus mesoscale combustion phenomena must take into account the wall effects. When the chamber size is in an order or even smaller than the flame thickness, there may not be any flame structure. The thermal kinetic wall effect is just as important as the gas phase combustion; this is the microscale combustion regime. In microscale combustion, non-equilibrium transport effects may play an important role when the process is diffusion controlled.

1.5 Scaling Impact in Transport Phenomena and Mixing

Most of the characteristic length of the micro-combustors being developed to date is sufficiently larger than the molecular mean-free path of the air. This means that the hypotheses of non-slip condition and continuum assumptions will still apply and the physical and chemical behavior is fundamentally the same as in macro scale. However, the small size of the micro-devices or their components causes particular characteristics of the fluid mechanics, heat transfer, and combustion involved in the device operation.

Some of the scaling issues involved in microcombustors can be understood by normalizing the conservation equations of momentum, energy, and species [37]. The one-

dimensional normalized form of the governing equations in the gas phase can be written as:

$$\frac{L}{t_c u_c}\frac{\partial u^*}{\partial t^*} + u^*\frac{\partial u^*}{\partial x^*} = -\frac{p_c}{p_c u_c^2}\frac{1}{p^*}\frac{\partial p^*}{\partial x^*} + \frac{1}{Re}v^*\frac{\partial^2 u^*}{\partial x^{*2}} + \frac{gL}{u_c^2} \tag{1.1}$$

$$\frac{L}{t_c u_c}\frac{\partial T^*}{\partial t^*} + u^*\frac{\partial T^*}{\partial x^*} = \frac{1}{Pe}\alpha^*\frac{\partial^2 T^*}{\partial x^{*2}} + Da\frac{Q}{C_p^* T_c}\dot{\omega}^{*"} \tag{1.2}$$

$$\frac{L}{t_c u_c}\frac{\partial y_i^*}{\partial t^*} + u^*\frac{\partial y_i^*}{\partial x^*} = \frac{1}{LePe}D^*\frac{\partial^2 y_i^*}{\partial x^{*2}} + Da\frac{1}{y_{ic}}\dot{\omega}^{*"} \tag{1.3}$$

Where *Da* is the Damkholer used in turbulent combustion and that corresponds to the ratio of chemical time scale and turbulent time scale.

The non-dimensionalized heat transfer equation on the solid wall can be represented in the following form:

$$\frac{\partial T_S^*}{\partial t^*} = Fo\alpha_S^*\frac{\partial^2 T_S^*}{\partial x^{*2}} \tag{1.4}$$

The relevant normalized boundary conditions for these equations are:

$$u^* = 0\,,\ \tau^* = \frac{\mu_c u_c}{\tau_c L}\mu^*\frac{\partial u^*}{\partial y^*} \tag{1.5}$$

$$T^* = T_w^*\,,\ \lambda_S\frac{\delta T_S^*}{\delta x^*} = \lambda\frac{\delta T^*}{\delta x^*}\frac{\delta T_S^*}{\delta x^*} = Bi(T_S^* - 1) \tag{1.6}$$

$$y_i^* = 0,\ \frac{\delta y_i^*}{\delta x^*} = (LePe)y_i^* \tag{1.7}$$

In macro-size combustors, the characteristic length is usually relatively large, and generally the Reynolds (Re) and Peclet (Pe) numbers are also large. The flows are mostly turbulent, and as seen in the above equations, the viscous and diffusive effects are small compared to the convective effects. As the size of the system is reduced, the Reynolds number and the Peclet number decrease indicating that the viscous and diffusive transports of heat and mass are now important and now the flow is primarily laminar.

As mentioned before, at large scale, even though the diffusion is slow compared to the convection, flow instability and turbulence can significantly enhance mixing at scales larger than the diffusion thickness. Furthermore, residence time is sufficiently long and mixing is usually not an issue especially in turbulent combustion. At small scale, since turbulent mixing is small, species mixing will primarily be by diffusion. In this regard the diffusion time is important since it must be smaller than the residence time for complete mixing to occur. That is, the Peclet number, which measures the ratio of the characteristic diffusion time and the characteristic residence time, has to be smaller than unity. The flow residence time is usually defined as:

$$t_r = \frac{\rho V}{\dot{m}} \sim \frac{L}{u_c} \tag{1.8}$$

The low Reynolds number coupled with the planar nature of small scale devices makes mixing of the reactants a potential problem in micro-systems. Although the small diameter of the channels significantly enhances the diffusive mixing, the residence time of the fluids in the channels is also reduced greatly, and may be insufficient to ensure complete mixing. Therefore, in some cases where the mixing of species needs to be

enhanced, different dynamic mixing approaches are introduced in enhancing the mixing rates of liquids [38-39]. Also efforts are being made in order to generate vortex to enhance the mixing inside a combustion chamber [40].

1.6 Chemical Reaction Issues: Thermal and Kinetic Quenching

Numerous issues on flame dynamics emerge as the size of the combustor is reduced [41-42]. For example, there is a minimum gap distance, known as the quenching distance, through which a gaseous flame will propagate without the aid of heterogeneous catalytic combustion.

Both thermal and kinetic quenching cause extinction and incomplete combustion and play an important role in small scale combustion due to the large surface to volume ratio. The chemical reaction time highly depends on heat loss and pressure, while the residence time depends on the characteristic chamber size and flow velocity. In micro-combustion devices, heat transfer by natural convection is small because the induced buoyancy effect is small. However, heat transfer by conduction through the gas to the surrounding solid surface is significant due to the high temperature gradients. Heat transfer by radiation also increases as the characteristics length decreases due to the large view factor. The significant increase of the heat loss will lead to flame extinction.

A flame cannot propagate below a quenching tube diameter as proven by Zel'dovich et al. [43] and Spalding [44]. The existence of a quenching diameter is a result of the increasing heat loss. The flame cannot propagate beyond a critical heat loss rate.

The concept of the quenching tube diameter is widely used in fire safety devices to prevent flame flashback and explosion.

Radical quenching is another mechanism that will deactivate the flame. Radical quenching is a heterogeneous kinetic process in which highly reactive radical intermediates undergo termination reactions at the solid wall surface. Since the reactive intermediates are crucial to the propagation of homogeneous catalytic cycles in the combustion mechanism, the removal of these radicals quenches the flame. As engine size or combustion volume decreases, the surface-to-volume ratio increases, resulting in increased combustor surface heat losses and increased potential destruction of radical species at the wall.

The effect of kinetic quenching depends on Lewis number and wall temperature. Kinetic quenching becomes dominant at high wall temperature or small Lewis number (defined as the ratio of thermal diffusivity to mass diffusivity). An increase of the wall temperature will significantly increase the critical Lewis number for the radical quenching to be important. At low wall temperature (high heat loss), radical quenching plays an important role only when the important radicals have small Lewis numbers. Since most of the radicals have a Lewis number close to unity, quenching is mostly cause by heat loss and radical quenching plays a less important role. The problem of wall quenching can be reduced or prevented by increasing the wall temperature or by using the concept of adiabatic wall. Elevated operating temperatures of the combustor walls not only help to prevent quenching, but also help counter the adverse effect of the small physical time inherent in micro-combustors by reducing the chemical time.

The heat loss and radical quenching on the wall at small scale will increase the chemical time and possibly prevent the onset of the gas-phase combustion reaction, or lead to quenching. As the length scale is decreased, the characteristic response time of the solid structure will decrease and the Fourier number (ratio of the heat conduction rate to the rate of thermal energy storage) increases, which results in a quasi-steady behavior of the solid temperature. In mesoscale combustion, the flame-wall interaction may dramatically change the nature of flame propagation in small scale devices. It can also enhance combustion in some cases. Other thermo-chemical management techniques that take the advantage or large surface to volume ratio and wall-flame coupling can yield the effect of the excess enthalpy and be used to overcome quenching and stabilize the flame.

In general, catalytic combustion [45-46] and excess enthalpy burners [47-48] have been widely studied to address the combustion enhancement through thermal and kinetic coupling between flow and structure. These approaches somewhat resolve the limitations on the combustor designs due to the thermal and radical quenching in small confinements. Although the performance and operating characteristics of Swiss-roll burners are extensively studied [49-50], degradation of the catalyst in excess enthalpy burners restricts the development of these combustor designs into practical systems. Both catalytic and excess enthalpy combustion concepts deposit thermal energy into the body structure and can also make thermal management much more difficult.

In addition to the thermal coupling, there could also exist kinetic coupling especially at microscale combustion. Since the gas phase reaction has large activation energy, the bulk gas has to maintain a relative high temperature around 1800K for the gas

phase reaction to complete. This results in high temperature gradient and heat loss. On the other hand, catalytic combustion has much lower activation energy and can happen at relatively low temperature (700K), which will significantly reduce the temperature gradient and heat loss. With the presence of both surface catalytic reaction and gas phase combustion, radicals from the surface reaction can participate in the gas phase combustion and reduce the quenching distance. Although the catalytic reaction is generally slower than the gas-phase reaction, the relative increase of surface area and the lower temperatures of the catalytic reaction suggest that micro-scale combustors using catalytic reaction may be easier to implement than those using gas-phase reactions.

1.7 Diffusion Flame in Mesoscale Combustion

Flame control, stabilization, and sufficient mixing become issues that need to be addressed in order to successfully develop micro combustors. Multiple isolated reaction zones, or flame cells, were observed in conditions both away from and close to extinction in the Y-shaped diffusion burner of Miesse et al. [51]. The mechanism responsible for this diffusion flame instability in microscale combustors has not been well understood. Therefore, fundamental understanding of the impacts of mixing and flame-wall interaction on non-premixed flames in mesoscale combustion must be addressed in order to successfully develop micro combustors. [52-53].

In turbulent combustion, large-scale unsteady flow motion together with micro-mixing mechanisms subsequently brings fuel and oxidizer into contact where products are formed within a thin reaction zone. The evolution of non-premixed flames in turbulent flow depends on the process of fuel and air mixing but also on the dynamics of

triple flames. Understanding the dynamics of triple flames and edge flames is relevant for explaining partial extinction phenomena and for development of ignition and turbulent flame stabilization.

Because of heat-release–induced effects, laminar triple flames promote a deviation of the flow in which they propagate; this deviation of the streamlines occurs upstream from the flame. In the vicinity of the triple point, the premixed flame is weakly curved and features a propagation velocity of which value is similar to that of the planar premixed flame velocity. This fact, in addition to the deviation of the flow upstream from the triple point together with conservation of mass, implies that burning velocities for triple flames take larger values than burning velocities for planar premixed flames. Hence, the triple-flame structure locally modifies, through heat release, the mixture fraction field, to keep the magnitude of the mixture fraction gradient evaluated at the triple point small enough to allow for the reaction to occur in the trailing diffusion flame. The triple-flame concept may be used to understand the flame structure at ignition, simply because when traveling along the stoichiometric line the size of the mixing layer decreases. Then, isoconcentration surfaces of fuel and oxidizer are brought together and the degree of premixing of the flow locally grows [54].

1.8 Motivation and Objectives of the Present Thesis

Recently there have been an important number of research efforts in the development of mathematical and numerical modeling in turbulent reacting flows. Such studies have been motivated by the need to understand and predict the combustion processes in devices such as gas turbine and ramjet combustors [55-56], liquid and

gaseous fueled furnaces [57], chemical lasers, and other propulsion devices such as ducted rockets. One of the motivations of this research thesis is to investigate different turbulence and chemistry modeling approach in the analysis of simple but practical industrial combustors.

In the literature there exist many studies and experiments conducted on coaxial jet type combustors. One of the best examples is Pierce and Moin [58] LES simulation on the Spadaccini burner [59]. Other examples are Vanka [60], and Kim and Chung [61] studies by different methods of the Lockwood burner [62]. The first part of this research thesis seeks to perform a numerical analysis of the effect of injection on the turbulent mixing quality in a simple combustor by the study of two grid geometries (2D and 3D) that are created to validate the results of the numerical simulation with the ones observed in experimental data. Later, numerical issues regarding this type of simulation such as the effect of grid arrangement (fine and coarse grid), boundary conditions (Schmidt number and turbulence intensity), and turbulence models (k-ε and LES) will be addressed and discussed. To conclude, the effect of injection geometry and the design on an improved configuration for high turbulent mixing quality and combustion efficiency inside the combustor is performed taking into consideration pollution formation. Another motivation of this thesis is to investigate what is the effect of injection geometry in the quality of the mixing to generate alternative means of achieving higher efficiencies at less environmental cost than the traditional preheating of the reactants methods.

Recently, experiments using mesoscale Swiss roll combustors [63], counterflow flames [64] and other devices, were conducted to study the heat recirculation effect at

small scales. The results revealed interesting coupling between flame and wall vie heat recirculation. Nevertheless due to some geometrical constraints some fundamental mechanisms of flame speed and extinction on wall properties were not understood. The effect of Lewis number on the existence of multiple flame regimes was not investigated. So far, it is not clear enough how flame curvature and local flame quenching will affect the flame speed and the transition of multiple flame regimes. Additionally, because the main focus of micro-scale combustion has been in premixed flames, there is not that much information about the effects of heat loss, flame scale, and reignition on the dynamics of triple flames. There is very limited work reported on small scale combustion systems experimental measurements or flame streets. Therefore, it results very attractive to investigate the mesoscale flame propagation and extinction theoretically and experimentally as well as to obtain a general flame dynamics for mesoscale flames due to wall-flame interaction through the analysis of non-premixed flames in a mesoscale mixing layer, where there is a strong interaction between wall temperature and flame. Having this as a motivation, a numerical analysis of a flame street in a fuel-air mixing layer insider a mesoscale combustor is performed. Between the fuel and the air stream there is a mixing layer zone along the flow direction. At the leading edge of this mixing zone, air and fuel mix fast and a premixed region with the stoichiometric line in the middle of the mixing layer. Therefore, experimentally it is going to exist an anchored leading triple flame due to the difference between the lower flows speed and the flame propagation speed. An important difference between non-premixed combustion at mesoscale and the normal scale is that in mesoscale after the first anchored tripe flame is shown a series of triple flames emerge, this is called the flame street. First, a three

dimensional grid was created to represent the actual experimental geometry. Second, the influence of different turbulence models such as k-ε,and k-ω, in the formation of the flame street is analyzed. Also the effect of the Schimidt number is assessed. Two different chemistry-turbulence interaction models are analyzed to evaluate the importance of transport kinetics. Finally, a flame street is reported and its behavior is studied under different wall temperatures and flow velocities. A comparison with experimental data by Xu [65] is made to validate the simulation.

By performing these simple studies in this thesis, the idea is to analyze the effect of injection geometries and flame dynamics in small scale to get a better understanding of the dynamics in turbulent and laminar flames, amongst its propagation and behavior in large and micro channels. Also, the objective is to get this understanding to improve industrial applications in terms of energy and environmental savings by using the numerical simulation tool.

Chapter 2

NUMERICAL SOLUTION METHODOLOGY

The present research work focuses on the modeling of combustion processes using Computational Fluid Dynamics (CFD). Computational combustion requires the coupling between fluid dynamics and chemical reactions and the accuracy is known to be highly dependent on the numerical formulation of the simulation problem. Therefore, in this Chapter, the basic CFD procedure and details including different types of chemistry and turbulent models are provided and discussed. The commercial software FLUENT, which is chosen to perform the simulation studies, is introduced.

2.1 Solution Procedure Overview

FLUENT is a commercial CFD software capable for modeling fluid flow and heat transfer in complex geometries and has been proven reliable in a broad range of applications in combustion modeling. It counts with a wide range of homogeneous and heterogeneous reacting flows such as furnaces, boilers, process heaters, gas turbines, and rocket engines [66-70]. It is demonstrated by these studies that FLUENT can give predictions of flow field and mixing characteristics, temperature field, species concentrations and particulates and pollutants.

A general overview of the computational methodology is provided here for completeness. In order to get accurate results and to avoid numerical convergence problems a detailed solution procedure should be carefully followed. As a first step the

solution parameters should be chosen (solver and discretization schemes), subsequently the initialization of the fluid should be performed and the convergence of the solution should be monitored. Finally, some parameters can be modified to accelerate convergence and/or to improve accuracy. The detailed solution procedure is depicted in Figure 2.1.

It is very important to explain in detail the solution parameters that were used throughout the numerical simulations of this thesis, therefore a complete explanation of the different parameters used is given in the proceeding sections.

2.1.1 Flow Solvers

To model the reactive fluid flow phenomena, the solution of the governing integral equations for the conservation of mass and momentum, and for energy and other scalars such as turbulence and chemical species are approximated using a control-volume-based technique, which consists of:

- Division of the domain into discrete control volumes using a computational grid.
- Integration of the governing equations on the individual control volumes to construct algebraic equations for the discrete dependent variables ("unknowns") such as velocities, pressure, temperature, and conserved scalars.
- Linearization of the discretized equations and solution of the resultant linear equation system to yield updated values of the dependent variables.

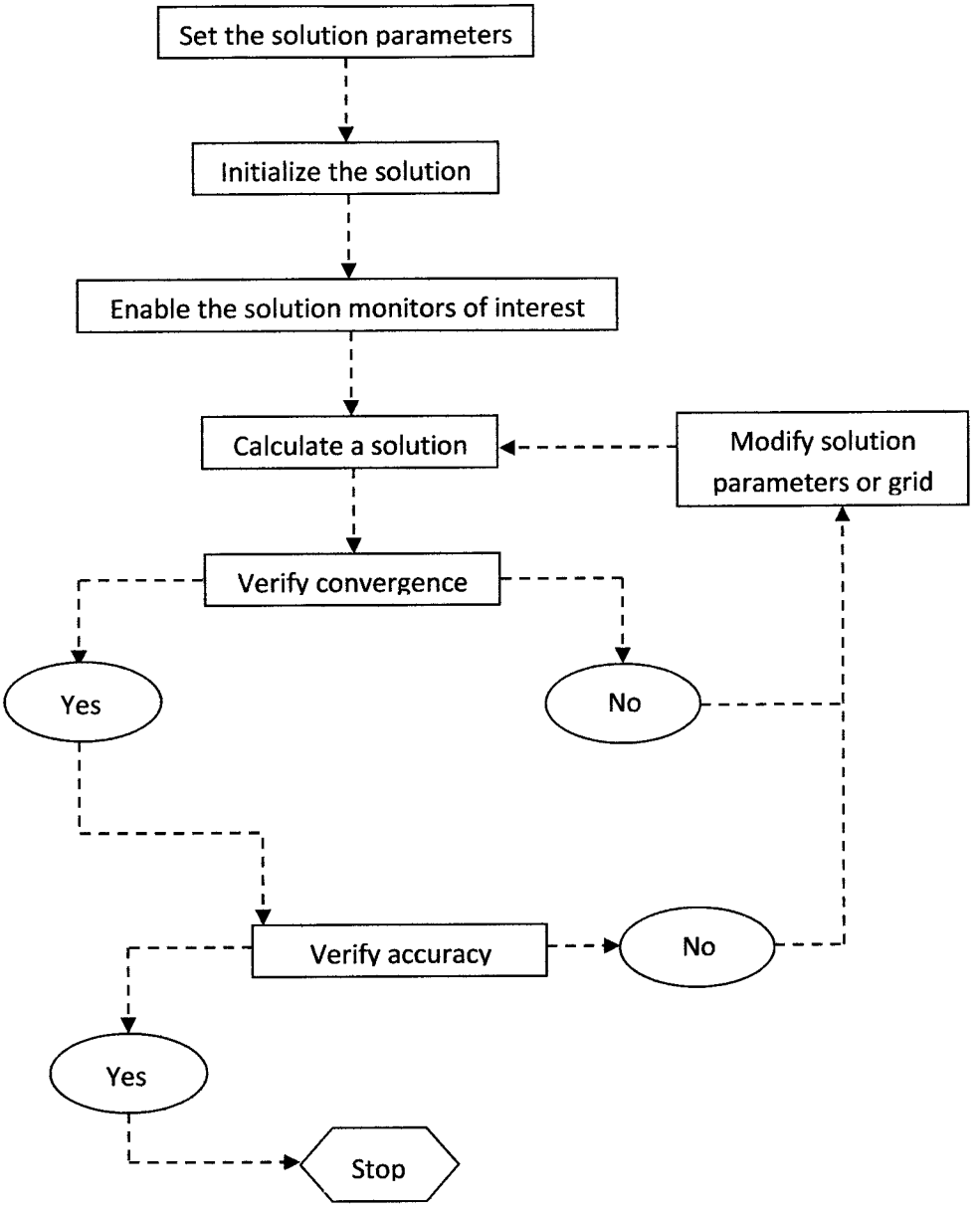

Fig. 2.1 FLUENT Solution Procedure Overview

The general algorithm of the solver used in this study for numerical simulations is based on a pressure-based approach. The pressure-based solver employs an algorithm which belongs to a general class of methods called the projection method [71]. In the projection method, the constraint of mass conservation (continuity) of the velocity field is achieved by solving a pressure equation. The pressure equation is derived from the

continuity and the momentum equations in such a way that the velocity field, corrected by the pressure, satisfies the continuity. Since the governing equations are non-linear and coupled to one another, the solution process involves iterations in which the entire set of governing equations is solved repeatedly until the solution converges. In Fluent, two pressure-based solver algorithms are available: a segregated algorithm and a coupled algorithm. The segregated solver solves for pressure correction and momentum sequentially while the coupled solver solves pressure and momentum simultaneously. These two approaches are outlined in Figure 2.2.

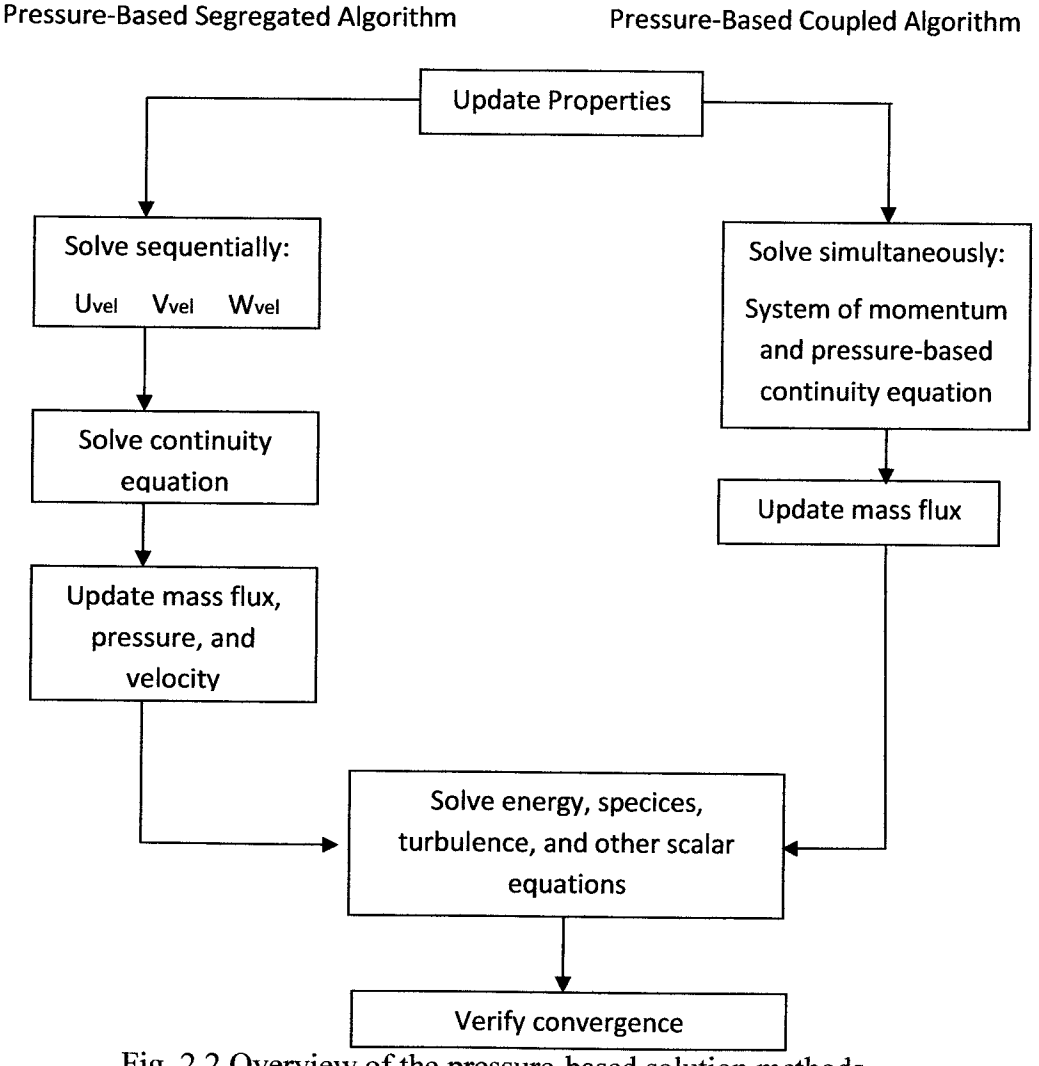

Fig. 2.2 Overview of the pressure-based solution methods

In choosing a solver it should be considered that the pressure-based solver is applicable for a wide range of flow regimes from low speed incompressible flow to high-speed compressible flow, requires less memory (storage), and allows flexibility in the solution procedure. The pressure-based coupled solver is applicable for most single phase flows and yields superior performance to the pressure-based segregated solver, nevertheless is not available for multiphase, periodic mass-flow and NITA cases, also it requires 1.5 – 2 times more memory than the segregated solver. The pressure-based segregated solver that is used in chapter 3 and the pressure-based coupled solver that is used in chapter 4 are the basis for the simulations performed in this work.

2.1.2 Discretization

Field variables (stored at cell centers) must be interpolated to the faces of the control volumes. This is accomplished by using an upwind scheme. Upwinding means that the face value is derived from quantities in the cell upstream, or "upwind", relative to the direction of the normal velocity. During the numerical simulations that are about to be shown in this thesis the first-order upwind and the second-order upwind discretization schemes were utilized.

When first-order accuracy is desired, quantities at cell faces are determined by assuming that the cell-centered values of any field variable represent a cell-average value and hold throughout the entire cell; the face quantities are identical to the cell quantities. Thus, when first-order upwinding is selected, the face value is set equal to the cell-centered value in the upstream cell. This scheme is the easiest to converge but only first-order accurate.

When second-order accuracy is needed, quantities at cell faces are computed using a multidimensional liner reconstruction approach [72]. In this approach, higher-order accuracy is achieved at cell faces through a Taylor series expansion of the cell-centered solution about the cell centroid. Thus, when second-order upwind is selected, the face value is computed using the following expression:

$$\varphi_{f,SOU} = \varphi + \nabla\varphi \times \vec{r} \qquad (2.1)$$

Where φ and $\nabla\varphi$ are the cell-centered value and its gradient in the upstream cell, and $\vec{r}$ is the displacement vector from the upstream cell centroid to the face centroid. The second-order upwind scheme uses larger stencils for 2nd order accuracy, essential with tri/tetrahedral mesh or when flow is not aligned with the grid, nevertheless the convergence could be slow.

2.1.3 Evaluation of Gradients and Derivatives

Gradients are needed not only for constructing values of a scalar at the cell faces, but also for computing secondary diffusion terms and velocity derivatives. The gradient $\nabla\varphi$ of a given variable φ is used to discretize the convection and diffusion terms in the flow conservation equations. Computationally, the gradients can be computed using the Green-Gauss cell-based approach. When the Green-Gauss theorem is used to compute the gradient of the scalar φ at the cell centered *c0*, the following form is written as:

$$(\nabla\varphi)_{c0} = \frac{1}{v}\sum_f \overline{\varphi_f}\,\vec{A}_f \qquad (2.2)$$

where φ_f is the value of φ at the cell face centroid. The summation is over all the faces enclosing the cell. It is perhaps important to point out that due to its nature the solution using the Green-Gauss cell-based approach may have false diffusion (smearing of the solution fields).

2.1.4 Discretization of Momentum and Continuity Equations

If the pressure field and face mass fluxes are known, the momentum equation can be solved using the discretization methods mentioned before. However, the pressure field and face mass fluxes are not known a priori and must be obtained as a part of the solution. An interpolation scheme is therefore required to compute the face values of pressure from the cell values.

An interpolation method for face pressure such as the PRESTO! is considered. The PRESTO! (PREssure Staggering Option) scheme uses the discrete continuity balance for a "staggered" control volume about the face to compute the "staggered" pressure. This method is used for highly swirling flows, flows involving steep pressure gradients, or in strongly curved domains.

Pressure-velocity coupling refers to the numerical algorithm which uses a combination of continuity and momentum equations and derives an equation for pressure (or pressure correction) when using the pressure-based solver. The numerical simulations of this thesis used the SIMPLE and Coupled approaches among different options available in Fluent. The SIMPLE algorithm uses a relationship between velocity and pressure corrections to enforce mass conservation and to obtain the pressure field while

the coupled algorithm solves the momentum equation and pressure correction equations separately. This algorithm results in slow convergence but it obtains a robust and efficient single phase implementation for steady-state flows, with superior performance compared to the segregated solution schemes.

2.1.5 Convergence

In order to get convergence in the numerical computations the following conditions should be satisfied: (1) all discrete conservation equations (momentum, energy, etc.) are obeyed in all cells to a specific tolerance or the solution no longer changes with subsequent iterations. (2) Overall mass, momentum, energy, and scalar balances are achieved.

There are two main ways to monitor convergence during the computations, by monitor residuals history or by monitor quantitative convergence. Generally, a decrease in residuals by three orders of magnitude indicates at least qualitative convergence. At this point, the major flow features should be established. Scaled energy residual must decrease to 10^{-6}. Scaled species residual may need to decrease up to 10^{-5} to achieve species balance. To monitor quantitative convergence it is necessary to monitor other relevant key variables/physical quantities for a confirmation and to ensure that overall mass/heat/species conservation is satisfied. Figure 2.3 shows a typical residual plot showing when the residuals values have reached the specified tolerance.

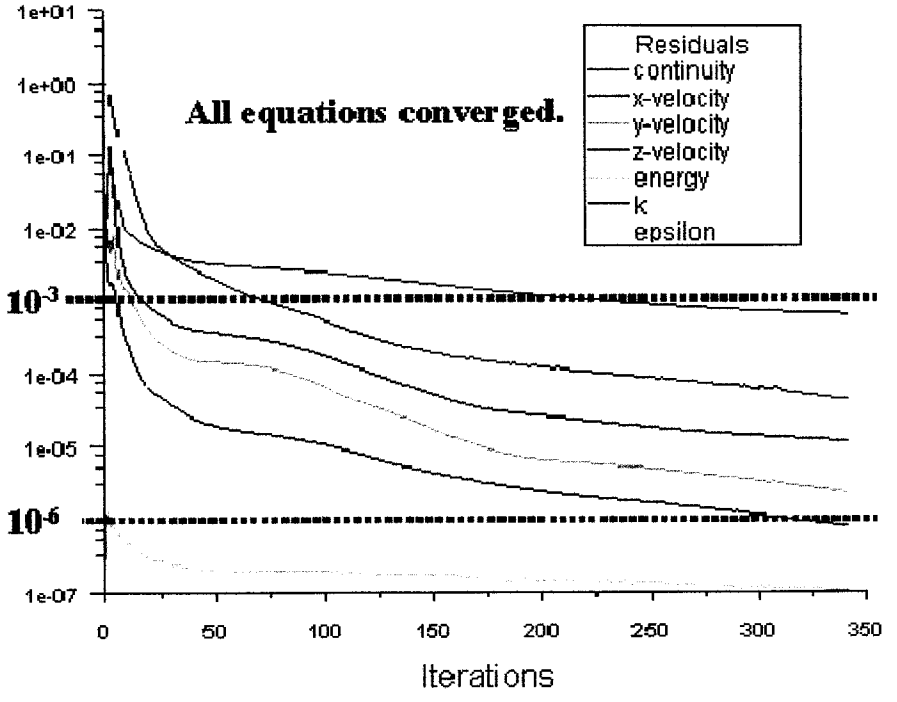

Fig. 2.3 Typical FLUENT residual plot [73]

Numerical stabilities can arise with an ill-posed problem, poor quality mesh, and/or inappropriate solver settings exhibited as increasing or "stuck" residuals, diverging residuals imply increasing imbalance in conservation equations. To avoid having convergence difficulties it is recommended to ensure that the problem is well-posed, compute an initial solution using first-order discretization scheme, decrease under-relaxation factors for equations having convergence problems, or remesh or refine cells which have large aspect ratio or large skewness.

2.2 Reacting Flow Models

There exist numerous difficulties in modeling reacting flows such as turbulence (most industrial flows are turbulent, DNS of non-reacting and reacting turbulent flow is

not possible because of the wide range of time and length scales), chemistry (realistic chemical mechanisms cannot be described by a single reaction equation, stiff kinetics), and turbulence-chemistry interaction (the sensitivity of reactions rates to local changes is complicated by enhances mixing of turbulent flows). Nevertheless methods are developed in the field of numerical combustion to overcome this difficulties by the use of finite rate/eddy dissipation approach (to simplify the chemistry), use of mixture fraction approach (to decouple chemistry from turbulent flow and mixing), and use of stiff solver (to model stiff chemistry) Figure 2.4 depicts an overview of reacting flow modeling.

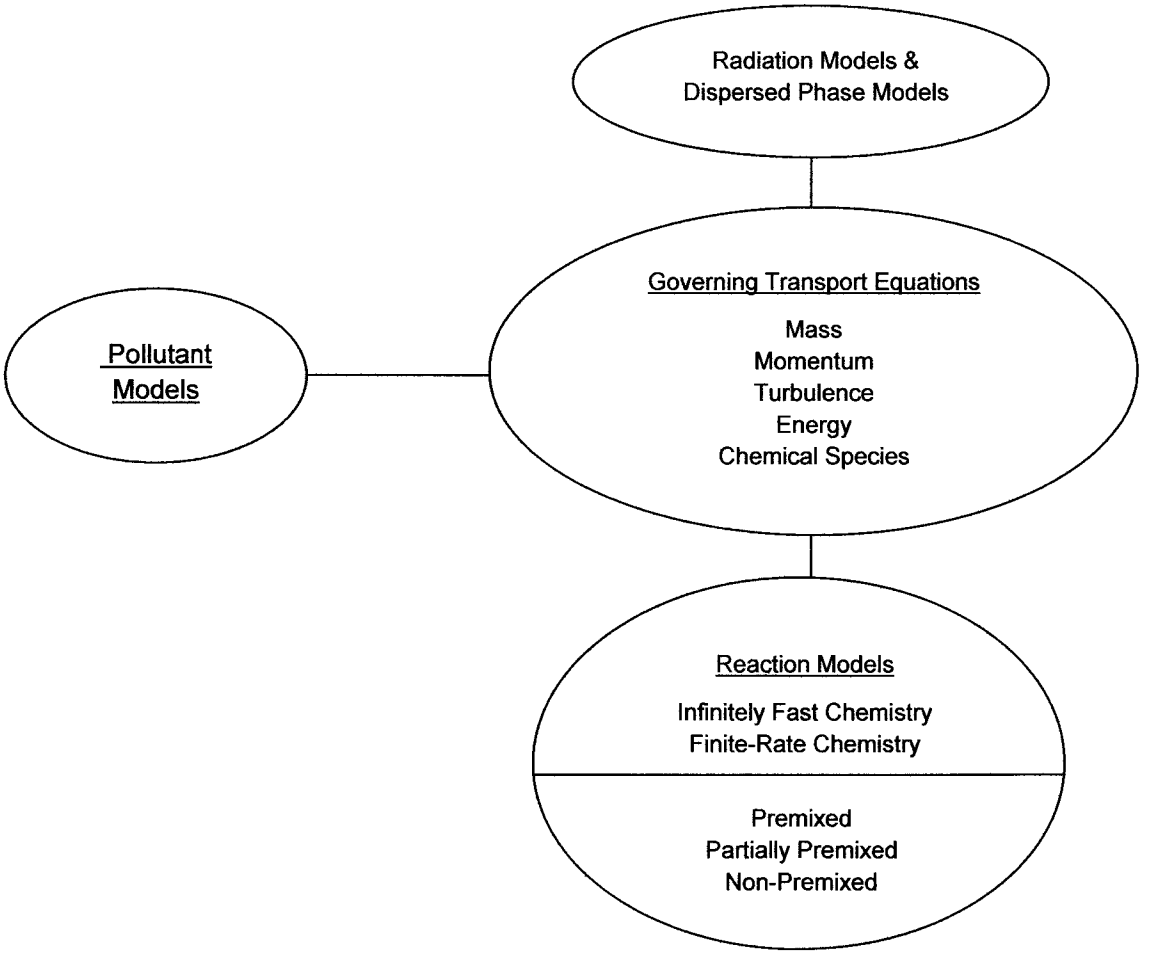

Fig. 2.4 Overview of reacting flow modeling

During the numerical simulations performed in this thesis several reacting flow models were used. Some essential features and characteristics of these different models are given below. First, table 2.1 illustrates the general overview of the non-premixed flow configuration models and approaches. These can be classified into two main approaches: fast chemistry models and finite-rate chemistry models. In the following sections an explanation of the models used for this study is given.

	Non-Premixed Flow Configuration
Fast Chemistry	**Eddy Dissipation Model** (Species Transport)
	Non-Premixed Equilibrium Model Mixture Fraction
Finite-Rate Chemistry	**Laminar Finite-Rate Model**
	Eddy-Dissipation Concept (EDC) Model
	Composition PDF Transport Model
	Laminar Flamelet Model **Steady / Unsteady**

Table 2.1 Overview of non-premixed flow configuration in FLUENT [73]

2.2.1 Fast Chemistry Models

2.2.1.1 Non-Premixed Combustion Model

For non-premixed combustion modeling, which involves the solution of transport equations for one or two conserved scalars (the mixture fractions); equations for individual species are not solved. Instead, species concentrations are derived from the predicted mixture fraction fields.

The thermochemistry calculations are preprocessed and then tabulated for look-up. Interaction of turbulence and chemistry is accounted for with an assumed-shape Probability Density Function (PDF).

The non-premixed modeling approach has been specifically developed for the simulation of turbulent diffusion flames with fast chemistry. The non-premixed model allows intermediate (radical) species prediction, dissociation effects, and rigorous turbulence-chemistry coupling. The method is computationally efficient in that it does not require the solution of a large number of species transport equations.

2.2.1.1.1 Mixture Fraction Theory

Definition

The basis of the non-premixed modeling approach is that under a certain set of simplifying assumptions, the instantaneous thermochemical state of the fluid is related to a conserved scalar quantity known as the mixture fraction, f. The mixture fraction can be written in terms of the atomic mass fraction as:

$$f = \frac{Z_i - Z_{i,ox}}{Z_{i,fuel} - Z_{i,ox}} \qquad (2.3)$$

where Z_i is the elemental mass fraction for element, *i*. The subscript ox denotes the value at the oxidizer stream inlet and the subscript fuel denotes the value at the fuel stream inlet. If the diffusion coefficients for all species are the same, then Equation 2.3 is identical for all elements, and the mixture fraction definition is unique. The mixture fraction is thus the elemental mass fraction that originated from the fuel stream.

Transport Equations for the Mixture Fraction

Under the assumption of having equal diffusivities, the species equations can be reduced to a single equation for the mixture fraction, *f*. The reaction source terms in the species equations cancel, therefore *f* is a conserved quantity. Whereas the supposition of identical diffusivities is delicate for laminar flows, it is generally acceptable for turbulent flows where turbulent convection overwhelms molecular diffusion. The Favre mean (density averaged) mixture fraction equation is:

$$\frac{\partial}{\partial t}(\rho \tilde{f}) + \nabla \cdot (\rho \vec{v} \tilde{f}) = \nabla \cdot \left(\frac{\mu_t}{\sigma_t} \nabla \tilde{f}\right) + S_m + S_{user} \qquad (2.4)$$

the source term S_m is due solely to transfer of mass into the gas phase from liquid fuel droplets or reacting particles. S_{user} is any user-defined source term. Additionally to solving for the Favre mean mixture fraction, one solves a conservation equation for the mixture fraction variance, $\overline{f'^2}$

$$\frac{\partial}{\partial t}(\rho \overline{f'^2}) + \nabla \cdot (\rho \vec{v} \overline{f'^2}) = \nabla \cdot \left(\frac{\mu_t}{\sigma_t} \nabla \overline{f'^2}\right) + C_g \mu_t (\nabla \tilde{f})^2 - C_d \rho \frac{\epsilon}{k} \overline{f'^2} + S_{user} \qquad (2.5)$$

where $f' = f - \bar{f}$. The default values for the constants σ_t ,C_g, and C_d are 0.85, 2.86, and 2.0, respectively, and again S_{user} is any user-defined source term.

Non-Premixed Model for LES

A transport equation is not solved for the mixture fraction variance. Instead, it is modeled as:

$$\overline{f'^2} = C_{var} L_s^2 \left|\nabla \bar{f}\right|^2 \quad (2.6)$$

where C_{var} is a constant (value of 0.5) and L_s is the subgrid length scale.

Relationship of f to Species Mass Fraction, Density, and Temperature

The power of the mixture fraction modeling approach is that the chemistry is condensed to one conserved mixture fraction. Under the supposition of chemical equilibrium, all thermochemical scalars (species fractions, density, and temperature) are exceptionally related to the mixture fraction.

For single mixture fraction, non adiabatic systems, such as those to be discussed later, the instantaneous values of mass fractions, density, and temperature are parameterized as:

$$\emptyset_i = \emptyset_i(f, H) \quad (2.7)$$

For a single mixture fraction system, where H is the instantaneous enthalpy. In non adiabatic systems, the local thermochemical state is related to f and to the enthalpy, H. The system enthalpy impacts the chemical equilibrium calculation and the temperature

and species of the reacting flow. Consequently, modifications in enthalpy due to heat loss must be accounted for when computing scalars from the mixture fraction as in equation (2.7).

In non-adiabatic systems, turbulent fluctuations should be accounted for by means of a joint PDF, $p(f,H)$. The computation of $p(f;H)$, however, is not realistic for most engineering applications. The problem can be simplified considerably by assuming that the enthalpy fluctuations are independent of the enthalpy level. With this assumption, $p(f,H) = p(f)\delta(H - \bar{H})$ and mean scalars are calculated as:

$$\bar{\emptyset}_\iota = \int_0^1 \bar{\emptyset}_\iota(f,\bar{H})p(f)df \qquad (2.8)$$

Determination of $\bar{\emptyset}_\iota$ in the non-adiabatic system therefore requires solution of the modeled transport equation for mean enthalpy:

$$\frac{\partial}{\partial t}(\rho\bar{H}) + \nabla\cdot(\rho\vec{v}\bar{H}) = \nabla\cdot\left(\frac{k_t}{C_p}\nabla\bar{\mathrm{H}}\right) + S_h \qquad (2.9)$$

where S_h accounts for source terms due to radiation, heat transfer to wall boundaries, and heat exchange with the dispersed phase.

Turbulence Chemistry Interaction

Equations (2.7) and (2.8) describe the instantaneous relationships between mixture fraction and enthalpy and species fractions, density, and temperature under the assumption of chemical equilibrium. The FLUENT calculation of the turbulent reacting flow, nevertheless, is concerned with prediction of the averaged values of these variable scalars. How these averaged values are related to the instantaneous values depends on the

turbulence-chemistry interaction model. FLUENT applies the assumed-shape probability density function (PDF) approach as its closure model when the non-premixed model is used.

The Probability Density Function, written as $p(f)$, can be thought of as the fraction of time that the fluid spends in the vicinity of the state f. Figure 2.5 plots the time trace of mixture fraction at a point in the flow (right-hand side) and the probability density function of f (left-hand side). The fluctuating value of f, plotted on the right side of the figure, spends some amount of time in the range denoted as Δf. $p(f)$, plotted on the left side of the figure, takes on values such that the area under its curve in the band denoted, Δf, is equal to the amount of time that f spends in this range. Written mathematically,

$$p(f)\Delta f = \lim_{T\to\infty} \frac{1}{T} \sum_i \tau_i \qquad (2.10)$$

where T is the time scale and τ_i is the amount of time that f spends in the Δf band. The shape of the function $p(f)$ depends on the nature of the turbulent fluctuations in f. In practice, $p(f)$ is unknown and is modeled as a mathematical function that approximates the actual PDF shapes that have been observed experimentally.

Using equations (2.7) and (2.8), it only remains to specify the shape of the function $p(f)$ with the purpose of determining the local mean fluid state at all points in the flow field.

The Assumed Shape PDF

For the numerical simulations performed in this thesis the shape of the assumed PDF, *p(f)*, is described by the β-function . The β-function PDF shape is given by the following function of $\bar{f}$ *and* $\overline{f'^2}$:

$$p(f) = \frac{f^{\alpha-1}(1-f)^{\beta-1}}{\int f^{\alpha-1}(1-f)^{\beta-1}df} \qquad (2.11)$$

Where

$$\alpha = \bar{f}\left[\frac{\bar{f}(1-\bar{f})}{\overline{f'^2}} - 1\right] \qquad (2.12)$$

And

$$\beta = (1-\bar{f})\left[\frac{\bar{f}(1-\bar{f})}{\overline{f'^2}} - 1\right] \qquad (2.13)$$

Notably, the PDF shape *p(f)* is a function of only its first two moments, namely the mean mixture fraction, and the mixture fraction variance. Therefore, given FLUENT's prediction of *f* and *f02* at each point in the flow field (Equations (2.4) and (2.5)), the assumed PDF shape can be computed and used as the weighting function to determine the mean values of species mass fractions, density, and temperature.

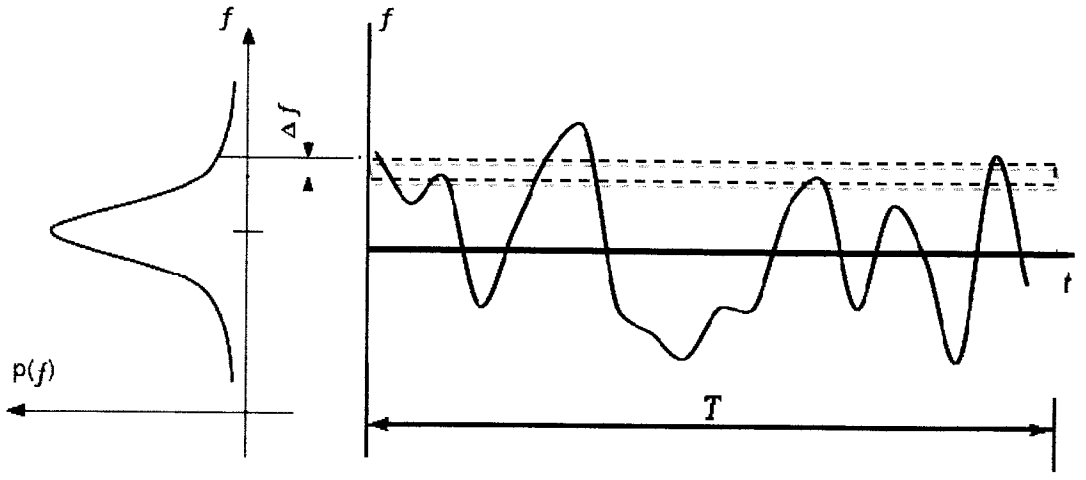

Fig. 2.5 Graphical description of the probability density function *p(f)*[73]

Chemistry Tabulation

In non-adiabatic systems, where the enthalpy is not linearly related to the mixture fraction, but depends also on wall heat transfer and/or radiation, a look-up table is necessary for each possible enthalpy value in the system. The result is a three-dimensional look-up table, which consists of layers of two-dimensional tables, each one corresponding to a normalized heat loss or gain. The first segment corresponds to the maximum heat loss from the system, the last portion corresponds to the maximum heat gain to the system, and the zero heat loss/gain slice corresponds to the adiabatic table. Slices interpolated between the adiabatic and maximum slices correspond to heat gain, and those interpolated between the adiabatic and minimum slices correspond to heat loss.

2.2.2 Finite-Rate Chemistry Models

Species Transport Equations

When conservation equations for chemical species are chosen to be solved a prediction of the local mass fraction of each species, Y_i, through the solution of a convection-diffusion equation for the ith species is made. This conservation equation takes the following general form:

$$\frac{\partial}{\partial x}(\rho Y_i) + \nabla \times (\rho \vec{v} Y_i) = -\nabla \times \vec{J_i} + R_i + S_i \quad (2.14)$$

where R_i is the net rate of production of species i by chemical reaction and S_i is the rate of creation by addition from the dispersed phase plus any other sources. An equation of this form will be solved for $N - 1$ species where N is the total number of fluid phase chemical species present in the system. Since the mass fraction of the species must sum to unity, the *Nth* mass fraction is determined as one minus the sum of the $N - 1$ solved mass fractions. To minimize numerical error, the *Nth* species should be selected as that species with the overall largest mass fractions.

Mass Diffusion

In turbulent flows, the mass diffusion is computed in the following form:

$$\vec{J_i} = -(\rho D_{i,m} + \frac{\mu_t}{Sc_t})\nabla Y_i \qquad (2.15)$$

where Sc_t is the turbulent Schmidt number. Note that turbulent diffusion generally overwhelms laminar diffusion, and the specification of detailed laminar diffusion properties in turbulent flows is generally not warranted

2.2.2.1 Eddy Dissipation Concept Model

The eddy-dissipation-concept (EDC) model provides a turbulence-chemistry interaction model and includes detailed chemical mechanisms in turbulent flows. It assumes that reaction occurs in small turbulent structure, called fine scales. The volume fraction of these fine scales is modeled according with the following expression:

$$\xi^* = C_\xi (\frac{\upsilon \varepsilon}{k^2})^{3/4} \qquad (2.16)$$

where * denotes fine-scale quantities and C_ξ is the volume fraction constant (2.1377) and υ is the kinematic viscosity.

Combustion at fine scales in FLUENT takes place at constant pressure, with initial conditions taken as the current species and temperature in the cell. Reactions proceed over a time scale, governed by the Arrhenius rates and are integrated numerically using the ISAT algorithm that is a powerful tool that enables realistic chemistry to be incorporated in multi-dimensional flow simulations by accelerating the chemistry calculations [74]. This algorithm can accelerate the chemistry calculations in a significant manner, offering substantial reduction in computational time.

The source term in the conservation equation for the mean species *i,* in equation 2.14 is modeled as

$$R_i = \frac{\rho(\xi^*)^2}{\tau^*[1-(\xi^*)^3]}(Y_i^* - Y_i) \qquad (2.17)$$

Where Y_i^* found from ISAT is the fine-scale species mass fraction alter reacting over time τ^*

In general, EDC coupled with one or two step mechanisms. For chapter 4 the reaction mechanism for methane oxidation can be expressed in two steps and with six volumetric species following the next reaction:

$$2CH_4+3O_2 \rightarrow 2CO+4H_2O$$

$$2CO+O_2 \rightarrow 2CO_2$$

2.3 Turbulence Models

Turbulent flows are characterized by fluctuating velocity fields. These fluctuations combine transported quantities such as momentum, energy, and species concentration, and cause these quantities to fluctuate as well. Since these fluctuations can be of small scale and high frequency, they are too computationally expensive to simulate directly in practical engineering calculations. Instead, the exact governing equations can be time-averaged to remove the small scales, resulting in a modified set of equations that are computationally less expensive to solve. Unfortunately, the modified equations

contain additional unknown variables, and turbulence models are required to resolve these variables in terms of known quantities.

It is unfortunate that no single turbulence model is universally accepted as being superior for all classes of problems. The choice of turbulence model will depend on considerations such as the physics encompassed in the flow, the established practice for a specific class of problem, the level of accuracy required, the available computational resources, and the amount of time available for the simulation. Tables 2.2 & 2.3 give a general perspective of all common turbulence models.

During the numerical simulations carried out in this thesis work three turbulence models are used: k-ϵ, k-ω and LES. Therefore, a detailed explanation of these three models is presented in the next section.

Model	*Description*
Spalart-Allmaras	A single transport equation model solving directly for a modified turbulent viscosity. Option to include strain rate in k production term for vortical flows.
Standard k- ε	The baseline two-transport-equation model solving for k and ε. Valid for fully turbulent flows only.
RNG K-ε	A variant of the standard k-ε model. Equations and coefficients are analytically derived. Significant changes in the ε equation. Additional options aid in swirling and low Reynolds number flows.
Realizable k- ε	A variant of the standard k- ε model. Its "realizability" stems from changes that allow certain mathematical constraints to be obeyed which ultimately improve the performance of this model.
Standard k-ω	A two –transport-equation model solving for k and ω, the specific dissipation rate (ε/k) based on Wilcox.
SST k-ω	A variant of the standard k-ω model. Combines the original model for use near walls and the standard k- ε model away from walls. No option to include compressibility
Reynolds Stress	Reynolds stresses are solved directly using transport equations. Use for highly swirling flows.

Table. 2.2 Turbulence models description [73]

Model	*Description*
Spalart-Allmaras	Economical for large meshes. Performs poorly for 3D flows, free shear flows, flows with strong separation. Suitable for quasi-2D external/internal flows and boundary layer flows under pressure gradient.
Standard k- ε	Robust. Widely used despite its limitations. Performs poorly for complex flows involving severe pressure gradient, separation, and strong streamline curvature. Suitable for initial iterations.
RNG K- ε	Suitable for complex shear flows involving rapid strain, moderate swirl, vortices, and locally transitional flows.
Realizable k- ε	Offers largely the same benefits and has similar applications as RNG. Possibly more accurate and easier to converge than RNG
Standard k-ω	Superior performance for wall-bounded boundary layer, free shear, and low Reynolds number flows. Suitable for complex boundary layer flows under adverse pressure gradient and separation. Can be used for transitional flows. Separation is typically predicted to be excessive.
SST k-ω	Offers similar benefits as standard k-ω. Dependency on wall distance makes this less suitable for free shear flows.
Reynolds Stress	Physically the most sound RANS model. Avoids isotropic eddy viscosity. More CPU time and memory required. Harder to converge due to close coupling of equations. Suitable for complex 3D flows with strong streamline curvature, strong swirl/rotation.

Table. 2.3 Turbulence model behavior and usage [73]

2.3.1 *k-ε* Turbulence Model

The simplest "complete models" of turbulence are two-equation models in which the solution of two separate transport equations allows the turbulent velocity and length scales to be independently determined. Due to its robustness, economy, and reasonable accuracy for a wide range of turbulent flows, the *k-ε* turbulence model it is gaining popularity in industrial flow and heat transfer simulations. This approach it's semi-empirical, and the derivation of the model equations relies on experimental considerations and empiricism.

The k - ε model used, is a semi-empirical model based on model transport equations for the turbulence kinetic energy (k) and its dissipation rate (ε). The model transport equation for k is derived from the exact equation, whereas the model transport equation for ε was obtained using physical logic and does not have much resemblance to its mathematically exact counterpart.

In the derivation of the k- ε model, the supposition is that the flow is fully turbulent, and the effects of molecular viscosity are negligible. The standard k- ε model is therefore valid only for fully turbulent flows.

The turbulence kinetic energy, k, and its rate of dissipation,ε, are obtained from the following transport equations:

$$\frac{\partial}{\partial t}(\rho k) + \frac{\partial}{\partial x_i}(\rho k u_i) = \frac{\partial}{\partial x_j}\left[\left(\mu + \frac{\mu_t}{\sigma_k}\right)\frac{\partial k}{\partial x_j}\right] + G_k + G_b - \rho\varepsilon - Y_M + S_k \qquad (2.18)$$

$$\frac{\partial}{\partial t}(\rho \varepsilon) + \frac{\partial}{\partial x_i}(\rho \varepsilon u_i) = \frac{\partial}{\partial x_j}\left[\left(\mu + \frac{\mu_t}{\sigma_\varepsilon}\right)\frac{\partial \varepsilon}{\partial x_j}\right] + C_{1\varepsilon}\frac{\varepsilon}{k}(G_k + C_{3\varepsilon}G_b) - C_{2\varepsilon}\rho\frac{\varepsilon^2}{k} + S_\varepsilon \qquad (2.19)$$

in these equations, G_k represents the generation of turbulence kinetic energy due to the mean velocity gradients, G_b is the generation of turbulence kinetic energy due to buoyancy, Y_M represents the contribution of the fluctuating dilatation in compressible turbulence to the overall dissipation rate. $C_{1\varepsilon}$, $C_{2\varepsilon}$, and $C_{3\varepsilon}$ are constants. σ_k and σ_ε are the turbulent Prandtl numbers for k and ε , respectively. S_k and S_ε are user-defined source terms.

The turbulent viscosity, μ_t, is computed by combining k and ε in the following way:

$$\mu_t = \rho C_\mu \frac{k^2}{\varepsilon} \quad (2.20)$$

where C_μ is a constant.

The term G_k , represents the production of turbulence kinetic energy, and from the exact equation for the transport of k, this term may be understood as:

$$G_k = -\rho \overline{u_i' u_j'} \frac{\partial u_j}{\partial x_i} \quad (2.21)$$

To evaluate G_k in a manner consistent with the Boussinesq hypothesis,

$$G_k = \mu_t S^2 \quad (2.22)$$

where S is the modulus of the mean rate-of-strain tensor, and is defined as:

$$S = \sqrt{2 S_{ij} S_{ij}} \quad (2.23)$$

When a non-zero gravity field and temperature gradient are present simultaneously, the k-ε models accounts for the generation of k due to buoyancy. For ideal gases such as the ones that are going to be subject of future study, the generation of turbulence due to buoyancy is given by:

$$G_b = -g_i \frac{\mu_t}{\rho Pr_t} \frac{\partial T}{\partial x_i} \quad (2.24)$$

where Pr_t is the Prandatl number for energy and g_i is the component of the gravitational vector in the *ith* direction. The default value for the Prandatl number of energy is 0.85.

It is clear from the transport equations for k (Equation (2.18)) that turbulence kinetic energy tends to be augmented ($G_b > 0$) in unstable stratification.

Turbulent heat transport is modeled using the concept of Reynolds' analogy to turbulent momentum transfer. The "modeled" energy equation is thus given by the following:

$$\frac{\partial}{\partial t}(\rho E) + \frac{\partial}{\partial x_i}[u_i(\rho E + p)] = \frac{\partial}{\partial x_j}\left(k_{eff}\frac{\partial T}{\partial x_j} + u_i(\tau_{ij})_{eff}\right) + S_h \quad (2.25)$$

where E is the total energy, k_{eff} is the effective thermal conductivity, and $(\tau_{ij})_{eff}$ is the derivatoric stress tensor, defined as,

$$(\tau_{ij})_{eff} = \mu_{eff}\left(\frac{\partial u_j}{\partial x_i} + \frac{\partial u_i}{\partial x_j}\right) - \frac{2}{3}\mu_{eff}\frac{\partial u_k}{\partial x_k}\delta_{ij} \quad (2.26)$$

and the effective thermal conductivity is denoted by:

$$k_{eff} = k + \frac{C_p\mu_t}{Pr_t} \quad (2.27)$$

where k is the thermal conductivity and the value of the Prandtl number is 0.85.

2.3.2 k-ω Turbulence Model

The k-ω model is based on the Wilcox k-ω model [75], which incorporates modifications for low-Reynolds-number effects, compressibility, and shear flow spreading. The Wilcox model predicts free shear flow spreading rates that are in close agreement with measurements for far wakes, mixing layers, and plane, round, and radial jets, and is thus applicable to wall-bounded flows and free shear flows. It is an empirical

model based on model transport equations for the turbulence kinetic energy (k) and the specific dissipation rate (ω), which can also be thought as the ratio of ε to k.

The turbulence kinetic energy and the specific dissipation rate are obtained from the transport equations:

$$\frac{\partial}{\partial x}(\rho k) + \frac{\partial}{\partial x}(\rho k u_i) = \frac{\partial}{\partial x_j}\left(\Gamma_k \frac{\partial k}{\partial x_j}\right) + G_k - Y_k + S_k \qquad (2.28)$$

$$\frac{\partial}{\partial x}(\rho \omega) + \frac{\partial}{\partial x}(\rho \omega u_i) = \frac{\partial}{\partial x_j}\left(\Gamma_\omega \frac{\partial \omega}{\partial x_j}\right) + G_\omega - Y_\omega + S_\omega \qquad (2.29)$$

In these equations, G_k, represents the generation of turbulence kinetic energy due to mean velocity gradients. G_ω represents the generation of ω. Γ_k and Γ_ω represent the effective diffusivity of k and ω, respectively. Y_k and Y_ω represent the dissipation of k and ω due to turbulence.

The effective diffusivities for the k-w model are given by:

$$\Gamma_k = \mu + \frac{\mu_t}{\sigma_k} \qquad (2.30)$$

$$\Gamma_\omega = \mu + \frac{\mu_t}{\sigma_\omega} \qquad (2.31)$$

where σ_k and σ_ω are the turbulent Prandtl numbers for k and w, respectively and μ_t is the turbulent viscosity.

In equation (2.28) the term G_k represents the production of turbulence kinetic energy. From the exact equation for the transport of k this term may be defined as

$$G_k = -\rho\overline{u_i' u_j'}\frac{\partial u_j}{\partial x_i} \qquad (2.32)$$

and the production of w is given by:

$$G_\omega = \alpha\frac{\omega}{k}G_k \qquad (2.33)$$

2.3.3 Large Eddy Simulation Model

Turbulent flows are characterized by eddies with a wide range of length and time scales. The largest eddies are typically comparable in size to the characteristic length of the mean flow. The smallest scales are responsible for the dissipation of turbulence kinetic energy.

The rationale behind LES can be summarized as follows

- Momentum, mass, energy, and other passive scalars are transported mostly by large eddies.
- Large eddies are more problem-dependent. They are dictated by the geometries and boundary conditions of the flow involved.
- Small eddies are less dependent on the geometry, tend to be more isotropic, and are consequently more universal.
- The chance of finding a universal turbulence model is much higher for small eddies.

The governing equations employed for LES are obtained by filtering the time-dependent Navier-Stokes equations in either Fourier space or configuration space. The filtering process successfully filters out the eddies whose scales are smaller than the filter

width or grid spacing used in the computations. The resulting equations thus govern the dynamics of large eddies.

A filtered variable is defined by

$$\overline{\emptyset}(x) = \int_D \emptyset(x')G(x,x')dx' \qquad (2.34)$$

where D is the fluid domain and G is the filtered function that determines the size of the computed eddies.

The finite-volume discretization itself implicitly provides the filtering operation:

$$\overline{\emptyset}(x) = \frac{1}{V}\int_v \emptyset(x')dx', \quad x' \in V \qquad (2.35)$$

where V is the volume of a computational cell. The filter function, $G(x,x')$ mentioned here is then

$$G(x,x') = \begin{cases} \frac{1}{V}, & x' \in V \\ 0, & x' \in otherwise \end{cases} \qquad (2.36)$$

Filtering the Navier-Strokes equations we can get the following relations:

$$\frac{\partial \rho}{\partial t} + \frac{\partial}{\partial x_i}(\rho \overline{u_i}) = 0 \qquad (2.37)$$

$$\frac{\partial}{\partial t}(\rho \overline{u_i}) + \frac{\partial}{\partial x_j}(\rho \overline{u_i}\overline{u_j}) = \frac{\partial}{\partial x_j}\left(\mu \frac{\partial \sigma_{ij}}{\partial x_j}\right) - \frac{\partial \bar{p}}{\partial x_i} - \frac{\partial \tau_{ij}}{\partial x_j} \qquad (2.38)$$

where σ_{ij} is the stress tensor due to molecular viscosity and it can be defined as

$$\sigma_{ij} \equiv \left[\mu\left(\frac{\partial \overline{u_i}}{\partial x_j} + \frac{\partial \overline{u_j}}{\partial x_j}\right)\right] - \frac{2}{3}\mu \frac{\partial \overline{u_l}}{\partial x_l}\delta_{ij} \qquad (2.39)$$

and τ_{ij} is the subgrid-scale stress defined by,

$$\tau_{ij} = \rho\overline{u_i u_j} - \rho\overline{u}_i\overline{u}_j \qquad (2.40)$$

The subgrid-scale stresses resulting from the filtering operation are unknown, and require modeling. The subgrid-scale turbulence models employ the Boussinesq hypothesis from,

$$\tau_{ij} - \frac{1}{3}\tau_{kk}\delta_{ij} = -2\mu_t\overline{S_{ij}} \qquad (2.41)$$

where μ_t is the subgrid-scale turbulent viscosity. The isotropic part of the subgrid-scale stresses τ_{kk} is not modeled, but aggregated to the filtered static pressure term. $\overline{S_{ij}}$ is the rate-of-strain tensor for the resolved scale and it's defined by,

$$\overline{S_{ij}} \equiv \frac{1}{2}\left(\frac{\partial\overline{u_i}}{\partial x_j} + \frac{\partial\overline{u_j}}{\partial x_i}\right) \qquad (2.42)$$

In order to resolve for μ_t the Smagorinski-Lilly model is employed where the eddy-viscosity is modeled by:

$$\mu_t = \rho L_s^2|\bar{S}| \qquad (2.43)$$

where L_s is the mixing length for subgrid scales and $|\bar{S}| \equiv \sqrt{2\overline{S_{ij}S_{ij}}}$ and for FLUENT $L_s = \min\left(kd, C_s V^{\frac{1}{3}}\right)$ where k is the Von Káramán constant, d is the distance to the closest wall, C_s is the Smagorinski constant (0.17) and V is the volume of the computational cell.

For the ongoing cases to be studied in subsequent chapters, The stochastic components of the flow at the velocity-specified inlet boundaries are neglected. Individual instantaneous velocity components are simply set equal to their mean velocity counterparts.

LES is an approach in which large eddies are explicitly resolved in a time-dependent simulation using the "filtered" Navier-Stokes equations. The underlying principle behind LES is that by modeling less of turbulence, the error introduced by turbulence modeling can be reduced. It is also believed to be easier to find a "universal" model for the small scales, since they tend to be more isotropic and less affected by the macroscopic features like boundary conditions, than the large eddies.

Filtering is essentially a mathematical manipulation of the exact Navier-Stokes equations to remove the eddies that are smaller than the size of the filter, which is usually taken as the mesh size when spatial filtering is employed as in FLUENT. The filtering process creates additional unknown terms that must be modeled to achieve closure.

All these characteristics that were discussed above are going to serve us to perform future simulations in this work. Both turbulence methods are going to be used in order to outline similarities and differences between them as well as to understand the effect of turbulence in the combustion process. The correct understanding of how to define turbulence and boundary conditions are a key element in the success of numerical simulations in combustion processes and in engineering simulation in general.

Chapter 3

NUMERICAL ANALISYS OF THE EFFECT OF INJECTION ON THE TURBULENT MIXING QUALITY IN A SIMPLE COMBUSTOR

3.1 Introduction

The design and development of combustion equipment are crucial areas in power engineering. A better understanding of the combustion mechanism in industrial furnaces (enclosures that receive energy from a combustion flame or from another process) and propulsion systems such as gas turbine has always been of great importance in engineering-related fields. The effect of turbulent mixing and resulting diffusion flames that may occur in these kinds of systems are one of the most challenging topics.

Combustion of fossil fuels is the main energy source in industrial, domestic and transportation applications. Nowadays there is an increasing knowledge of the limited supply of fuels and due to the importance that they have in modern society a lot of effort has been made toward the development of alternative energy sources being the design of the engineering systems one of the most critical areas of development. As it was mentioned before, there exist currently several methods to achieve better energy efficiency [76], yet an important effort has to be made in the design of combustion systems since is one of the most important methods.

With the increasing environmental concerns there is another important incentive to have more efficient combustion systems, which is the reduction of pollutants emission. If complete combustion is not achieved not only low combustion efficiency is going to be present but high pollutant formation is going to be formed since unburned fuel is considered to be a pollutant. Therefore a very useful manner to describe the burner performance is trough combustion efficiency (completeness of combustion).

There are several methods to define completeness of combustion such as the residence time and the swirl number but one very useful criterion to define this concept is by measuring the percentage of carbon monoxide in the combustion products [77] observing that there is a relation between fuel wasted and combustion efficiency as indicated in Figure 3.1. This efficiency is a good indicator of furnace performance and will be used in this chapter.

As the combustion completeness increases the combustion efficiency increases as well and less pollutant formation is observed. Nevertheless, most efficient combustion is achieved at high temperatures that are favorable to the formation of nitrogen oxides. Therefore, there is a compromise to be made, either to reduce the nitrogen oxides formation by working with lower temperatures and less combustion efficiency or having higher temperatures but more pollutant formation.

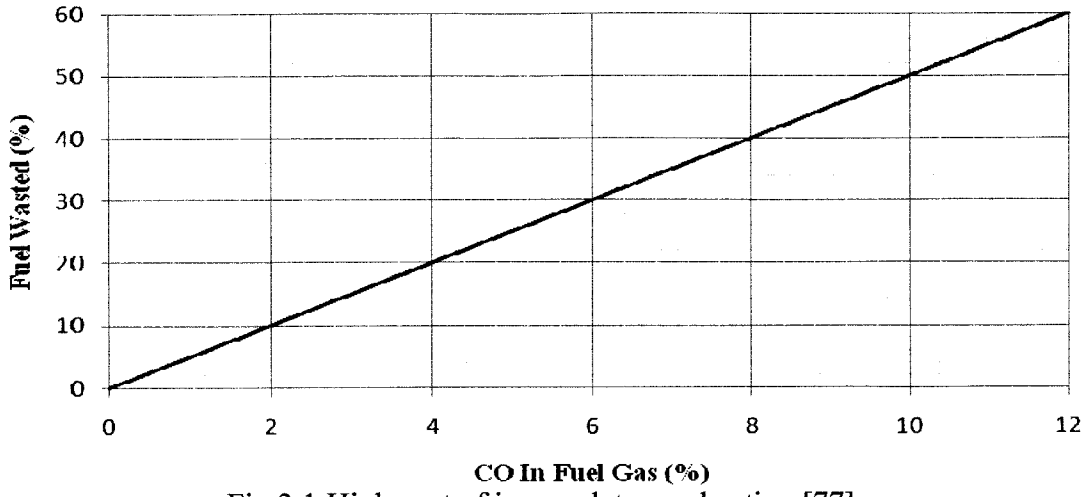

Fig 3.1 High cost of incomplete combustion [77].

In the past, advances in the development of industrial combustion devices had been slow due mainly to the economical factors involved in building costly models and prototypes and the elevated cost of gathering real testing data. Computational techniques are now available for the prediction of turbulent reacting flows in furnaces of arbitrary geometry [78]. It provides not only the fundamental understanding of the turbulent mixing and turbulence in unsteady flows, but also a useful tool for engineering design.

Several studies [79-83] have been performed with regard to the development of mathematical and numerical modeling for turbulent reacting flows. These studies were motivated by the need of a better understanding of combustion mechanisms in industrial applications such as gas-turbines, ramjet combustors and space shuttle engines. The prediction of the combustor flowfield is desirable not only for understanding and interpreting experimental data but also for engineering design optimization.

Computational techniques contain physical models for turbulence and chemical reactions which require verification either by previous experimental data or by

predictions based on experimental data. There exists in the literature some experimental data for the analysis of turbulent mixing in traditional industrial combustors [61, 62, 83]. This thesis seeks to acquire the results of the numerical simulation of these reference cases and then validate them with experimental data to further analyze other parameters that would influence the combustor efficiency. Numerical issues regarding this type of simulation such as the effect of grid arrangement, boundary conditions and turbulence models will be addressed and discussed. The final goal of this thesis is to investigate computationally the effect of injection geometry and to design an improved configuration for high turbulent mixing quality and combustion efficiency inside the combustor taking into consideration pollution formation.

3.2 Experimental Data

In the present study, the experimental data gather by Lockwood [62] is selected for validation of the numerical simulations; moreover, the study made by Kim and Chung [61] is used to compare the accuracy of the numerical simulations results with a similar study that utilized the finite element analysis approach. The experiment setup by Lockwood is described as a cylindrical furnace, axially fired with natural gas from a concentric tube burner. It consists of a cylindrical combustion chamber with 0.21 m in internal diameter by 1.9 m in length. A double concentric-tube jet burner was secured, axially aligned to one end of the chamber. As for the burner, the annular air delivery tube has an inner and outer diameter of 0.044 m and 0.078 m, respectively. The diameter of the fuel delivery tube was 0.0195 m. The simulated combustor chamber geometry schematic and inlet conditions, as well as the full 2D grid created for the simulation is

shown in Figure 3.2 and Table 3.1. Town gas was used as the fuel and air was used as the oxidizer. The composition and relevant properties of the town-gas fuel are given in Table 3.2. The burner fuel pipe and air annulus were made 0.7 m in length to provide fully developed and settled flow at the burner exit plane.

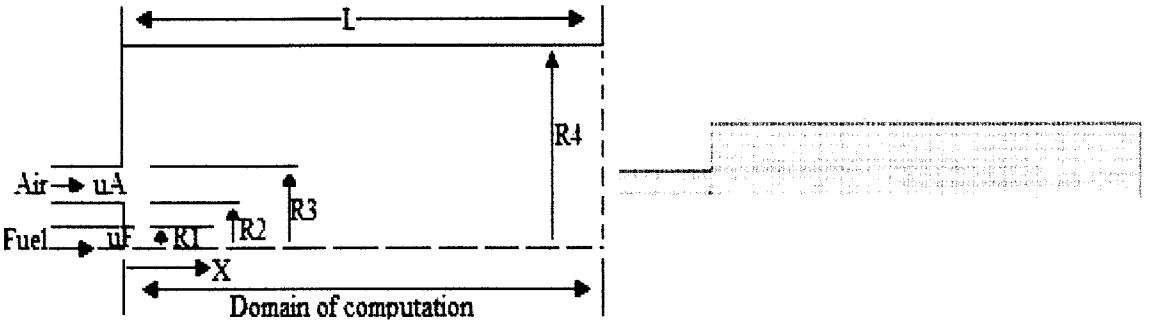

Fig 3.2 Combustion chamber geometry created for the simulation

Inlet fuel velocity (m/s)	21.92
Inlet air velocity (m/s)	14.94
Fuel side inner radius R_1 (m)	0.0095
Fuel side outer radius R_2 (m)	0.022
Air side inner radius R_3 (m)	0.039
Outlet radius R_4 (m)	0.105
Combustor length L (m)	1.9

Table 3.1 Inlet conditions for the simulation

CH_4	27%
CO_2	8%
N_2	4%
H_2	55%
CO	4%
C_2H_6	2%
Calorific Value	2.63×10^4 kJ / kg
Stoichiometric air-fuel ratio by mass	10.59
Molecular Weight	25.8

Table 3.2 Town gas composition and properties

3.3 Numerical Simulation Approach

The furnace dimensions are small enough to eliminate significant radiation effects but large enough to ensure that the flow was fully turbulent. The problem is simulated two-dimensionally first, just half of the actual cylindrical combustor. Three-dimensional simulations are then presented for both a very coarse and a fine mesh to demonstrate the importance of the grid arrangement. When the 2D and 3D results show a satisfactory agreement with the experimental data from [62], five different inlet geometries will be investigated in order to achieve a better configuration for high turbulent mixing quality and combustion efficiency inside the combustor.

In more numerical details, for the two-dimensional case an axisymmetric geometry was chosen so only half of the combustor was modeled. The resulting mesh of

that simulation consists of 58,800 quadrilateral cells with a constant grid arrangement, for the half 2D slice of the combustor. For the three dimensional case, as the inlets are concentric it is only necessary to perform a simulation on a quarter of the total volume. The resulting meshing for the quarter of the three-dimensional model consisted of 45,125 hexahedral cells; this cell size was proven to be enough for the present problem. For the case were a very coarse mesh was employed the model consisted of 18,875 hexahedral cells. For the cases were an improved configuration of the combustor is studied, one axisymmetrical geometry and four three dimensional are selected.

Turbulence is first represented by the k-ε model, which provides an optimal choice between accuracy and economy for most turbulent reacting flows. As discussed in chapter 2, the k-ε turbulence model uses an equation for the turbulent kinetic energy which can be derived like a conservation equation. However this model depends on the geometry and on the nature of the problem considered. Despite its shortcomings this model is in wide use because it represents significant savings in computational resources.

There are three parameters which are important, the Schmidt number, the Rich Flammability Limit (RFL), and the Turbulence Intensity. The effect of the Schmidt number and the turbulence intensity in the quality of the mixing in the combustor is going to be discussed later on in this study. To validate the numerical simulation with the experimental data, these three parameters values are tabulated in Table 3.3.

Schmidt Number	0.15
Rich Flammability Limit	0.10
Air inlet Turbulence Intensity	7
Fuel inlet Turbulence Intensity	4
Outlet Turbulence Intensity	5

Table 3.3 Schmidt Number, RFL and turbulence intensity values for the Lockwood combustor

The Schmidt number is a dimensionless number defined as the ratio of momentum diffusivity (turbulent viscosity) and mass diffusivity (turbulent diffusivity), and is used to characterize fluid flows in which there are simultaneous momentum and mass diffusion convection processes. When doing the simulation the FLUENT default value of the Schimidt number was adjusted due to attain better convergence.

A mixture that has less than a critical amount of fuel, known as the Lean or Lower Flammability Limit (LFL), or greater than a critical amount of fuel, known as the Rich or upper Flammability Limit (RFL), will not be flammable. To work with the assumption made in [62] of chemical equilibrium throughout the flow, and according to the way to input the RFL in FLUENT the value to be used for this parameter is 0.1. The Turbulence Intensity is defined as the ratio of the root-mean-square of the velocity fluctuations to the mean flow velocity; in general it is a quantity that characterizes the intensity of gusts in

the airflow. As mention earlier, the effect of the Schmidt number and the turbulence intensity parameters in the quality of the mixing will be analyzed later.

Density and viscosity values are calculated from the ideal gas law and from the fluids characteristics provided in [62]. According to this ideal gas assumption the temperatures for the air and town gas are 335K and 300K, respectively.

3.4 Results and Discussion

For comparison and validation, the previous work done by [62] and by [61] is used as a reference of validation for the numerical simulation. The way of comparison of the simulations is through the axial profiles of the mixture fraction. From Kim and Chung it is shown that the predicted values of the mixture fraction have the same qualitative trends as the experimental data.

We must be careful when comparing both profiles as those from Kim and Chung uses a normalized distance x/D on the horizontal axis, where the profile generated during the simulation uses the distance from the burner x. Therefore a comparison between the mixture fractions measured in [62], predicted in [61] and the present 2D simulation is shown in Figure 3.3, having the distance from the burner as the reference frame. We notice that the values or profile obtained for the 2D numerical simulation for the mixture fraction have the same qualitative trends as in [62] and [61] data, and show a very good agreement after 0.3m with respect to Lockwood experimental data. It can be seen that, close to the inlet where the velocity gradient in both the axial and radial distributions are

steep, the experimental measurements exhibit a faster decay rate than do the numerical simulations.

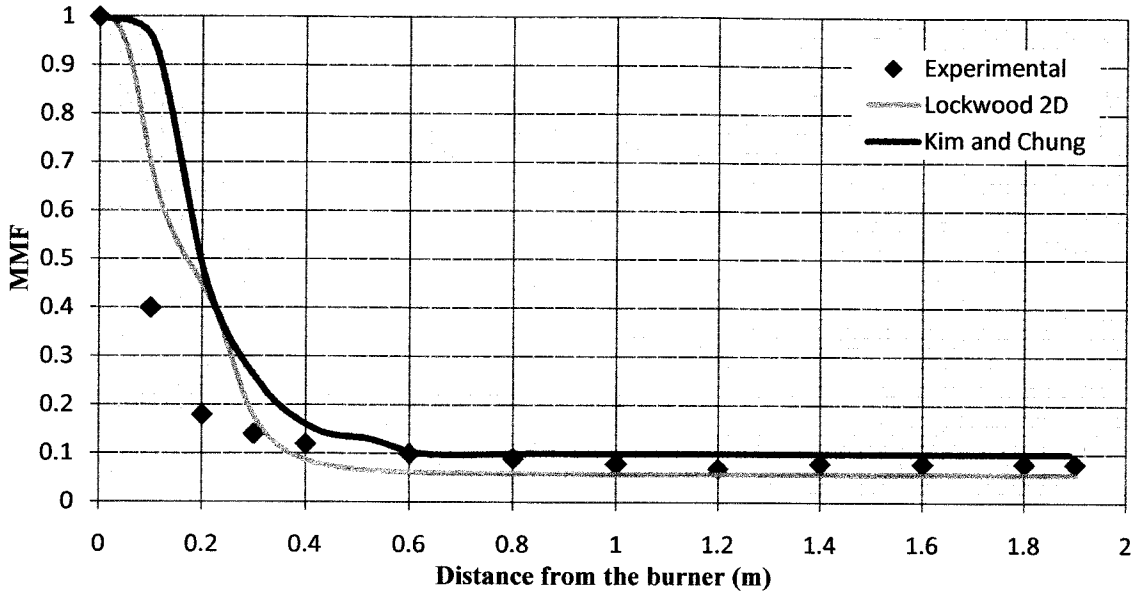

Fig 3.3 Axial variation of mixture fraction in a turbulent diffusion flame for the 2D case

Equivalent simulations were performed, however with a three-dimensional geometry. Only a quarter of the full geometry is used in the simulations. Special attention was required in order to simulate accurately all boundary conditions in order to get a physical result. Two different simulations are performed on the three-dimensional geometry, the first one with a coarse cell number and the second with a much finer mesh cell number. The goal of this section is first to validate the numerical simulation with the experimental data as done previously with the 2D case to validate the use of this type of geometry in future analysis. Also the realization of simulations for two kinds of meshes aims to demonstrate the importance of the grid arrangement.

Again, the way of comparison of the simulations is through the axial profiles of the mixture fraction. These values or profiles will then be compared with the values generated in the numerical simulation in the 3D fine mesh case (the coarse mesh case will be discussed later). Once more, we must be careful when comparing both profiles with those from Kim and Chung because the normalized distance *x/D* on the horizontal axis. Therefore a comparison between the mixture fractions measured in [62], predicted in [61] and the present 3D fine mesh simulation is shown in Figure 3.4. It is notice that the values or profile obtained for the 3D numerical simulation for the mixture fraction have the same qualitative trends as in [62] and [61] data, and show a very good agreement after 0.5m with respect to Lockwood experimental data. Similar trend as in the 2D case was observed.

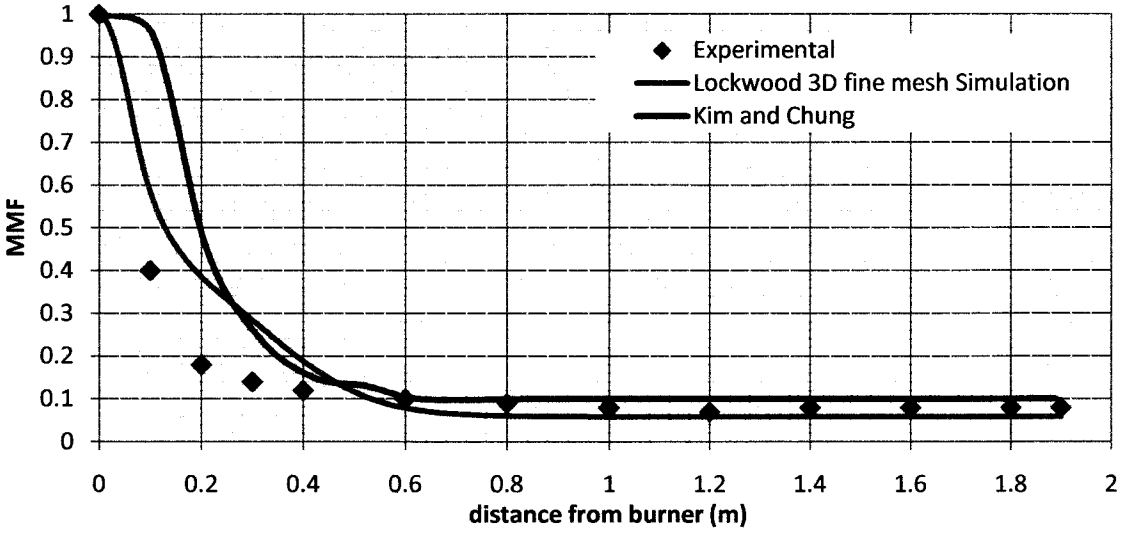

Fig 3.4 Axial variation of mixture fraction in a turbulent diffusion flame for the 3D case

In order to assess the effect of the meshing in the quality of the mixing, the 3D case is simulated with a coarse cell number. The grid for the simulation with the coarse mesh consists of 18,875 hexahedral cells.

The MMF profile along the center axis of the 3D combustor is shown is Figure 3.5. It can be clearly seen that the simulations results have the same qualitative trend as per the 3D case, 2D case and experimental results; nevertheless the rate of decay at the inlet is slower for this case as it is for the standard 2D case. It is also shown that an agreement is reached after 0.5m with respect to Lockwood experimental data, this value being the same than the ones demonstrated in the other cases concludes that for the 3D case there is not much impact on the results with the refinement of the mesh, this is positive because major computational time can be saved if the coarse mesh approach is used in this particular case.

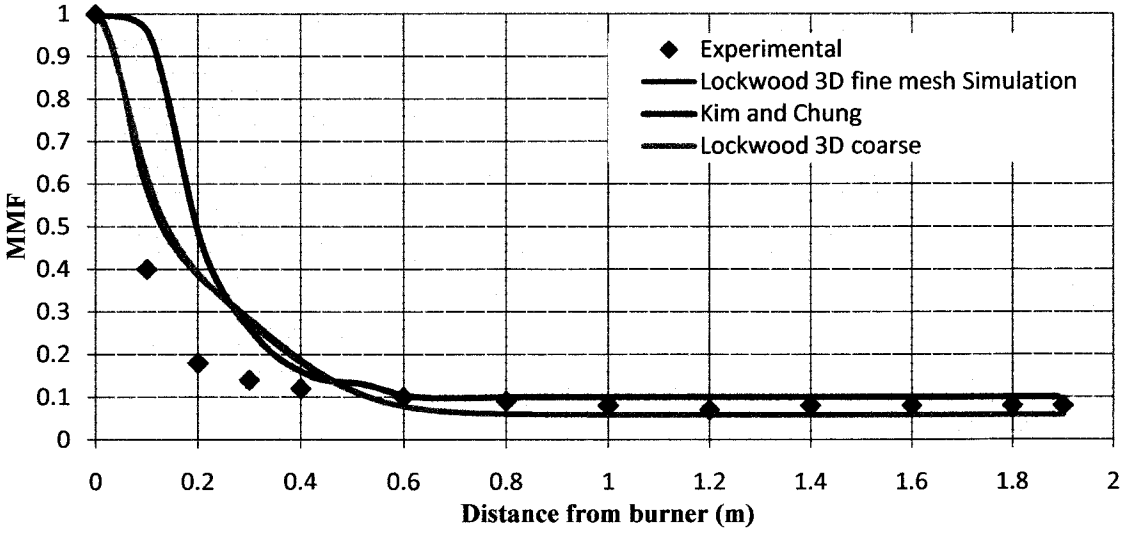

Fig 3.5 Three dimensional coarse mesh MMF profile along the center axis

As mentioned earlier, there are three important parameters affecting the quality of the mixing of a simple combustor: the Schmidt number, the Rich Flammability Limit

(RFL), and the Turbulence Intensity. The effect of the Schmidt number and the turbulence intensity parameters is going to be studied in the proceeding section. The effect of the RFL is not going to be modeled in order to have similarity with [62] where it is assumed that chemical equilibrium prevails throughout the flow. Because of this the value of the RFL = 0.1 in all the simulations, nevertheless, it is recognized that it is an important parameter in the quality of the burning process and temperature distribution of a simple combustor. In order to assess the importance of these quantities the simple 2D combustor configuration was chosen.

The different values for the Schmidt number and the turbulence intensity are depicted in Table 3.4.

Schmidt Number	Turbulence Intensity on air inlet
0.3	4%
0.8	10%
	17%

Table 3.4 Different values for Schimidt number and turbulence intensity on air inlet for a 2D simulation of a simple combustor

For the variation in the Schmidt number the comparison between the two proposed Schmidt numbers cases and the standard 2D Lockwood simulation (Schmidt number = 0.15) and the experimental data is shown in Figure3.6. It can be clearly seen that these two cases have the same qualitative trend than the previous seen cases;

however, it is clear that as the Schmidt number increases the rate of decay at the inlet decreases as well, showing an important deviation from the original experimental data, this is due to the increase in turbulent viscosity originated by the raise in the Schmidt number. It is also shown that an agreement is reached after 0.8 and 1.4 m for the 0.3 and 0.8 cases respectively, with respect to Lockwood experimental data. It is proven then, that an increase in the Schmidt number is not desirable to get simulations that are close enough to the experimental data.

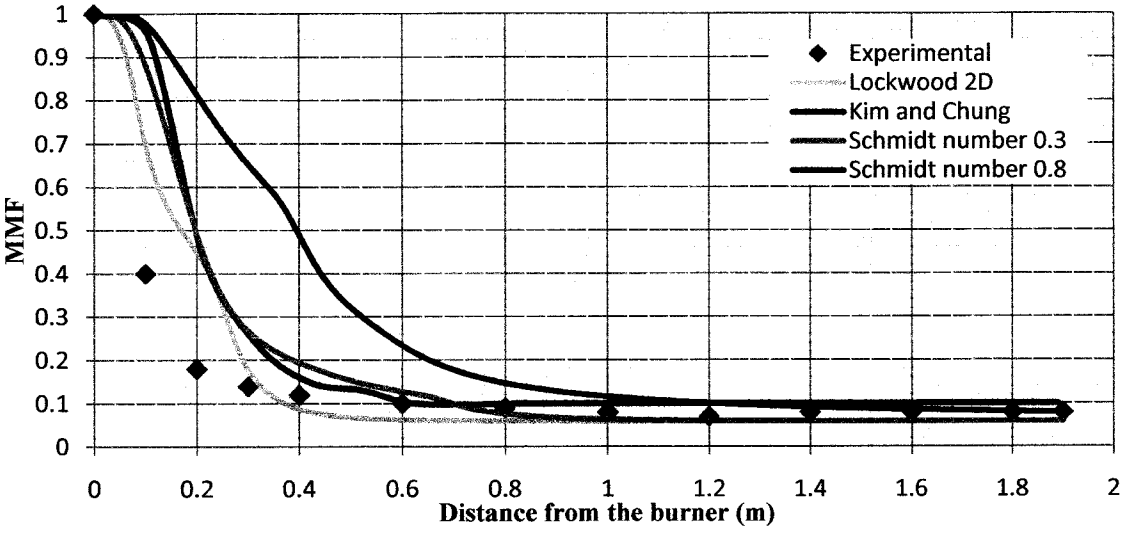

Fig 3.6 MMF comparisons for various values of Schmidt number

For the variation in the turbulence intensity the comparison between the three proposed turbulent intensity numbers cases and the standard 2D Lockwood simulation (turbulence intensity = 4%) and the experimental data is shown in Figure 3.7. One can see that these three cases have the same qualitative trend as the previous cases; however, it is clear that as the value of the turbulent intensity increases, the rate of decay is higher. The 17% turbulence intensity case is in agreement with the experimental data. It is also

shown that an agreement is reached after 0.2 and 0.5 m for the 17% and 10% and 4% cases respectively, with respect to Lockwood experimental data.

Another important parameter to analyze is the effect of the turbulence model on the turbulent mixing of the combustor. As explained before, all the previous simulations are done using the k-ε turbulent model and the results show very good qualitative agreement. Nevertheless, another approach is also considered here in order to compare the effect of a change in the turbulence model approach with respect to the experimental data. The model proposed for these new simulations is the Large Eddy Simulation approach (LES).

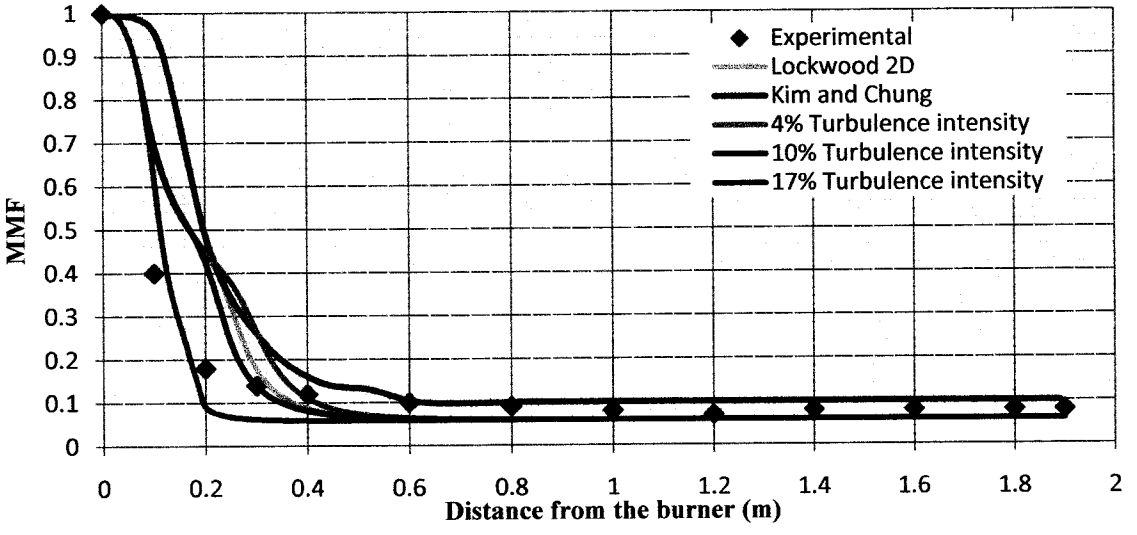

Fig 3.7 Turbulence Intensity comparisons for various values of Schmidt number.

Large eddies continuously undergo dissipation cascade becoming multiple eddies at small scale. The large scales are generated as a consequence of multiple factors such as viscous shear of the fluid and geometric constraints. As one examines eddies scales from largest to smallest, the smaller scales become more and more geometry-independent. It is

widely believed that at some small scale, imbedded inside of the flow, the turbulence can be described by an isotropic model. This indicates a filter scale or grid scale below which the flow is isotropic and above which the flow is problem-specific. With LES, the filter scale is between the largest and the Kolmogorov scale. Above this filter scale, one solves the Navier Strokes Equations; below this scale, turbulence models are used [84].

The underlying principle behind LES is that by modeling less of turbulence, the error introduced by turbulence modeling can be reduced. Filtering is essentially a mathematical manipulation of the exact Navier-Stokes equations to remove the eddies that are smaller than the size of the filter, which is usually taken as the mesh size when spatial filtering is employed as in FLUENT. The filtering process creates additional unknown terms that must be modeled to achieve closure.

The MMF contour along the center axis for the LES simulation is shown in Figure 3.8. Again it can be said that the LES simulation keeps a very good qualitative agreement with respect with the experimental data and a very similar behavior in comparison with the k-ε method. There is a zone between 0.2 and 0.6 m where the MMF for the LES method shows a better behavior than the k-ε and closer to the experimental data because of the filtering process and the size of the eddies in that recirculation area.

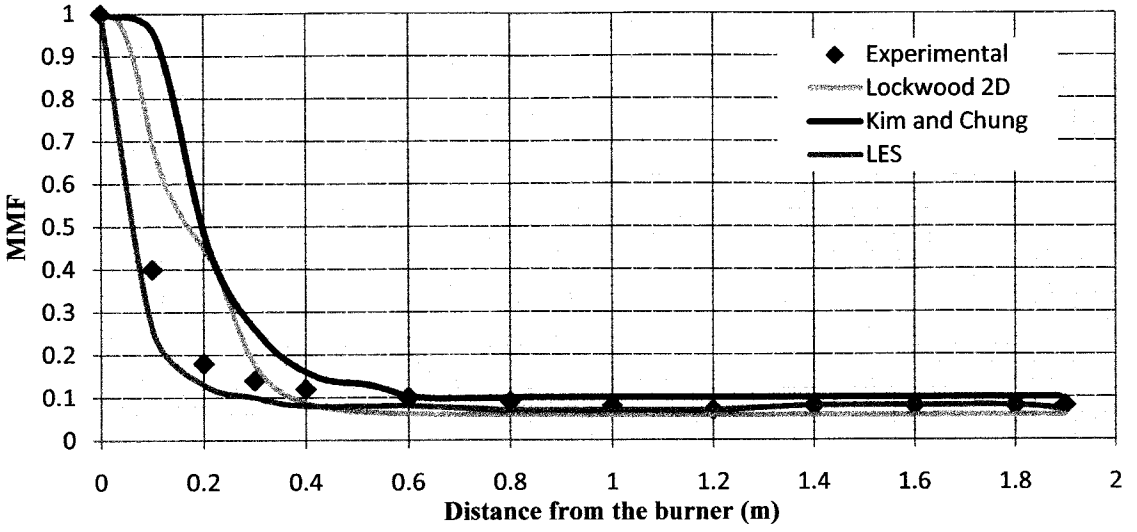

Fig 3.8 MMF profile along the centerline using LES turbulent model

It can be seen that for the LES method the rate of decay in the first part of the combustor is faster than in the traditional k-ε method and faster than the experimental data. It is important to say that the Schmidt number "tuning" was not necessary in LES which supports the idea that explicit computation of mixing at smaller scales, alleviates uncertainty in using the constant Schmidt number assumption. This indicates that isotropic eddy viscosity models whether used as k-ε method (RANS) for the main flow predictions or used as a simple algebraic model for sub-grid modeling, results in mixing that is under-predicted.

3.5 Effect of injection on the quality of the mixing of a simple combustor

As mentioned before, there are several methods to achieve better energy efficiency but still the most important method to achieve this is through the design of better combustion systems. Because of this, the effect of injection geometry to achieve better combustion efficiency will be analyzed. As the previous simulations are validated, the effect of changing the fuel and air inlet geometries is going to be analyzed. Four different geometries are compared to the 'traditional' Lockwood configuration. The first configuration proposed (Lockwood 2D) keeps the air and fuel inlet concentric, but the fuel inlet is elongated. The second configuration consists of setting the air inlet under a 30° angle and keeping the fuel inlet in its original position. A third configuration will assume a vertical air inlet in which two different distances from the combustor edge will be discussed. The last configuration proposed is to set both air and fuel inlet under a 30° angle and in opposite directions.

The first configuration will be simulated on a 2D approach basis to illustrate that this approach is acceptable as demonstrated in previous sections. The rest of the simulations will be done in 3D because its geometry allows a better visual representation of the results. The standard $k - \varepsilon$ turbulence model is chosen due to the savings in computational time. However, LES model will be used to analyze the case with the best performance. Among these new configurations the Schmidt number is 0.15 as in previous cases and all the other inlet conditions are kept the same to have a same frame of

reference for all the cases analyzed. Figure 3.9 shows the different proposed geometries for the simple combustor.

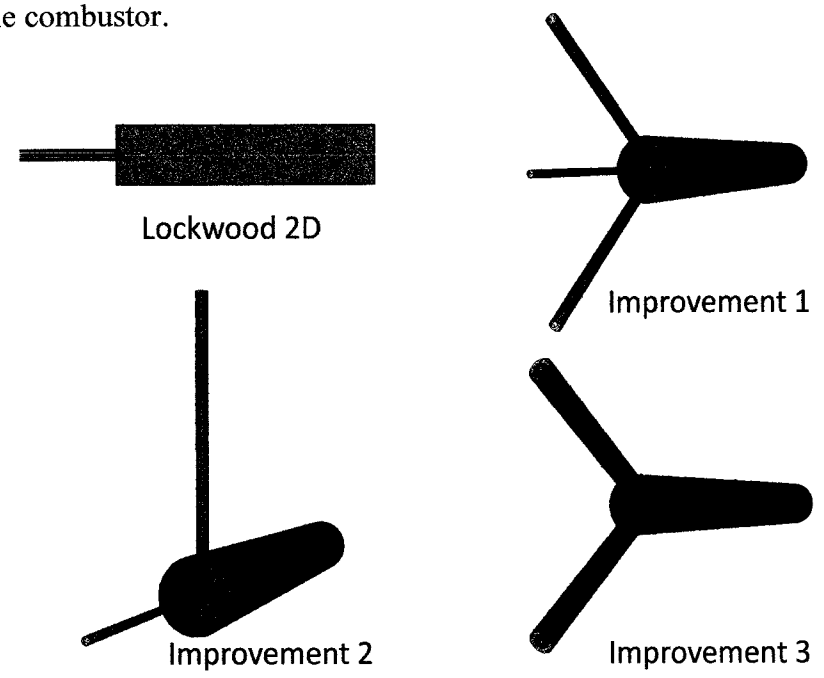

Fig 3.9 Different geometries proposed for the simple combustor: (a) fuel inlet elongated, (1) air inlet at an angle, (2) vertical air inlet, (3) fuel and air inlet at an angle

a) Fuel inlet elongated (Lockwood 2D)

In order to make an evaluation between this proposed geometry and previous cases the MMF and temperature will be used as a standard value of comparison.

The elongated fuel inlet configuration consists of the same concentric tubes as seen before but with the fuel inlet elongated by 5cm thus having a magnitude of 75 cm. The numerical model had 34709 quadrilateral cells and the simulation was performed only on the upper half of the combustor due to the symmetry, therefore being analyzed as axisymmetric.

The MMF contour along the centerline can be seen in Figure 3.10. It is clear that with this new geometry the rate of decay of the MMF is significantly slow in comparison with the experimental data and the 2D geometry resulting in an important over prediction of the mixing. It is interesting to note that only a small increment in the length of the fuel injector of 5 cm creates a big effect on the quality of the mixing, primary due to the shift of the recirculation zone. It can be seen that the results start showing an agreement after 1.2 m that is a higher value than the 0.4 acquired for the other simulations. This difference in the quality of the mixing is due to the fast expansion of the air at the inlet that makes the fuel stream not to have the same degree of mixing as in the previous case. Therefore it can be said that the implementation of this geometry change does not add any value or improvement to the quality of the mixing as it was expected.

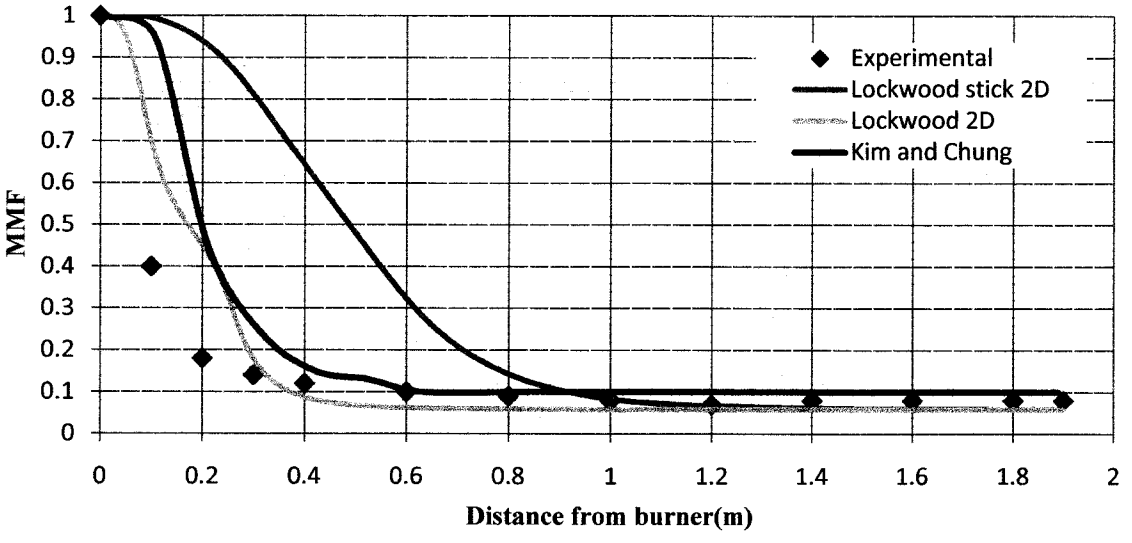

Fig 3.10 MMF distribution along the center axis for the "Fuel inlet elongated" configuration

Also, looking at the temperature distribution along the centerline shown in Figure 3.11 in comparison with the "traditional" 2D combustor and the experimental data it can be seen that the temperatures achieved throughout the combustor are not as high as the ones calculated in previous cases, making this another reason to account for the non-improvement in the mixing quality in this configuration.

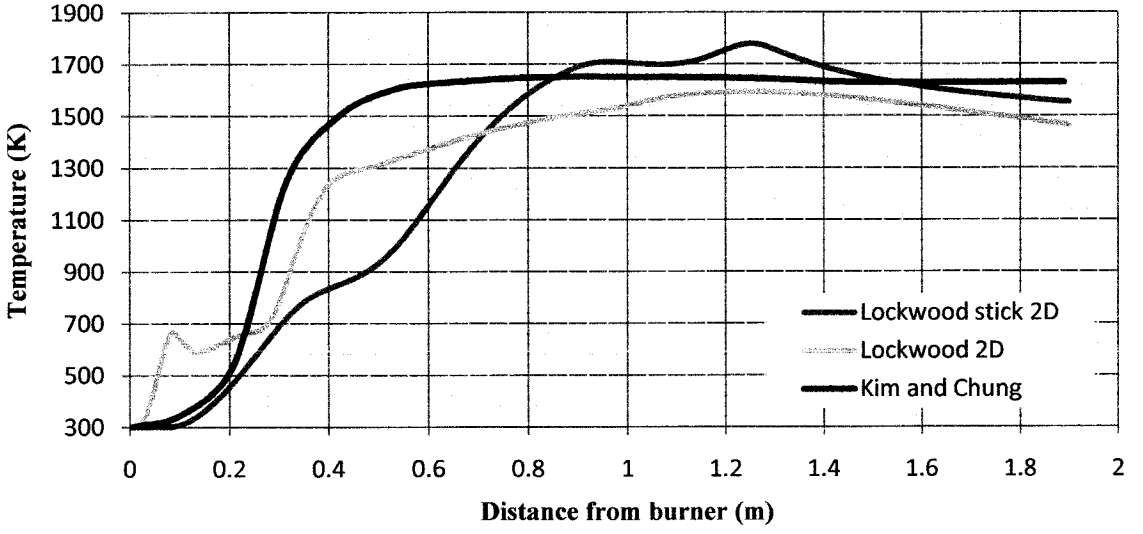

Fig 3.11 Temperature distribution along the center axis for the "Fuel inlet elongated" configuration

It is important to note here that the Schmidt number for this configuration has a very close agreement with a bigger Schmidt number simulation like the ones shown in Figure 3.6. Therefore, for this case the "tuning" of the Sc number seems to have little effect on the quality on the mixing because several simulations were performed with bigger Sc numbers (0.3, 0.5, and 0.8) and the MMF distribution remains very close in all of those cases.

b) Air inlet at a 30° angle

For this case the air inlet will be simulated as an annulus to maintain as much similarity as possible with respect to the previous simulations and experimental data. This

annulus will have an inclination of 30° while the fuel inlet will remain in the original position.

This model consists of 265,276 hexahedral cells and this number is considerably bigger than the "conventional 3D" case that would consist of 180,500 hexahedral cells considering the entire combustor geometry. This cell size was proven to be suitable for this problem and provides significant savings in computational time than a much smaller cell size without any loss in accuracy.

For this case one can see significant improvements in the quality of the mixing as shown in Figure 3.12. The rate of decay for the MMF for this case is faster than for the experimental data or the 3D case, thus providing a better mixing at the inlet. This trend is very similar to the one seen in the LES case and this can be due to the fact that the primary mixing happens at a very close distance to the inlet.

Also as shown in Figure 3.12, the MMF profiles reaches a stable value at 0.18 m, confirming that the mixing happens at a faster rate and closer to the inlet; additionally the results have a good qualitative agreement with previous data and an excellent agreement after 0.4 m. Because of the angle under which the air inlet are set, fuel and inlet get in contact faster and in a more efficient way that in the previous examined cases. This angle creates a better union between the molecules of the two reactants. Therefore, this is a good attempt to get a better mixing quality in the cylindrical combustor. It should be noticed as well that the final amount of fuel unburned in this configuration is a little bit higher in comparison with the "traditional 3D" combustor and the experimental data. This can lead to portions of CO at the end of the combustion process.

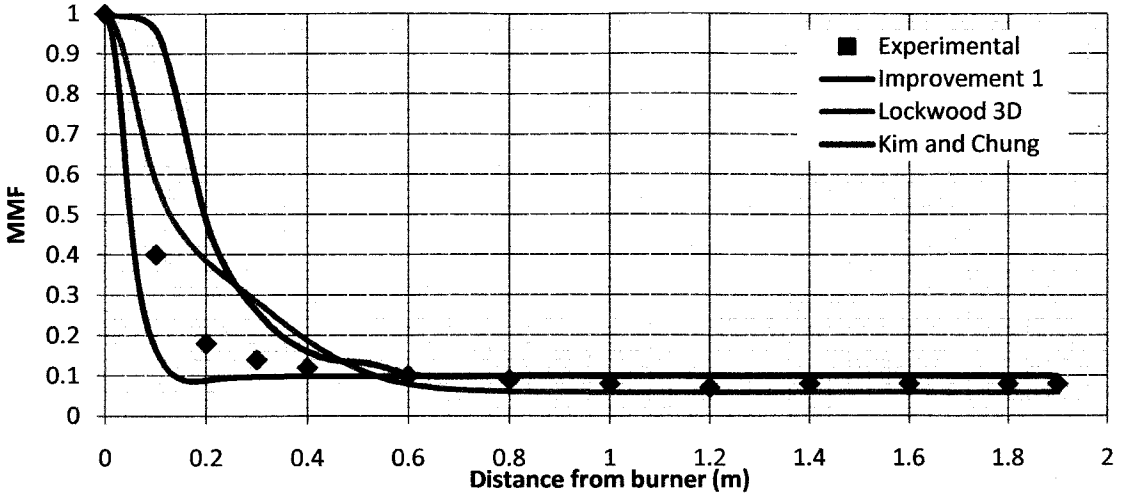

Fig 3.12 Mean Mixture Fraction distribution along the centerline for an "Air inlet under 30°" case

The temperature distribution shows that a higher temperature is to happen in the primary mixing zone because of all the burning process and the flame location. It can be seen in Figure 3.13 that in general higher temperatures are reached in this type of combustion, thus satisfying one of the aforementioned "T's of combustion". It is noticeable that at 0.2m from the burner (mixing zone) there is an increment of about 200% in the total temperature that after 0.8m finds agreement with the rest of the other configurations.

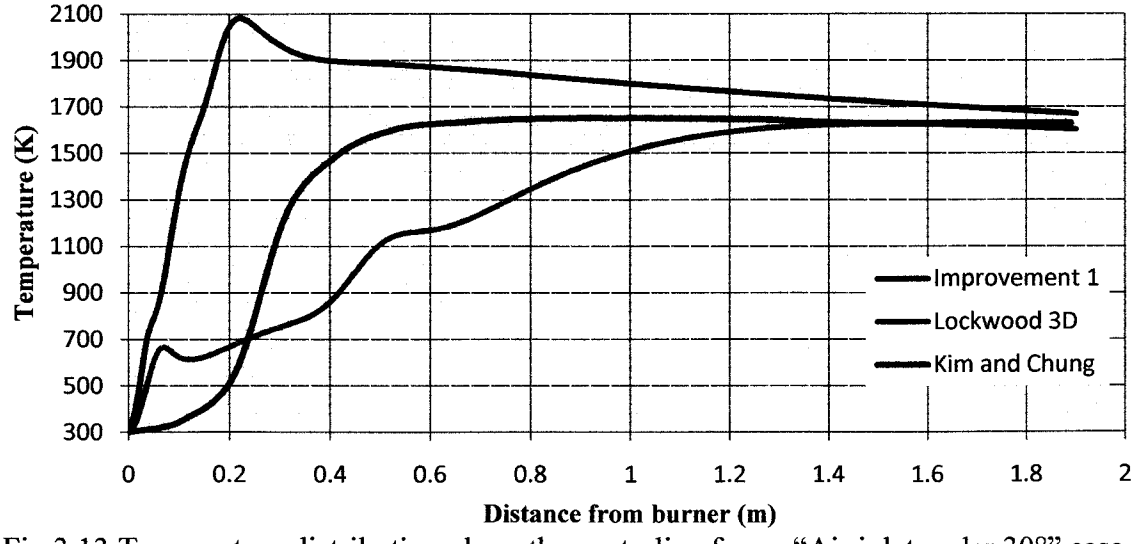

Fig 3.13 Temperature distribution along the centerline for an "Air inlet under 30°" case

c) Vertical air inlet

For this case, this air inlet annulus will have a vertical orientation with respect to the combustor and two different geometries will be revised. The first one corresponding to a distance of 5cm between the combustor inlet and the air inlet, and in the second case there will be no distance between the fuel inlet and the combustor edge; this means that the air annulus will be situated right away at the beginning of the combustor geometry.

This model consists of 289,129 hexahedral cells, this number is again considerably bigger than the "conventional 3D" case but in good agreement with the "air at a 30° case". Illustrated in Figure 3.14 the effect of modifying the distance of the air inlet is minimum and it is only observed a shift of the graph by 5cm this being as expected because the 5cm difference between both air inlet configurations.

Because the air stream mixes with the fuel stream in a vertical position a zone of fast mixing is created at the location of the air stream providing a very fast but incomplete initial mixing. Nevertheless, as the distance from the inlet increases this mixing decreases in quality because the initial mixing happens at a very fast rate that as both fluids move along the combustor they cannot mix in the same manner as in the inlet of the combustor because this mixing is not "strong" enough to carry on trough the rest of the combustor where it can be seen that there is more fuel-air products at the end of the combustor that in the original studied cases. Therefore, it can be said that this case provides a good mixing rate at the inlet of the combustor but the overall quality of the mixing is not as good as previous cases, keeping this case as an alternative for cases where the initial mixing is an important parameter.

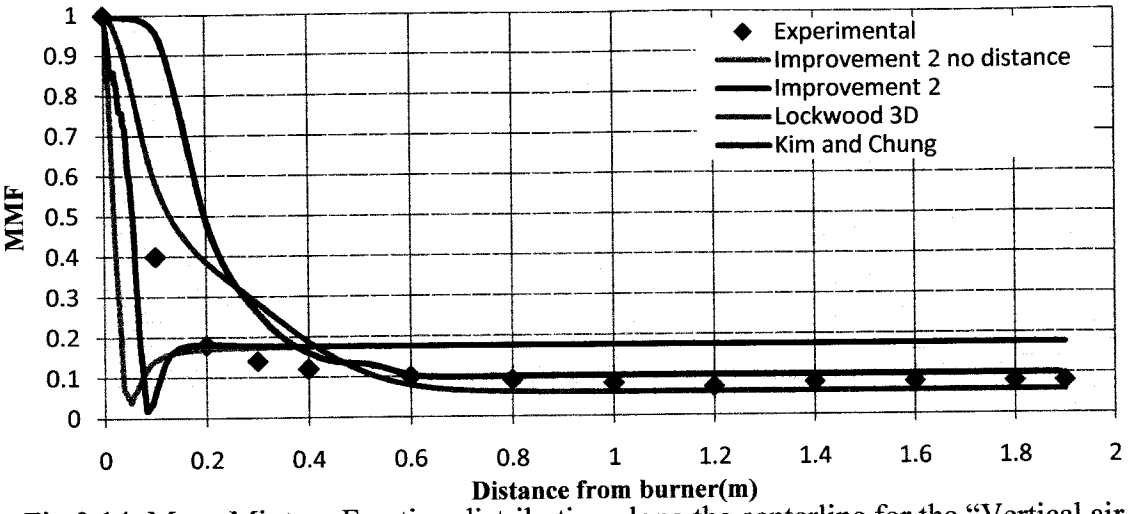

Fig 3.14 Mean Mixture Fraction distribution along the centerline for the "Vertical air inlet" case

Regarding the temperature distribution, again it can be seen that the inlet temperature is higher than the "traditional 3D design" but as expected the temperature along the combustor decays rapidly and lower temperatures are achieved at the end of the combustor, being this characteristic an important drawback of this design. This can be seen in Figure 3.15.

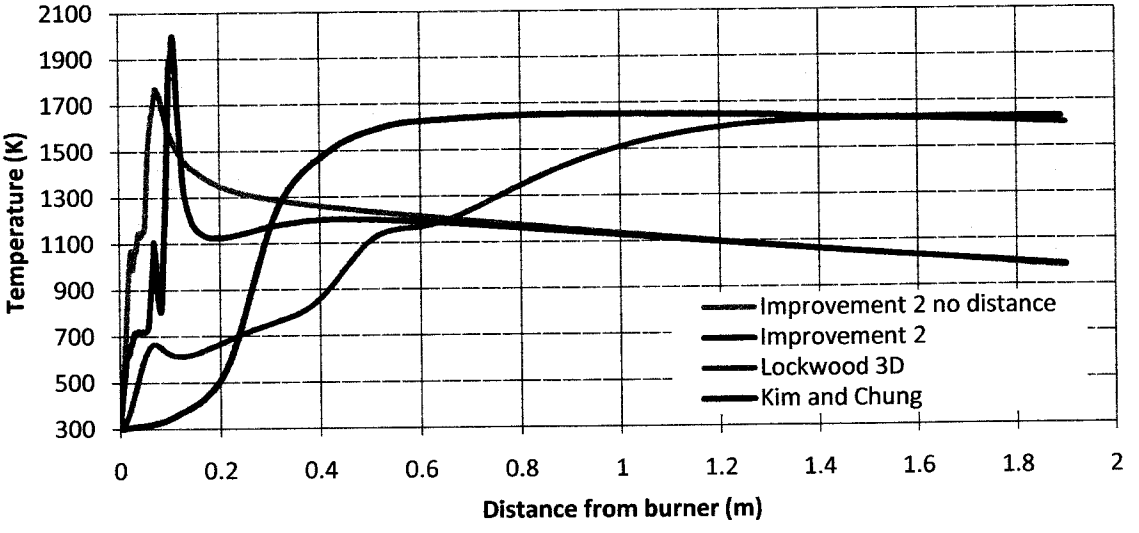

Fig 3.15 Temperature distribution along the centerline for the "Vertical air inlet" case.

d) Fuel and Air inlet at a 30° angle

For the last proposed geometry under investigation, both the air inlet and fuel inlet will be concentrically aligned but will have a 30° inclination with respect to the center axis of the combustor. This model consists of 274,449 hexahedral cells, this cell number is again considerably larger than the "conventional 3D" case but once more is reasonable taking into consideration previous cases of study.

In Figure 3.16, it shows that again a faster rate of decay in the MMF is experienced, at the inlet there is a better mixing zone because the two streams mix in a more efficient way when they are under an angle as seen in previous cases due to a better angle of mixing at the inlet.

After 0.2 m it is shown that there is a very good agreement with the experimental data but having less reactants remaining at the end of the combustor chamber. This is a good characteristic if a reduction of CO at the end of the combustor is to be achieved. As it is seen in Figure 3.16 this geometry also offers an advantage over the experimental data and the 3D case especially at the inlet and in the amount of reactants at the end of the process. This is why this case is considered also as a good improvement of the cylindrical combustor chamber.

Also it can be seen in Figure 3.16 for the propose configuration the value of the MMF is low because it shows the MMF distribution along the centerline and in this region there is not that much mixing in that region of the combustor.

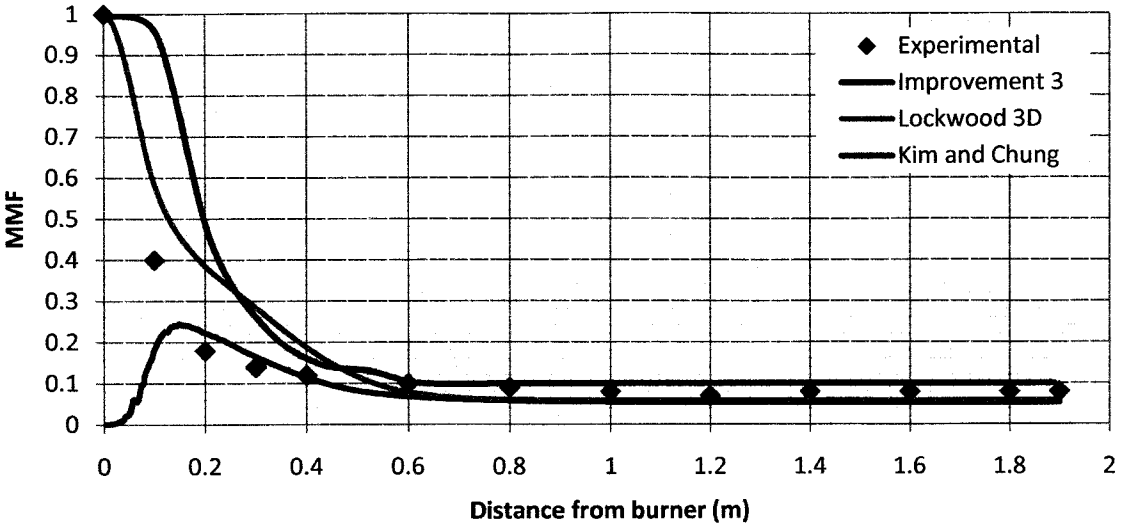

Fig 3.16 Mean Mixture Fraction distribution along the centerline for the "Fuel and air inlet at a 30° angle" design.

The temperature distribution is again higher in the primary mixing zone but rapidly reaches an agreement with Kim and Chung [61] data. This sudden drop in temperature is mainly due to the fast mixing at the inlet of the combustor and to the viscous forces interacting right after the mixing zone. This drop in the temperature can be beneficial in the reduction of NOx emission because of the high dependence between those two factors. Temperature distribution along the center axis is depicted in Figure 3.17.

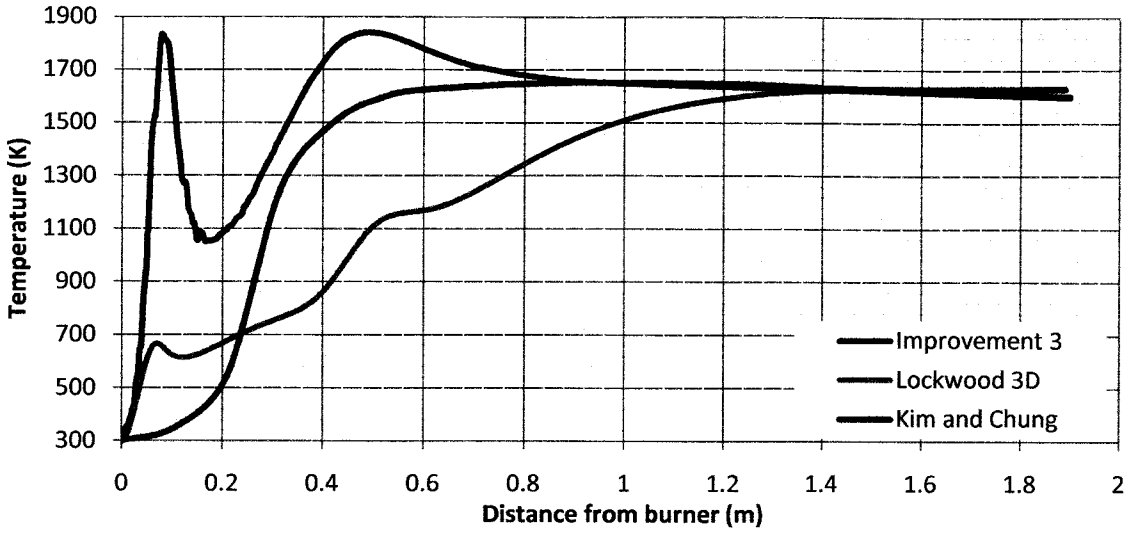

Fig 3.17 Temperature distribution along the centerline for the "Fuel and air inlet at a 30° angle" design.

After the analysis of these four cases it can be seen that setting the inlets at an angle provides the best mixing quality in the simple combustor. This inclination at the inlets provides a faster primary mixing zone and as expected higher temperatures. These two configurations seem to be the better design improvements of the ones discussed in this work.

To assess the difference between these two configurations the emissions of CO and NOx are studied in order to define which combustor is the most energy efficient. The NOx emission study is performed by the postprocessor of FLUENT under very simple yet realistic assumptions of thermal NOx emissions and equilibrium assumptions. Thus, this assessment is only to compare the two different geometries proposed.

Figure 3.18 shows the contours of CO emission for the "air inlet at a 30° angle" and the "fuel and air inlet at a 30° angle" respectively. It can be seen that in the first case

there are more emissions of CO in the recirculation zone than in the second case. This phenomenon was expected because as we saw in Figure 3.12 there was more fuel unburned in the combustion process than in all the rest of the configurations. In the second case we could see in Figure 3.16 that there was less unburned fuel than in the rest of other configurations and this is confirmed by the fact that there are very small emissions of CO in the combustor. The main zone of emission is just downstream of the main burning zone. Additionally, we can see that at the end of the combustor for the first case there are some emissions of CO and in the second case there are no CO emission making this design very beneficial for the environment.

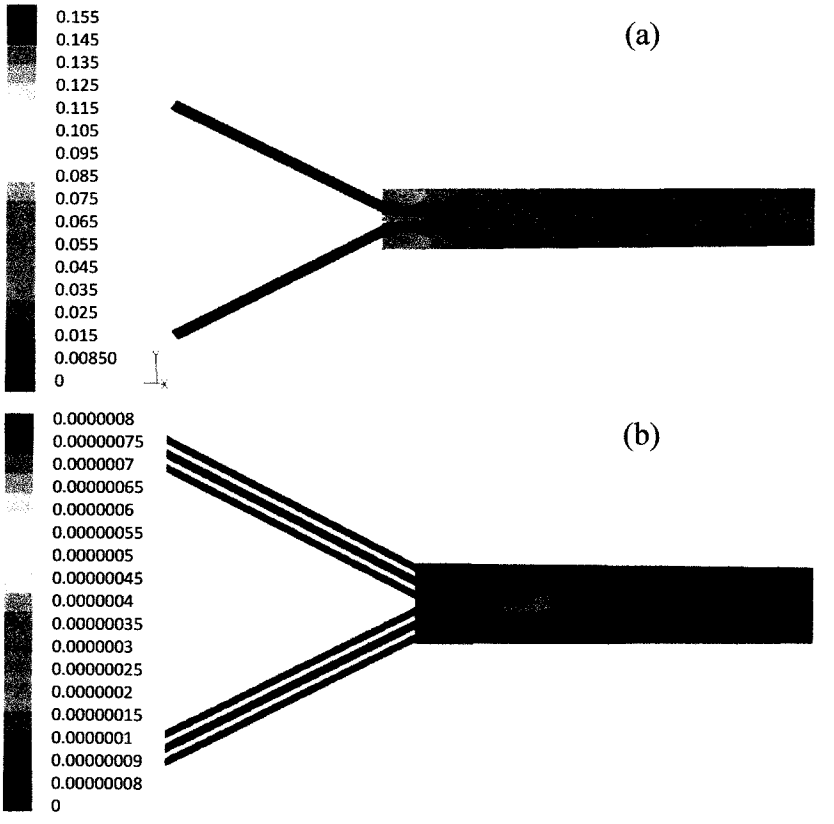

Fig 3.18 CO mass fraction contours for (a) air inlet at a 30° angle and (b) Fuel and air inlet at 30° angle.

The NOx distribution along the centerline can be seen in Figure 3.19. It is noticeable that as expected the first case has the most NOx emission along the center axis. This bigger amount of emission is because this case had the bigger temperatures in the mixing zone as shown before.

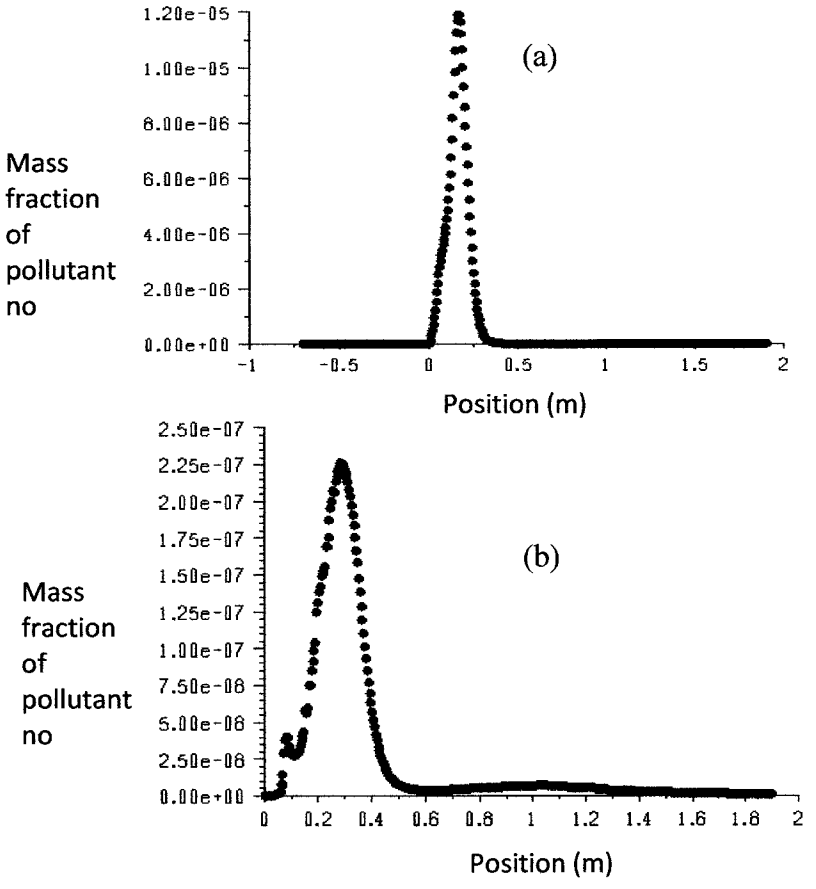

Fig 3.19 NOx distribution along the center axis for (a) air inlet at 30° angle and (b) Fuel and air inlet at 30° angle.

The NOx emission concentrations happen almost at the same place in both configurations, something expected because the recirculation zone is very similar in all the cases to be 1.4D (D = diameter) as shown also by Kim and Chung [61].

It can also be seen that at the end of the combustor there are very small amounts of NOx concentration that leads the very energy efficient systems, nevertheless the second case (*Fuel and Air inlet at a 30° angle)* shows in general less emission. Therefore it can be said that the *Fuel and Air inlet at a 30° angle* represents the better design in the objective of acquire better combustion and energy efficiency.

Figure 3.20 shows the MMF distribution along the centerline for the *Fuel and Air inlet at a 30° angle* using the LES turbulence approach. It can be seen that as discussed earlier because of the filtering process the trend shows a better agreement with the experimental data in a larger range of distances, while in the $k - \varepsilon$ simulation the agreement with the experimental data is seen after 0.2 m from the burner, in the LES simulation the agreement is reached at 0.1 m from the burner showing a more realistic representation of the physical phenomena. It is shown as well that still the rate of decay is better than in the previous cases and inclusively it shows a better agreement with the experimental data in the 0.2 m – 0.4 m regions than the $k - \varepsilon$ model, proving its better accuracy, with the drawback of the increase in computational time.

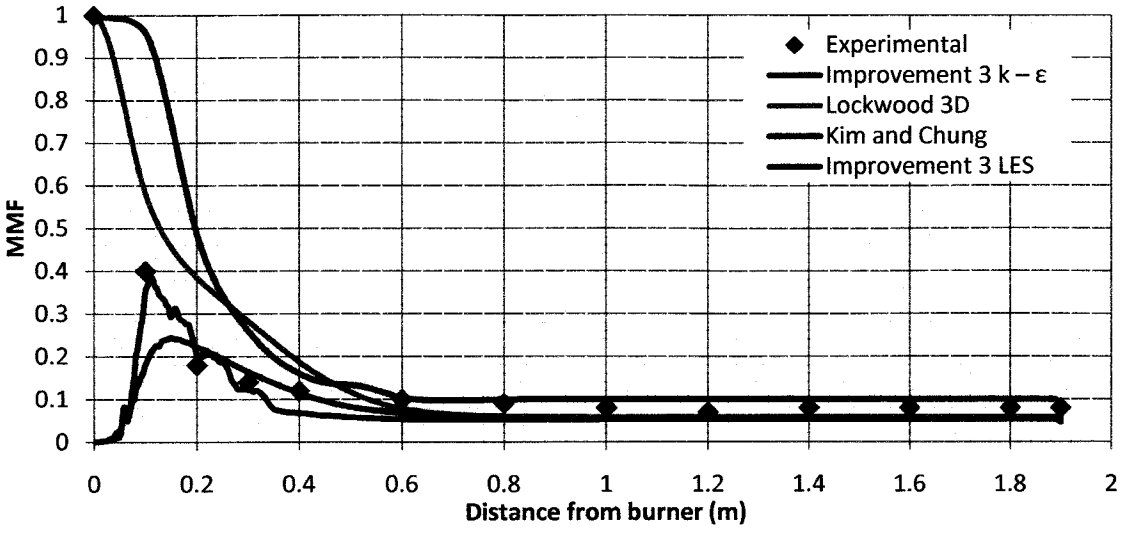

Fig 3.20 Mean Mixture Fraction distribution along the centerline for the "Fuel and air inlet at 30°" design using LES turbulence approach.

3.6 Concluding Remarks

A detailed numerical analysis was performed to assess the effect of injection on the turbulent mixing quality in a simple combustor. A numerical simulation was performed in a 2D model to validate experimental data with the simulations performed. Once the model was validated for a 2D geometry, a simulation on a 3D case was performed to evaluate the differences between these two geometrical dimensions. Different factors were analyzed such as grid cell number, effect of Schmidt number, turbulence intensity and turbulence model to identify the proper models and constants to use to model the changes in the injection geometry. Four different inlet geometries were proposed to achieve a better combustion efficiency and better energy efficiency. The first geometry discussed was an elongation in the fuel inlet in 2D, this configuration shows a poor improvement in the quality of the mixing and lower temperatures. The second configuration was setting the air inlet at a 30° angle; with this case it was seen better

mixing at the inlet of the combustor as well as higher temperatures in the same zone that leads to some CO and NOx formations. The third geometry analyzed was setting the air inlet in a vertical position, this shows better mixing at the inlet but higher amount of unburned fuel at the end of the combustor, additionally lower temperatures were seen. The last case seen had the fuel and air inlet at a 30° angle showing a better mixing at the inlet of the combustion and higher temperatures along the system without having CO and NOx formations proving to be the case that provides better combustion and energy efficiencies. Finally, the latter case was simulated with LES turbulence approach which shows a better agreement along a bigger range of distances and better efficiency although it has a higher computational cost.

Chapter 4

NUMERICAL ANALYSIS OF A NON-PREMIXED FLAME STREET IN A MESOSCALE CHANNEL

4.1 Introduction

The study of laminar flames remains a topic of fundamental importance to the field of combustion. Historically, one-dimensional analyses of flame fronts have proven to be very important and have provided significant insight into the physical mechanisms underlying more complicated systems. A new trend of combustion technologies for which the classical one-dimensional solutions are not adequate has sparked a great deal of renewed interest in the study of laminar flames. One of those rising area is the study of combustion at length scales below classical quenching limits. Recent developments in microfabrication technology have led to great interest in microscale combustion and power generation. Such work is motivated by the fact that hydrocarbon fuels contain about 100 times more energy per unit mass than lithium-ion batteries, and this any device capable of conversion of fuel to electricity at an efficiency better than 1 represents a potential improvement in the state of the art for portable electronic devices and other battery-powered equipment.

While numerous research groups worldwide are involved in the development of micro power generators and micro-combustors [85-87], few have used numerical modeling as a design tool despite the fact that microscale devices are extremely hard to instrument and this built-test-modify engineering is unlikely to lead to successful designs. The challenges associated with microscale combustion modeling are entirely different from those of macroscale devices.

If microcombustors are successfully developed and combined with appropriate energy conversion devices to account for their advantages, lighter and longer lifetime electrical power sources could be made. Development of micro-scale combustors, however, faces various technical difficulties, especially heat losses. As devices are scaled down, their surface area to volume ratio becomes larger. To overcome this problem and establish stable heat generation in micro-scale combustors, thermal management and catalytic reaction might be required [88-90].

Classical combustion experiments suggest that it may not be possible to sustain a flame at small length scales, and show that quenching distances for typical hydrocarbon-air flames are on the order of 1-2 mm [91]. As mentioned in previous chapters, the two primary mechanisms responsible for flame quenching are thermal quenching due to excessive heat loss through the burner walls and radical quenching as key combustion radicals become adsorbed to the wall surface, rendering them unavailable to participate in the chain-branching and chain-propagation reactions that are essential to the existence of hydrocarbon flames.

Various thermal-management techniques have been proposed to reduce heat losses to the ambient and recirculate thermal energy produced by the flame to preheat the incoming reactants. One technique that has been examined experimentally and theoretically is the recirculation of the hot post-flame combustion products through the burner wall as a source of preheating. A single pass burner, and a 3-D "Swiss Roll" combustor [92-93] based on the excess-enthalpy burner proposed by Weinberg [94] have been developed that utilized this concept. Thermal energy is transferred between the

products and reactants through a highly conductive wall medium. It has been recognized that it is possible to transfer heat through the wall in the axial direction to serve as a flame stabilization mechanism. This configuration has been studied for methane/air and propane/air flames in a 2-D channel [53, 95]. The effects of wall thickness, conductivity, channel thickness, and external heat loss on the stability limits of these flames are discussed. The propagation of flames in thin, non-adiabatic channels has been studied by Daou and Matalon [96] and Ciu et al. [97]. Some others studies have been held to assess the effect of the channel wall on flame structures [98-100].

The past experimental works [101] have proved that it is possible to propagate flames in a small gap around millimetre scale. To develop a micro-combustor system, one of the most challenging task is to maintain stable combustion in a micro-scale combustion chamber, which is normally considered to be around the flame quenching distance in the traditional sense, to constantly convert the chemical energy to the thermal energy. Some theoretical analysis of the combustion mechanism in simple micro-chambers has been performed [102] to show the feasibility of stable combustion in micro-combustor.

The fundamental understanding of combustion mechanism in micro-scaled chambers, which is very essential to the design and optimization of power MEMS devices, is not understood well at the moment. Due to the difficulties in conducting spatially resolved measurements of combustion characteristics in micro-scale devices, the numerical simulation can be a cost-effective approach to study the micro-combustion

mechanism. For example, Kamali et al. [103] performed a numerical simulation of wall treatment effects on the micro-scale combustion.

To follow the research direction in micro-combustion, this chapter performs a numerical analysis of a flame street in a fuel-air mixing layer insider a mesoscale combustor to further validate and compare them with experimental data. First, a three dimensional grid was created to represent the actual experimental geometry. Second, the influence of different turbulence models such as k-ε, k-ω, and LES in the formation of the flame street is analyzed. Also the effect of the Schmidt number is assessed. Two different chemistry-turbulence interaction models are analyzed to evaluate the importance of transport kinetics. The final goal of this chapter is to study the effect of the wall temperature and flow velocities, in a non-premixed street in a mesoscale channel.

4.2 Experimental Data and Setup

In the present study, the experimental data obtained by Xu and Ju [65] is selected for validation of the numerical simulations; additionally, this study is used to compare the accuracy of the numerical simulations results and to compare the effect of wall temperature and inlet velocity with the experimental data. The experiment setup by Xu and Ju [65] is described as a two horizontal silicon carbide plates, 241 mm long, 95 mm wide and 6 mm thick. To allow optical access to the channel two rectangular quartz windows were positioned between the silicon carbide plates, this also ensures a constant channel height of 6 mm. The final mesoscale channel combustor (241 x 95 x 6 mm^3) is represented in Figures 4.1 & 4.2. To provide a uniform wall temperature distribution the silicon carbide plates have a high thermal conductivity as well as low thermal expansion.

Two ceramic support rims separate the silicon plates from an aluminum frame and the support rims sit on a silica foam block. Between these two structures a metal heating coil is used to control the temperature of the silicon carbide plates. This heating coil allows the temperature of the silicon carbide plates to be raised up to 700 K and 1000 K, respectively, by using one or two heating coil. In the experimental setup the plates temperature was measured using a K-type thermal couple. To provide uniform discharge flows of fuel and oxidizer between the two parallel plates and to generate a mixing layer between the fuel and air streams at the inlet, a 400 cell ceramic honeycomb was mounted into the inlet connector. The fuels used by Xu and Ju [65] are methane and propane.

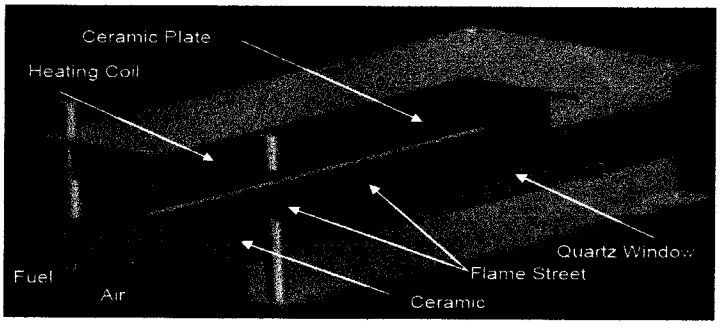

Fig. 4.1 Schematic of the channel combustor [65]

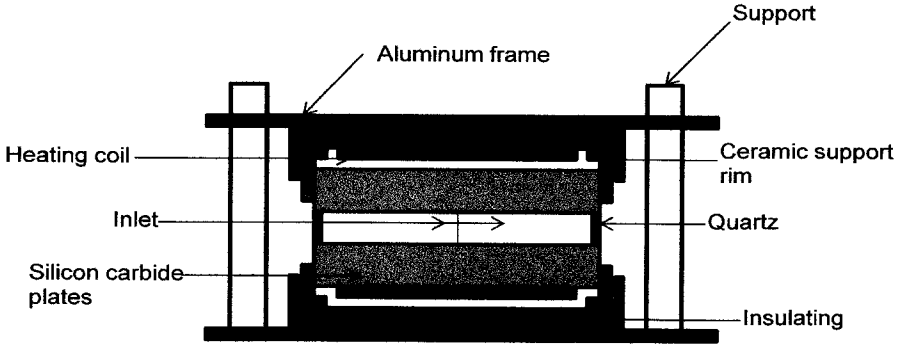

Fig. 4.2 Section view of the channel combustor from the end

The simulated combustor chamber geometry was performed in 3D due to the nature of the experimental setup; neither a 2-D approach nor a 2-D axisymmetrical approach would give accurate results due to the geometry of the problem. Several approaches are taken to create an accurate model of the geometry of the experiment. This is a critical step during the realization of the numerical simulation, because the physics behind mesoscale combustion is not well understood yet, there are some difficulties that should be addressed to consider the very strong connection between the wall and the inside of the combustor chamber. Several parameters such as different inlet lengths, different inlet widths, and different mesh sizes are modified throughout the creation of a mesh to accurately represent the geometry to be studied.

The first parameter that is studied and modified is the effect of different sizes in the inlet notch. Figure 4.3 represents temperature contour of the three different approaches taken in this step in a representation of the middle plane of the combustor. Three different geometries are created having different inlet notch sizes. The size of the combustor chamber remains the same for the three cases (241 x 95 x 6 mm^3). Additionally, all the geometries have the same inlet depth (6mm) and the same distance between the fuel and oxidizer streams (1mm). The geometries consider inlet notch lengths of 20mm, 5mm, and 1mm, respectively.

In the first case a "long" inlet is considered looking to achieve a fully developed flow, in the second approach a "medium" length is modeled to reduce the inlet length and facilitate the mixing of the two streams; finally the third geometry considers a very small inlet size to cause immediate mixing in the inlet of the combustor. It is seen that in the

first two configurations there is no convergence and in the third configuration there is convergence in 130 iterations. Additionally, in the first two simulations there is no presence of a flame street in the results and in the very small inlet length case there can be seen some flamelets. These simulations are performed using some defaults values provided by FLUENT, these values are going to be modified later in this chapter to get better physical results and an authentication is made in the inlet length size to validate the results obtained with the standard values. Therefore, the inlet size chosen to carry on in the numerical simulation is 1mm that enhances the mixing right in the inlet of the combustor.

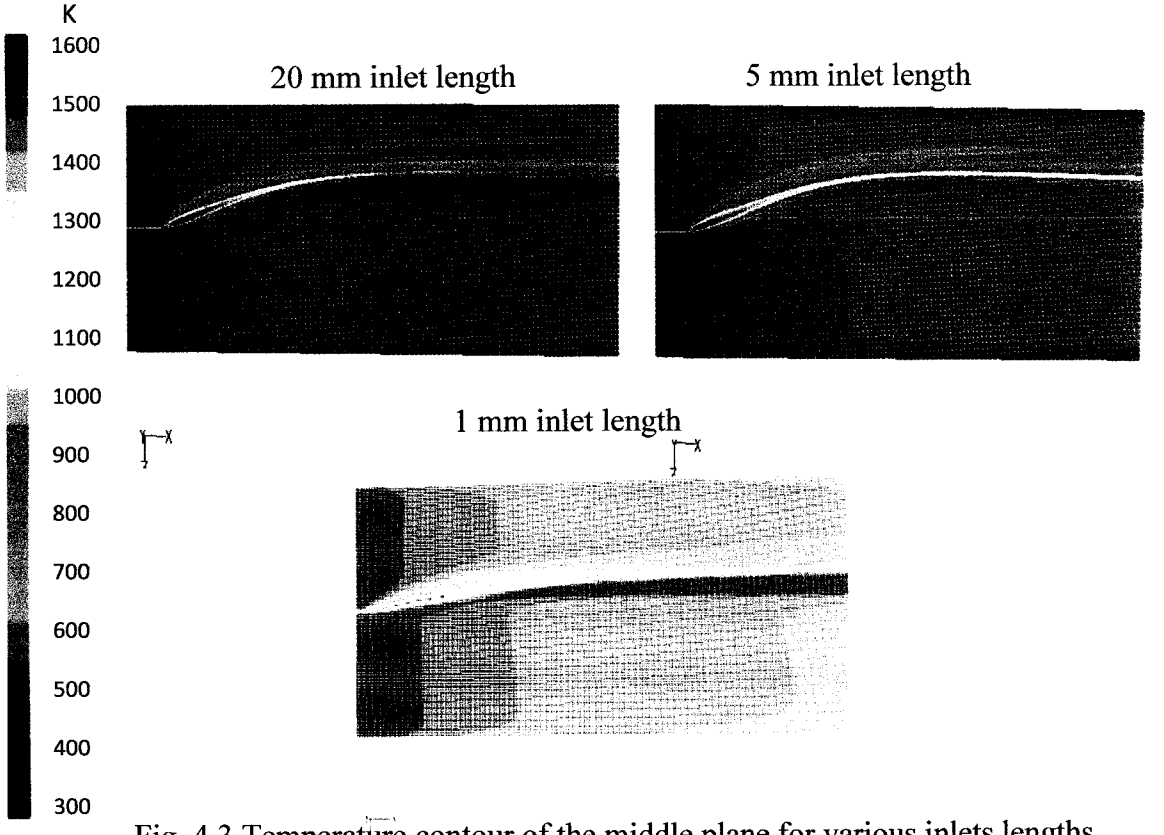

Fig. 4.3 Temperature contour of the middle plane for various inlets lengths

Another parameter that is investigated is the width of the air and fuel streams inlet. Figure 4.4 shows the two different approaches taken for this modeling in a temperature contour of the middle plane of the combustor. Again, the size of the combustor chamber remains the same for both cases and the 1mm inlet length is applied to both cases as well. To modify the inlet width of the two streams the distance between the fuel and the oxidizer inlet is changed from 1 mm to 2 mm, this creates inlets widths of 47mm and 46.5 mm, respectively. It can be seen that by using a wider inlet for both streams there is a slightly higher temperature in the combustor chamber and the flame street becomes more visible, additionally it can be seen that a "cold zone" of about 300K is located in the middle of the combustor creating an unphysical situation that will be discussed later on. Therefore, the inlet width of 47 mm is going to be considered as the default width.

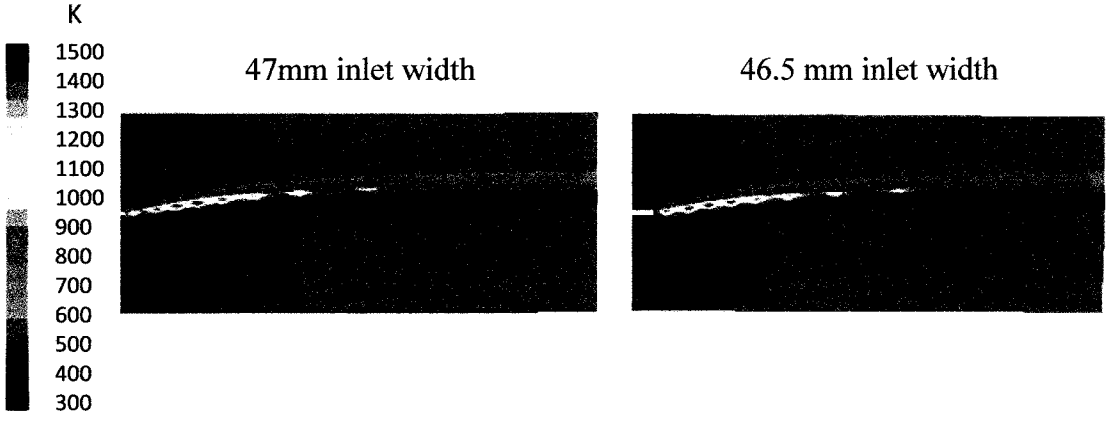

Fig. 4.4 Temperature contour of the middle plane for different inlet width

The most important parameter in the construction of the geometry mesh is to find an adequate size for the mesh. Figure 4.5 illustrates the temperature contour plot of different mesh sizes that are taken into consideration. Four different mesh sizes are analyzed with the objective of getting a more accurate result possible employing a minimal computational time cost. The interval sizes that are used to study the effect of the grid resolution on the numerical simulations are 3 mm, 2.5 mm, 2 mm, and 0.6 mm. The combustor chamber size is maintained the same and the inlet length and width are being matched to the optimal values. The default values provided by FLUENT used in previous simulation are kept constant as well. By changing the size of the mesh, a careful analysis should be made on the results because if the mesh size is too big the results from that mesh can lead to incorrect or misleading answers. On the other hand if the mesh size is too small a lot of computational cost can be incurred in the analysis, thus a really careful interpretation of the results should be made. Figure 4.5 demonstrates the results achieved with the different mesh sizes.

Using the interval size of 3mm convergence was attained after 145 iterations with a chamber temperature of 1204.8 K and three weak flamelets are seen. With the 2.5 mm interval size case there was no convergence achieved but still with the appearance of 3 flamelets and a maximum temperature of 1237 K. Decreasing the interval size to 2 mm shows after 76 iterations that 5 flamelets are seen with a maximum temperature of 1172.4 K. As it can be seen in Figure 4.5 the quality of the results is poor and as the mesh size becomes smaller and the appearance of a "cold stream" zone is noticeable (300 K), thus giving us unrealistic results. It is evident to see that this zone has no physical meaning in

the combustor because this temperature is lower than the wall temperature used during the simulations.

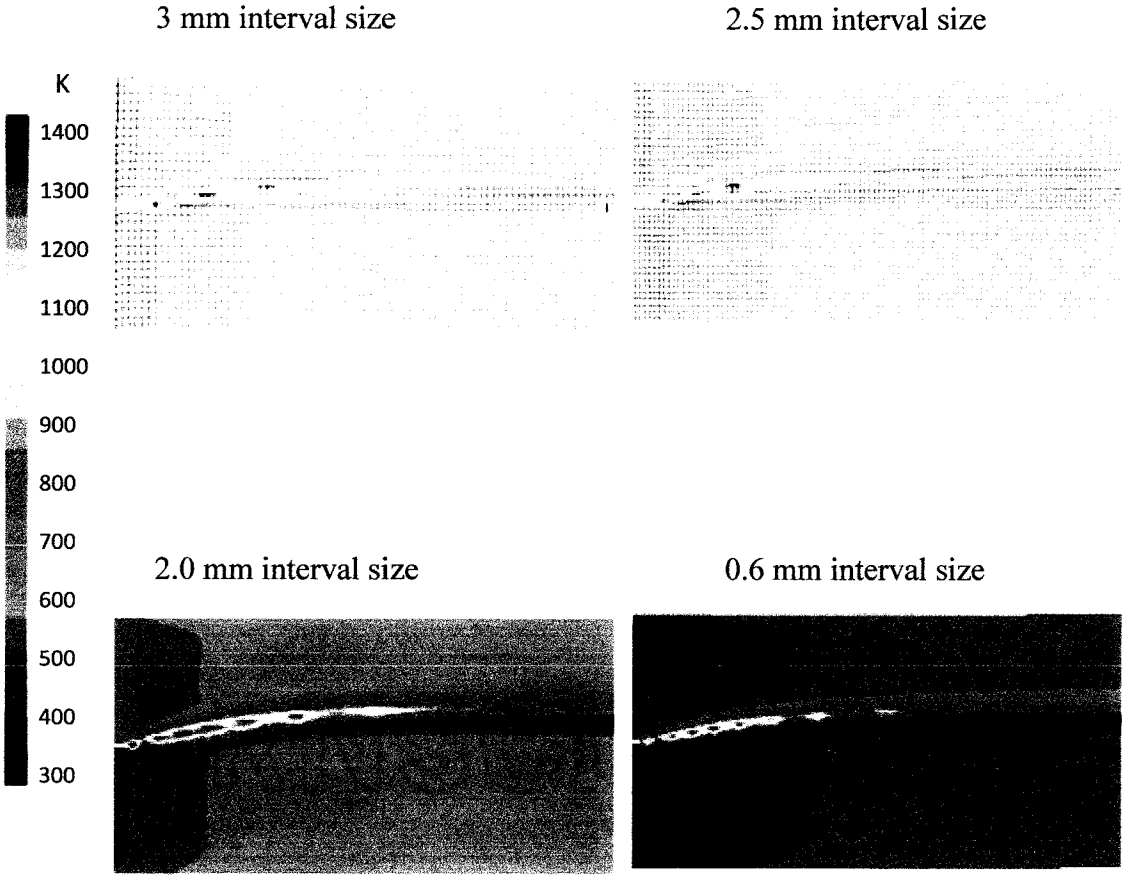

Fig. 4.5 Temperature contour of the middle plane for different mesh size

Therefore, although it is more computationally expensive, another mesh configuration is studied. In this configuration the interval size is 0.6mm where it can be seen that the quality of the results improved significantly and that more physical results can be achieved if some parameters from the FLUENT standard ones are modified. As a result with this interval size the entire geometry consists of 634 500 hexahedral cells. In

this configuration the presence of the flame street is very remarkable but still the problem of the "cold zone" needs to be solved. It is important to note that at this stage if the mesh size is refined more flamelets are seen (only approximately four flamelets are expected) in the combustor chamber because FLUENT is able to solve in more detail the chemistry involved in this process.

After all the analysis was done, figure 4.6 shows the final 3-D geometry that is going to be used throughout all the subsequent numerical simulations. This geometry provides a very good representation of the experimental data and eradicates mistakes and errors that can be presented by a bad election of parameters in the geometry model.

Detailed information about the "cold stream" zone and the physics of the flamelets or flame streets is provided in the following section. The main purpose of this section is only to get an optimal set of parameters to model the 3-D geometry of the mesoscale combustor channel.

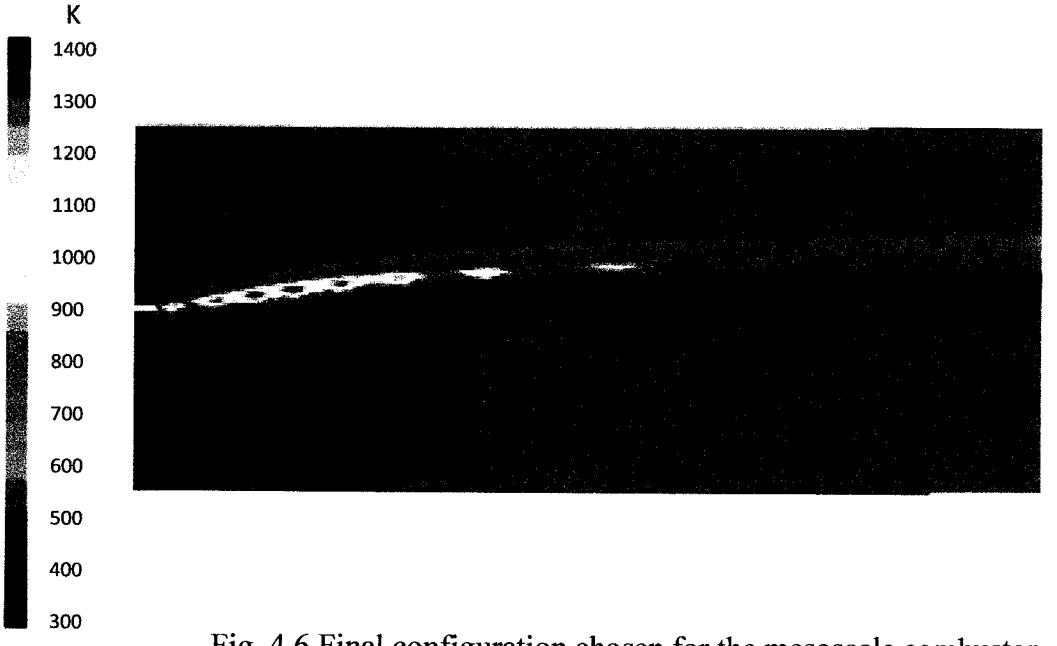

Fig. 4.6 Final configuration chosen for the mesoscale combustor

4.3 Non-premixed flame street

In order to understand the non-premixed flame street phenomena, the schematic top view of the formation of fuel/air mixing layer and the flame street (multiple flamelets) is shown in Figure 4.7. Between the fuel and the air stream there is a mixing layer zone along the flow direction. At the leading edge of this mixing zone, air and fuel mix fast and a premixed region with the stoichiometric line in the middle of the mixing layer. Therefore, experimentally it is going to exist an anchored leading triple flame due to the difference between the lower flows speed and the flame propagation speed. An important difference between non-premixed combustion at mesoscale and the normal scale is that in mesoscale after the first anchored tripe flame is shown a series of triple flames emerge, as referred to as the flame street.

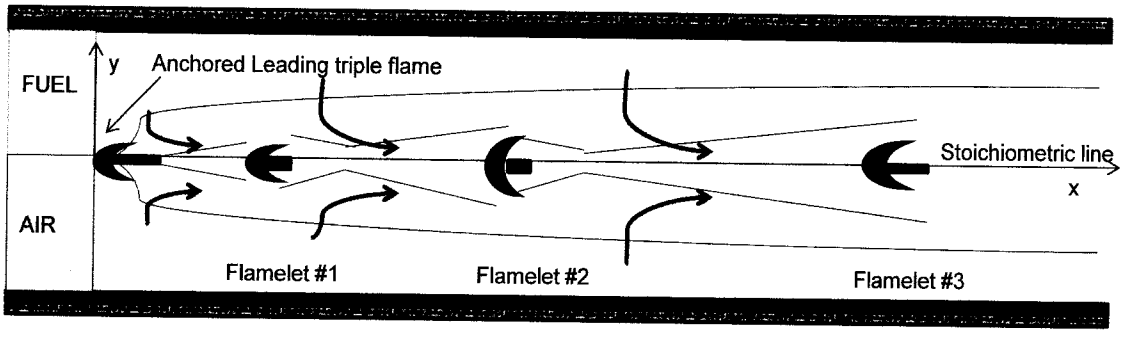

Fig. 4.7 Non-premixed flame formed in the mixing layer

This flame street is the result of the triple flame coupling with fuel diffusion and heat losses. After each flame, the diffusion flame part extinguishes due to the external heat loss and the lack of diffusion of reactants. Then, the reactants keep diffusing into the mixing layer. After a delay time, the flammability limit is attained in the center of the mixing layer and a new triple layer is formed. Finally, the triple flame propagates upstream at a decreasing flame speed and is stabilized at a point where the local flame

speed is balanced by the flow speed. This process repeats and forms a number of triple flames until the reactants gradients become small enough to support another triple flame. Consequently the triple flame structure will be primarily dominated by the flow diffusion time and the heat loss with the wall.

According to Xu and Ju [65] if the flow velocity and wall temperature are controlled there exist two flame regimes: the non-premixed flame street regime and the bimodal flame regime. The bimodal flame regime exists at low flow rates while the multiple triple flamelets exist at relatively high flow speed. The flame street boundary is broader at high wall temperature. At higher wall temperature, the flame can burn much leaner and it can be stabilized at a lower flow speed. Therefore, the non-premixed flame street depends on the wall temperature and the flow velocity.

The start of these triple flamelets can be illustrated with Figure 4.7. Because of the dilution of previous flamelets and the increase of the dissipation rate the flame speed decreases along the stoichiometric line. The flame curvature increases and the flame size decreases. If the flow velocity is relatively low, the flame will be extinguished because of the effects of the diffusion time and wall heat transfer. Nevertheless, if the flow velocity is high, the flame can be stabilized and the triple flame street can be created. Figure 4.8 shows different views of a flame street and the structure of these flamelets from the experiment carried by Xu and Ju [65].

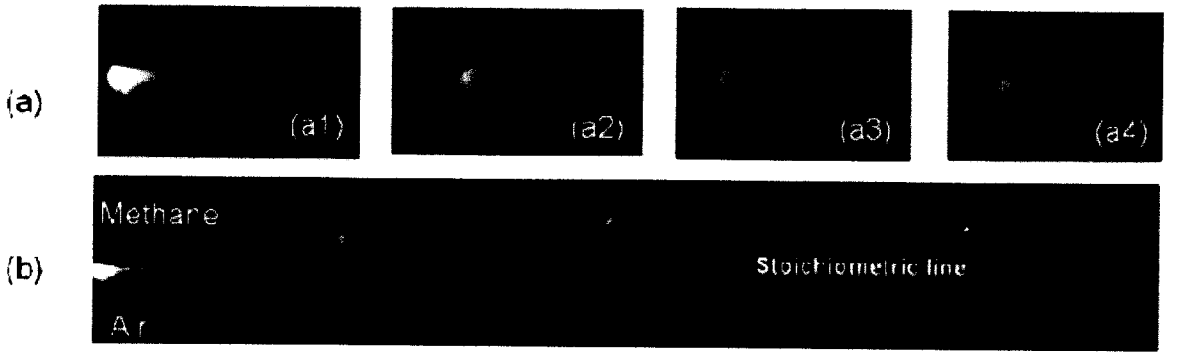

Fig. 4.8 The methane triple flame street from (a) top view of the four flamelets (b) top view of the flame street [65]

4.4 Numerical Simulation Approach

As mentioned before the simulations are performed in a 3-D geometry and the mesh created in the previous section is used throughout the analyses. There are four main parameters affecting the non-premixed flame street in the mesoscale channel: the turbulence model employed, the Schmidt number, chemistry model and simulation solution parameters. The fine tuning of these parameters lead to a successful simulation of the correct interaction of wall heat transfer and diffusion time.

In order to assess the effect of these parameters some sort of uniformity has to be employed in certain parameters to give validity to the simulations. Throughout all these series of simulations some parameters are considered standard and are the same for each study. The geometry adopted was the one developed in the previous step; the wall temperature was considered to be at ambient temperature (300 K); the silicon carbide plates were modeled to be 553.15 k; the inlet velocity for the air and fuel streams are 0.45 m/s and 0.13 m/s as described by Xu and Ju [65]; both oxidizer and fuel streams are considered to be at 300 K, the turbulent intensity for the inlets in both streams was

considered to be 1% because the flow is laminar and the hydraulic diameter of the inlets is 0.01064 m. The experiment was considered to be at ambient pressure. It is important that the main goal of this section is to seek for the optimal set of assumptions that will ensure meaningful results. In this process of tuning the boundary conditions there exist two main problems that are faced and that through the manipulation of the initial parameters are going to be solved. These parameters are the appearance of a cold zone of about 300 K in the middle of the combustor implying that there exist a zone of ambient temperature inside the combustor, the representation of the flamelet street, and the achievement of numerical convergence.

A fist parameter to be studied is the turbulence model. Two different turbulence models are used: the k-ε turbulent model and the k-ω turbulent model. To make these simulations the non-premixed chemistry approach was taken and the 2^{nd} order upwind scheme is used. Additionally it is seen that it is necessary to get numerical convergence to modify the under-relaxation factor by approximately 0.2 to get adequate results.

For the k-ε turbulent model, convergence was achieved after 125 iterations but no triple flamelet street is seen but the cold zone in the middle of the combustor does not exist. On the other hand, when the k-ω model is used numerical convergence is achieved after 108 iterations, the presence of the cold zone is observed but a sketch of the flamelet street is present. It can be seen that by using the k- ε model the presence of the cold stream zone is gone. However, because of the limited interaction between the wall and the flow it is hard to model the heat transfer with the wall. After these analyses are performed it is concluded that the k-ω model should be the turbulence model to use during the rest of the

numerical simulations. Since it incorporates modifications for low-Reynolds-number effects, compressibility, and shear flow spreading; predicts free shear flow spreading rates that are in close agreement with measurements for far wakes, mixing layers, and plane, round, and radial jets, is thus applicable to wall-bounded flows and free shear flows like the case that is being analyzed. Figure 4.9 shows a comparison between the use of the k-ε model and the k-ω model.

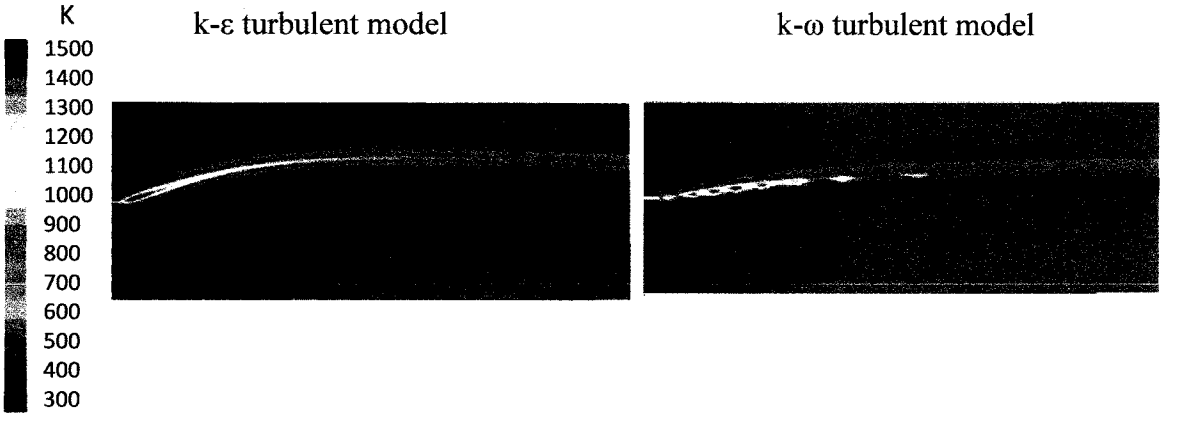

Fig. 4.9 Temperature contour of the middle plane for different turbulent model

The second parameter that is modified is the Schmidt number. This parameter is suggested to be an important factor in the prediction of mixing in non-premixed combustion as discussed in Chapter 3. Three different Schmidt number values are going to be used to verify if this parameter is important in the development of the flamelet street. The default value that FLUENT adopts for the Schmidt number is 0.80 so studies are conducted in reducing the value of this parameter to be 0.5 and 0.15. The k-ω turbulence model is used in these simulations.

Where the Schmidt number is equal to 0.15 no numerical convergence is achieved in the simulation. While if the Schmidt number is 0.5 convergence is attained in 154 iterations. Again just a sketch of the flamelet street is seen and there is presence of the

cold zone. The 0.80 case sees convergence after 120 iterations but once more the behavior of the cold zone and the flame street remains the same. Figure 4.10 illustrates the effect of modifying the Schmidt number. It is clearly seen that for this case the Schmidt number has no effect on the behavior of the triple flame street or the cold zone, this being understood as that the Schmidt number will only affect the initial mixing of the fluids and not the dissipation time downstream. Hence, it has a minimal effect on the flame street. The standard value of 0.80 will be used in the rest of the simulations to use as much as possible FLUENT standard parameters.

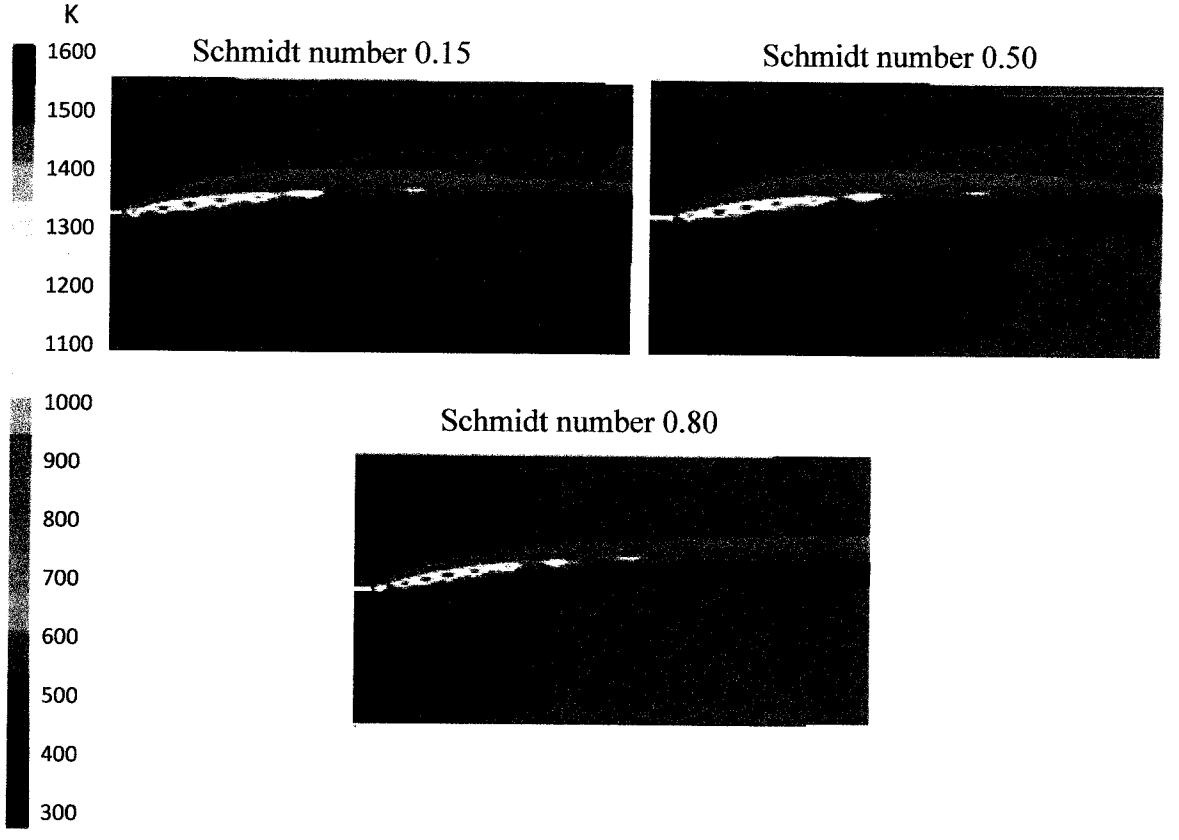

Fig.4.10 Temperature contour of the middle plane for different Schmidt number

The chemistry model employed in previous simulations in chapter 3 is the non-premixed approach or the pdf assumption. Because of the diffusion and wall heat transfer as well as the governing mechanisms for the triple flames street, it is believed that by modeling the mixing and transport of chemical species by solving conservation equations that describes convection, diffusion and reaction sources for each component species should be a good approach to take into consideration during the simulations.

The chemistry model that is suitable for this kind of task is the finite rate chemistry model; therefore the effect of this different chemistry model is analyzed. An appropriate approach to have a proper modeling of the dissipation time is the eddy dissipation concept model. For this case, volumetric reactions are accounted for as well as thermal diffusion. Still the k-ω turbulence model is being used. The results obtained for these simulations can be seen in Figure 4.11. Convergence was attained at 103 iterations and as can be seen from the figure there is a more remarkable presence of the triple flame street along the combustor, instead of the flamelets being all close to the inlet of the combustor, but there is still the presence of the cold zone. This change of chemistry model coupled with the k-ω turbulence model permits to account for the close interaction of the wall heat transfer and the diffusion time. Therefore, as expected these parameters exhibit the best behavior in representing physically the triple flame street phenomena. Yet, there is still a physical unfeasibility in the model with the appearance of the cold zone that has to be solved by modifying some of the simulation solution parameters.

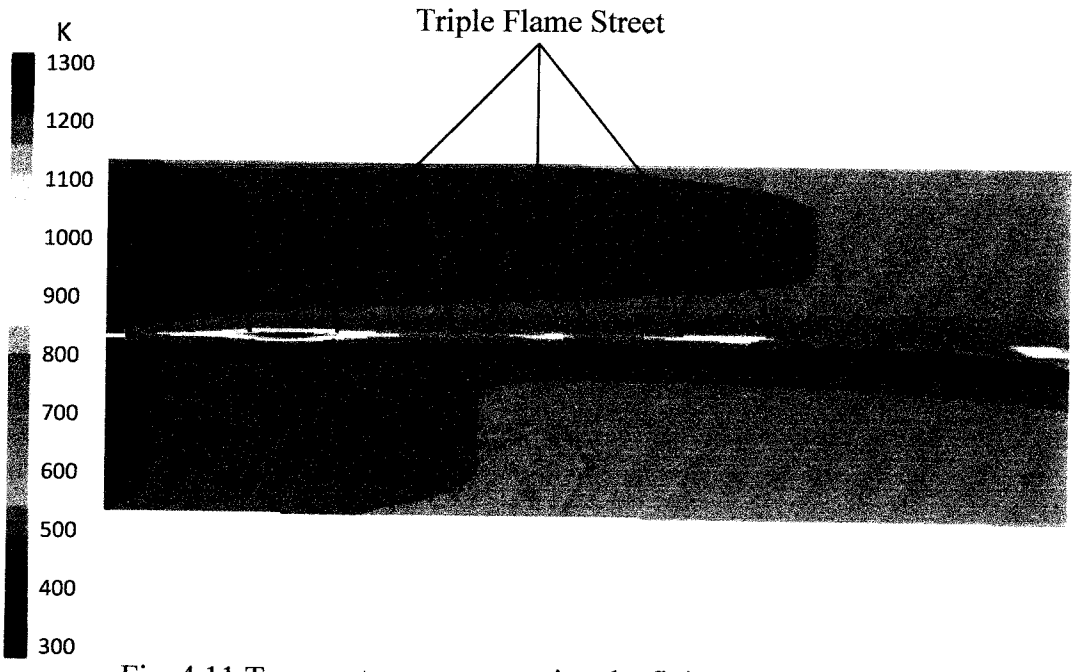

Fig. 4.11 Temperature contour using the finite rate chemistry model

In order to eradicate that cold zone, some solution parameters have to be modified to get an accurate and realistic representation of the physics behind the non-premixed flame street in mesoscale combustion. There are two important parameters to be modified in order to get accurate results: the pressure output of the combustor and the pressure-velocity coupling in the solution control of the simulation. The original scheme used to simulate the outside of the combustor was the pressure outlet option that permits to establish a constant pressure at the exit of the combustor; originally this value was maintained at atmospheric pressure. Because the cold zone in the middle of the combustor is due mainly to a big density drop originated by a big pressure gradient the pressure outflow option is more appropriate to model the outlet of the model. The pressure outflow option calculates according with the properties in the combustor the correct value of output pressure, thus eliminating all the big pressure gradients that can be incurred if we set as fixed a determined pressure value at the output of the combustor.

Additionally, the coupling between the velocity and the pressure had to be modified to account for the change in the pressure outlet. The coupled scheme is used as it solves the momentum equation and pressure correction equations separately. As seen in chapter 2 of this thesis, this algorithm results in slow convergence but it obtains a robust and efficient single phase implementation for steady-state flows, with superior performance compared to the segregated solution schemes providing more detailed information in the pressure-velocity coupling and avoids the big pressure gradients. Figure 4.12 illustrates the behavior of the triple flame street if the pressure output and the pressure-velocity coupling are modified. As it can be seen the effect of the wall heat transfer and diffusion time remains the same as in the previous case but now the cold zone in the middle of the combustor chamber does not longer exist giving us a very accurate and realistic representation of the experimental data.

4.5 Results and Discussion

The previous set of assumptions forms the foundation for the numerical simulations in order to study the effect of wall temperature and flow velocity in the formation of the triple flame street, methane is the fuel chosen to perform the numerical simulations.

The temperature of the silicon carbide plates is modified to verify that the wall temperature is a dominant parameter in the development of the triple flame street in mesoscale combustion. Four different temperatures are simulated in accordance with the work made by Xu and Ju [65] being 465.15 K, 553.15 K, 673.15 K, and 773.15 K. This broad range of temperatures will permit to understand the behavior of the flamelets street

at relative low, medium and high temperatures to confirm the effect of the wall heat transfer in this process.

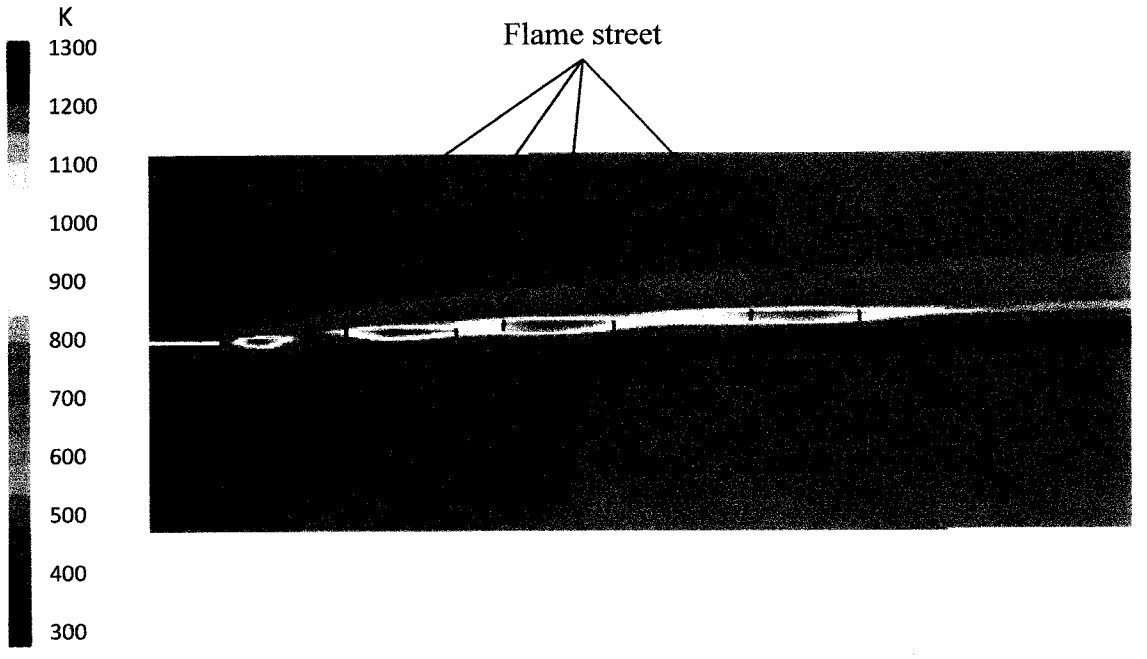

Fig. 4.12 Temperature contour of the mesoscale channel under the effect of the modification of all the parameters studied.

The top view of the flamelets at different wall temperatures corresponding to Xu and Ju's [65] experimental data can be seen in Figure 4.13 and the top view of the flamelets from the numerical simulation temperature contour using FLUENT can be seen in Figure 4.14. The results from the experimental data and the numerical simulation have the same trend and behavior for all of the temperature ranges from the experimental data.

It is clear that at a higher wall temperature, the heat loss from flame to the wall is less and this causes that a flamelet can be stabilized at more diluted conditions, and the flame separation distance decreases. This can be seen in Figure 4.15 (a) as illustrated also

in the experimental data from Xu and Ju [65] in Figure 4.15 (b). It can be seen that the heat loss to the wall is a critical component in the quenching of the triple flame. As it is observed in Figure 4.13 at very high wall temperature the diffusion flame does not quench and all the flamelets merge forming a big leading single diffusion flame structure. It can be seen too that the results obtained from the numerical simulations have a very good agreement with the experimental results, thus validating all the fine tuning process made prior to the change in wall temperature.

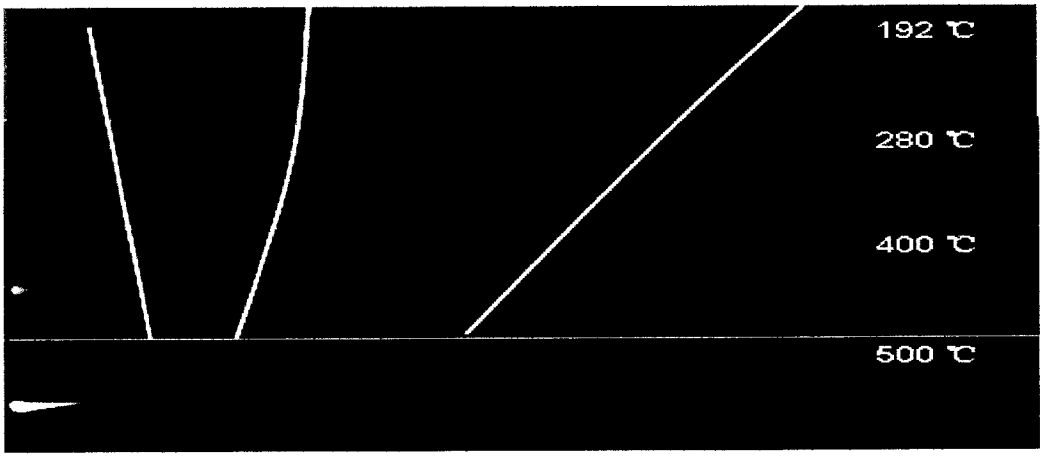

Fig. 4.13 Top view of Flame Street at different wall temperatures for experimental data [65]

As it was mentioned before the second important parameter in the development of the triple flame street is the flow speed. Therefore, a series of simulations are done to assess the effect of changing the velocity at the air inlet. The value of the fuel stream velocity is kept the same to have accordance with the experimental work from Xu and Ju [65]. Three different air velocity values are chosen for these simulations: 0.25 m/s, 0.45 m/s, and 0.58 m/s. Again, this range of velocities is enough to verify the behavior of the triple flames when this parameter is modified.

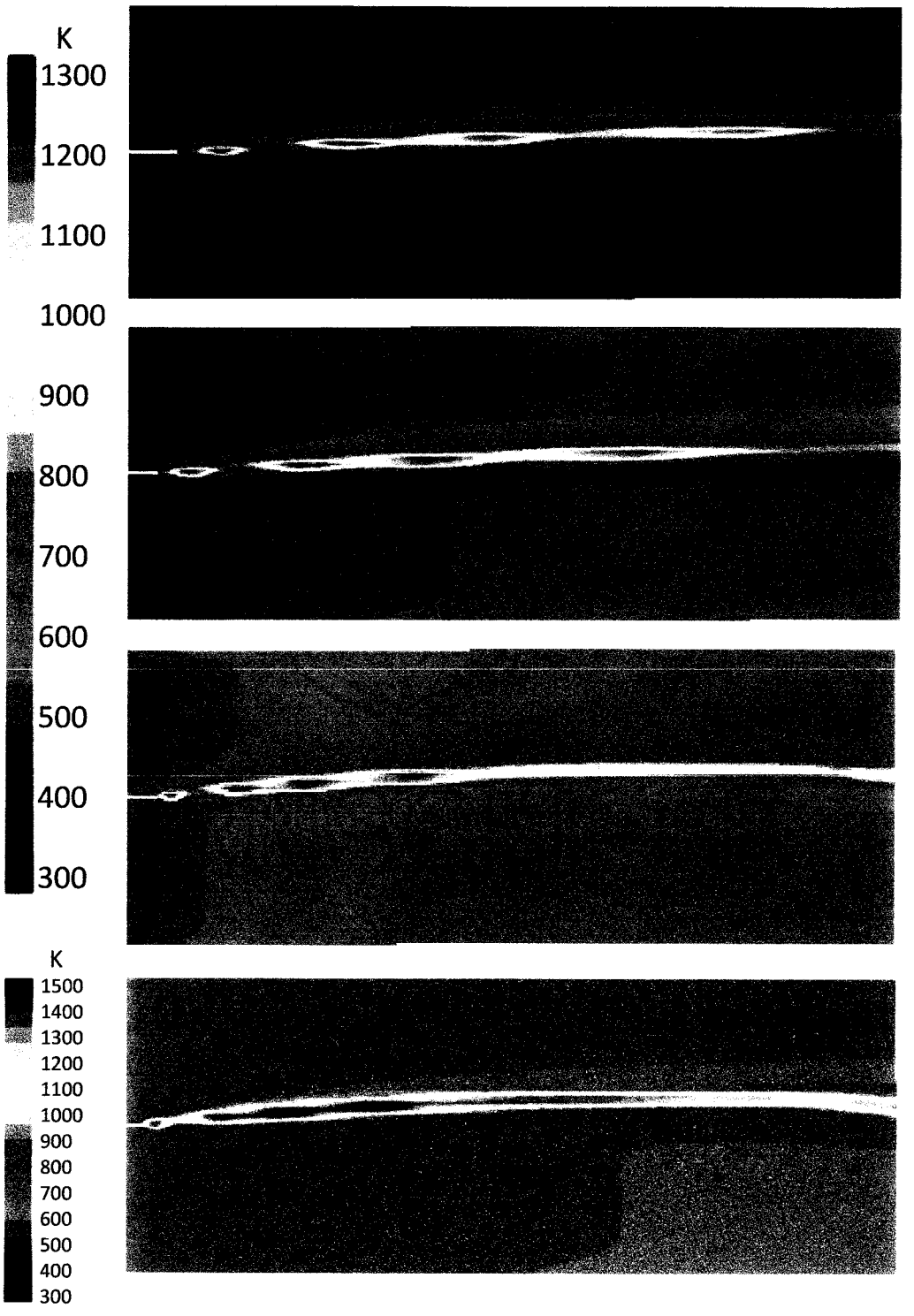

Fig. 4.14 Top view of Flame Street at different wall temperatures for numerical simulation

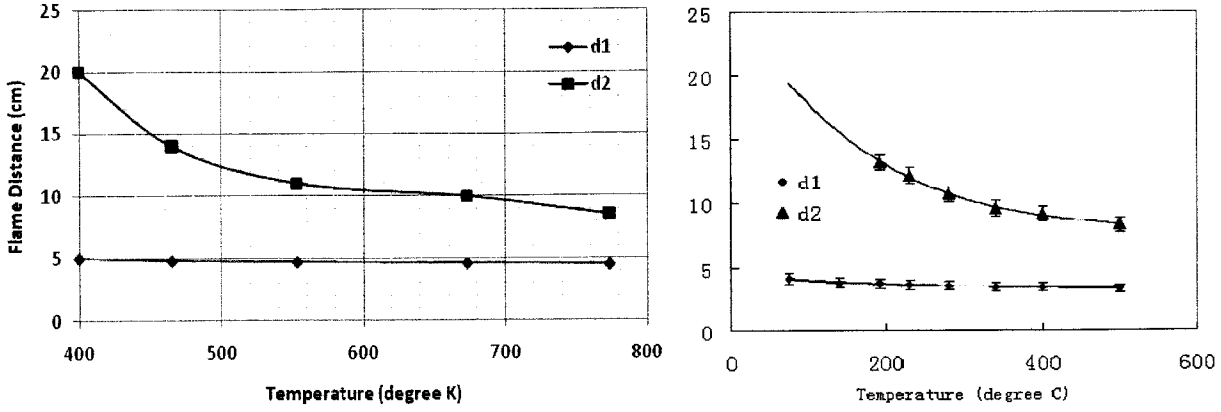

Fig. 4.15 Flame separation distance Vs Temperature for (a) numerical simulation (b) experimental data

Figure 4.16 shows the temperature contour of the numerical simulation at different air flow speeds. Figure 4.17 represents the measure flame distances measured by Xu and Ju [65] and by the numerical simulation. As seen by Xu and Ju [65] it is clear that the distances between the flamelets increases nonlinearly with increasing air flow speed. It is noticeable that at certain wall temperature and flow rate conditions, as a result of the dilution effect from the previous flamelet and the increase of the diffusion length scale, the flame distance of a certain flamelet is larger than the previous one. It is clear that the results show again a good agreement with the experimental data and that behavior of the flame street is well reproduced.

In order to have a better understanding of how the flame street develops with time a time dependent numerical simulation for a wall temperature of 553.25 K is performed to see the time that it takes for the flame street to develop. Figure 18 shows the time that it takes to each flame street to be developed. The flame at a first moment is anchored, because of the heat loss and lack of diffusion of the reactants the diffusion flame branch extinguishes. At 0.06 seconds because the flammability limit is reached in the center of

the mixing layer, the second triple flame is formed. At 0.09 sec the triple flamelet is shown and at 0.13 sec the last flamelet is formed. This Figure clearly illustrates the process of creation of the triple flame street. It is clear to see based on the preceding analysis that the mesoscale triple flame street generation is mainly dependent on the wall heat transfer and the diffusion time.

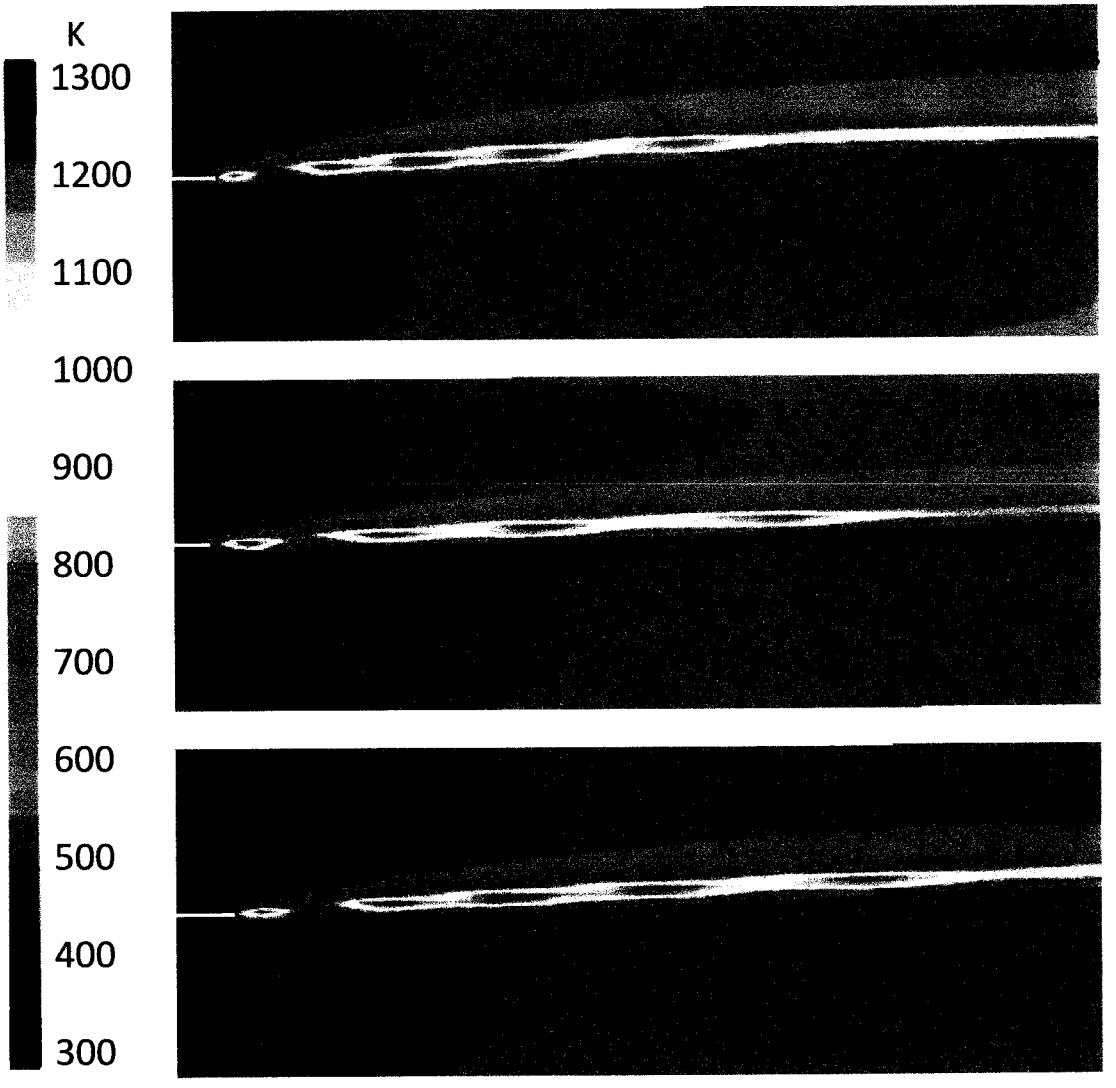

Fig. 4.16 Temperature contour of the numerical simulation at different air flow speeds

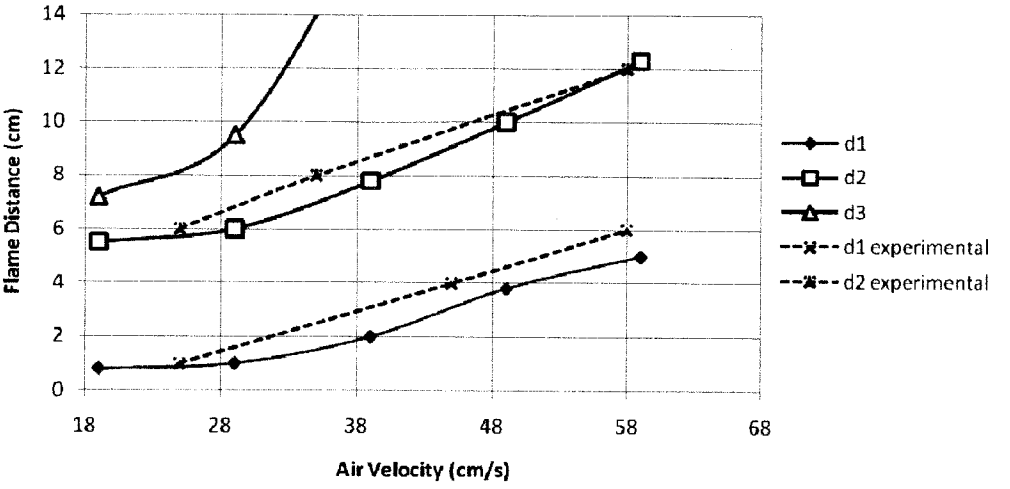

Fig. 4.17 Flame Distance Vs Temperature for numerical simulation and experimental data

The sensitivity of flame position to the air flow velocity depends on the location of stoichiometric line. To look at this effect, similar simulations were performed using propane as fuel. Note that higher fuel diffusivity and stoichiometric air-fuel ratio shift the stoichiometric line to the air side. Propane (C3H8) has a smaller diffusivity than methane and that may modify the behavior of a flame street. The measured distances of propane flames gathered by Xu and Ju [65] and the ones gotten by the numerical simulation are shown in Fig. 4-19 at same wall temperature. Propane has slightly smaller flame distance due to its large flame speed at high wall temperature. The dependence in sensitivity of flamelet distance with air velocity is very similar for both fuels. However, the third flame shows a higher sensitivity for methane fuel, implying that the flame distance is affected strongly by the increase of air flow speed due to a higher diffusivity of methane.

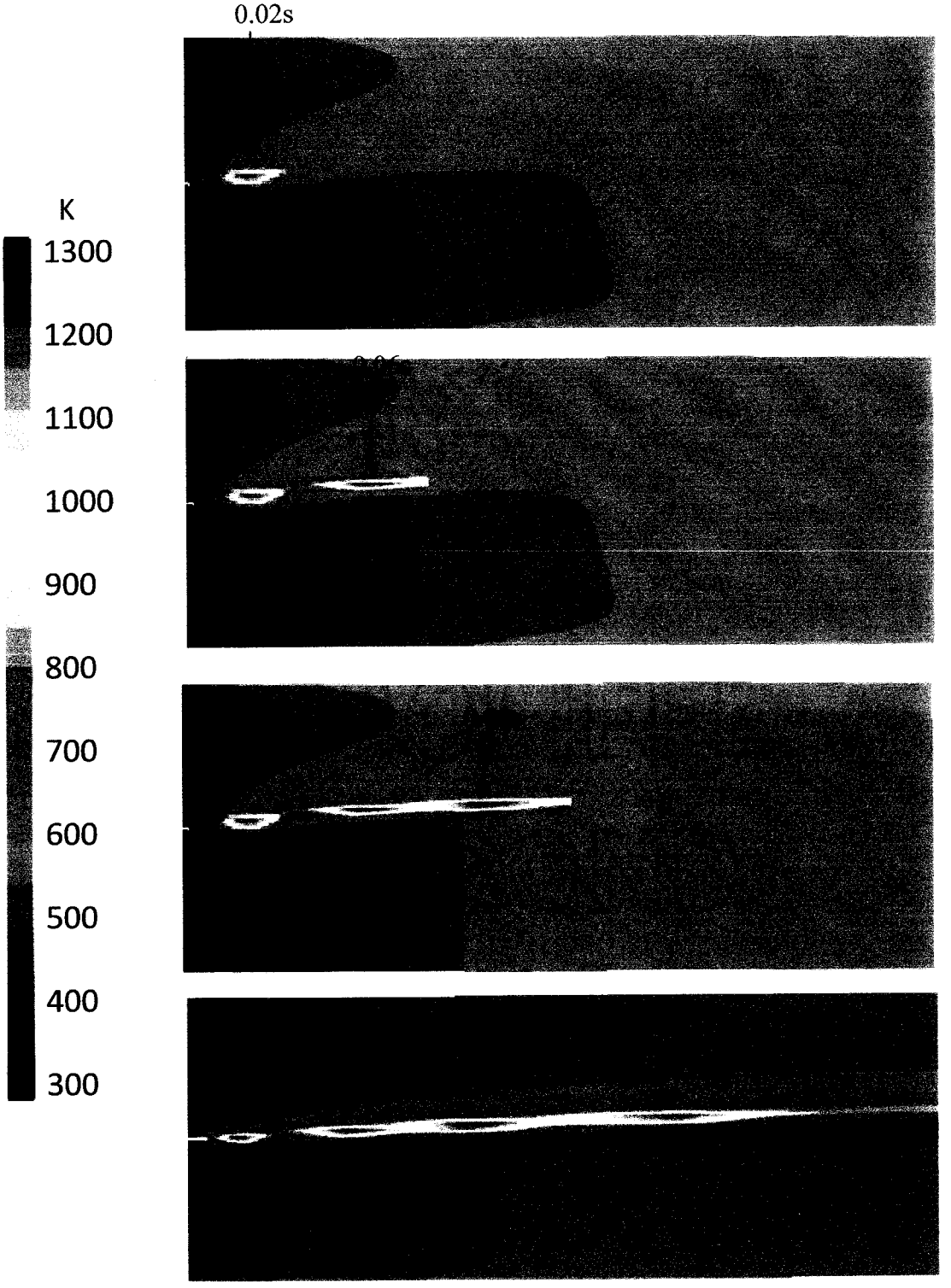

Fig. 4.18 Development of the Triple Flame Street with time.

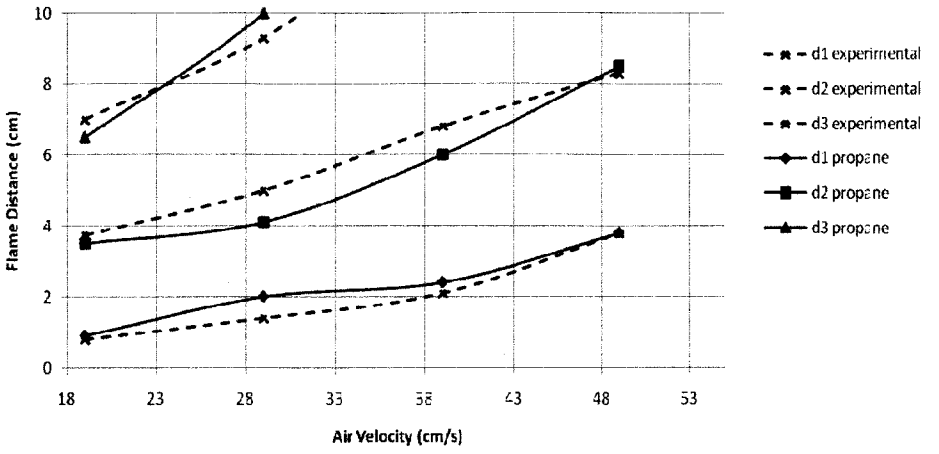

Fig. 4.19 Flame Distance Vs Air velocity for numerical simulation and experimental data using propane as the fuel

4.6 Concluding Remarks

A numerical analysis was performed to assess the effect of wall temperature and flow velocity on the development of a non-premixed flame street in a mesoscale channel. A numerical simulation was performed on a 3D model of a rectangular shaped mesoscale burner to compare the results obtained in the numerical simulations with experimental data. In order to make this comparison, different factors were analyzed in the 3D model such as different inlet length, different inlet widths, and different mesh sizes throughout the creation of a mesh to accurately represent the geometry to be studied. Additionally, four main parameters affecting the non-premixed flame street in the mesoscale channel are investigated: the turbulence model, the Schmidt number, chemistry model and simulation solution parameters to get the optimal configuration of the mesoscale combustor and accurate boundary conditions.

Four different wall temperatures, three flow velocities and two different types of fuels are studied to see the effect of wall heat transfer and diffusion time in the behavior of the triple flame street. Non-premixed flamelets of a mixing layer within the constrained channel are observed. A flame street is formed by several steady triple flames and its behavior clearly depends n the flow rate and surface temperature. The distance between two close flamelets increases with increasing the flow speed. Also as the temperature of the wall is increasing the triple flames tend to merge into a unique anchored flame that propagates along the channel. It can be said that this phenomenon is expected regardless of the kind of fuel that is used and that the behavior of the flamelet street is very similar. It is concluded then that the two main parameters affecting the development of a non-premixed flame street in a mesoscale channel being the heat transfer to and from the wall and the diffusion time of the flow.

Chapter 5

CONCLUSION

5.1 Concluding Remarks

Non-premixed turbulent combustion processes control most practical applications of combustion. Studying these mechanisms has been the objective of numerous theoretical and experimental works in the last century. In recent years numerical simulations have become an essential tool to understand and model turbulent combustion. By using this tool numerous experimental problems can be avoided without losing any accuracy in the results describing turbulent flames. Microfabrication technologies have made possible the development of Power Micro Electro-Mechanical System (Power MEMS) devices. Due to the higher energy density of hydrogen and hydrocarbon fuels, combustion process based miniature power generators have the potential to be more compact and longer-lived than chemical batteries. Successful miniaturization of combustion components demands a complete and broad understanding of microfluid dynamics and microcombustion phenomena. It is not clear whether or not the presently available theories and databases are adequate to predict the combustion behavior and flow dynamics in submillimeter systems. While flame propagation at the submillimeter scale is feasible, the interplay of fluid dynamics, kinetics and transport in flame stability and combustion characteristics of these systems is poorly understood.

During this dissertation, two numerical simulations are performed. First a numerical analysis of the effect of injection on the turbulent mixing quality in a simple combustor followed by a numerical analysis of a non-premixed flame street in a

mesoscale channel simulations are presented. All the simulations are conducted with the commercial software Fluent ®. A concise explanation and survey of the fluent code is presented. The description of the turbulence models as well as the combustion models used in this research work are outlined and explained. All the important parameters and solution methodology used throughout the simulations are detailed.

One of the limitations to design combustion equipments, or even predict simple flames, is the resolution of the mathematical formulation. Analytical solutions are not feasible, and numerical techniques have thus received enormous interest. The general numerical tools provide an accurate prediction of the phenomena of interest, including both turbulent mixing and the dynamics of flame propagation in small scale. Through the problems investigated in this work, it is shown that the numerical simulations can provide a reasonable description of the phenomena by comparing with experimental results. Because of this, numerical tool have become a very powerful tool that solves the problem of costly and hard to implement experimental tests.

Special attention has to be paid while performing numerical simulations because the success of this technique relies enormously in the way the simulation is set up because the results are very sensitive to these numerical details. The first parameter that has to be implemented in detail is the numerical resolution, as it was seen in this dissertation a poorly resolved calculation (bad mesh quality, low grid resolution) can lead to mistakes in the simulation results that can change in a radical way the behavior of the problem. On the other hand, having a very high grid resolution can lead to an excessive computational cost in the simulations, therefore is essential to find the fine balance that permits to get accurate results with savings in computational time. Another parameter

that has to be meticulously done is the definition of the geometry. It is very important for the ease of the simulations to establish beforehand well defined boundaries and computational zones in order to have a smooth and reliable calculation. The proper election of the turbulent model is another factor that will dominate the results of the problem. Since the initial set up of the problem the behavior that is expected and which interactions are involved in the process should be defined, once these two considerations are defined, a turbulent model that closely matches the requirements of the simulation is imperative. As it was seen during this work by choosing the k- ε turbulence model is the most common model used nowadays but it performs poorly for complex flows involving severe pressure gradient, separation, and strong streamline curvature while the k-ω model has superior performance for wall-bounded boundary layer, free shear, and low Reynolds number flows. The k-ω model is suitable for complex boundary layer flows under adverse pressure gradient and separation but separation is typically predicted to be excessive. The role of the Schmidt number in modeling non-premixed combustion at large scale is a dominant factor during the simulations. The correct "tuning" of this parameter can resolve all the under predictions and over predictions that can be seen if this parameter is not taken into consideration having thus a more accurate result. Finally the proper choice of the chemistry model can prevent lots of misleading errors in the problems. If a "zoom in" at the chemistry and fluid interaction wants to be performed the finite-rate model is the model of choice while if the chemistry can be look with a "zoom out" the pdf approach provides significant computational savings with no compromise in accuracy.

5.2 Contribution to Knowledge

Despite of being simplified problems, the numerical works carried in this project has meaningful applications. By analyzing the injection geometries and flame dynamics in small scale, one can improve our current understanding of the dynamics behind turbulent and laminar flames, its propagation and its behavior in large channels and in micro channels, and in interactions with its enclosures. Additionally by having a full understanding of the mechanisms behaving these kind of flames, this knowledge can be used to improve industrial application in term of energy saving, efficiency, achievement of better mixing qualities; and by using the numerical simulation tool significant economical savings can be achieved by avoiding costly experimental setups.

The results presented in this dissertation are only a small amount of the physics that need to be understood to make of meso- and microscale combustion a really robust technology. There are a numerous questions still that need to be answer and there is plenty of research work to be done in this area like sub-millimeter scale catalytic reaction, using gas/liquid hydrocarbon fuels at small scale, and planar laser induced fluorescence. The topic of microcombustion will remain an important area for the combustion research. A future step to continue with this work should be to keep on developing other combustor configurations that will permit more ecological configurations, as well as to simulate the large combustor using the finite-rate chemistry to see if with a closer look at the chemistry involved better configurations can be achieved. On the other hand, it is recommended to perform some analysis on emission at the mesoscale level as well as the possibility for design improvements.

REFERENCES

[1] Epstein, A. H. Senturia, C.D. and Anathasuresh, G. and Ayon, A. and Breuer, K. and Chen, K.S. and Ehrich, F.E. and Gauba, G. and Ghodssi, R. Power MEMS and Microengines. *IEEE Conf. on Solid State Sensors and Actuators* 1997. Vol. 2:753-756.

[2] Pisano, A. Microelectromechanical Systems (MEMS) Program. *DARPA / ETO* 1997. BAA 97-43.

[3] Fernandez-Pello, A. C. Micropower generation using combustion: issues and approaches. *Proceeding of the Combustion Institute* 2002. Vol. 29: 883-899.

[4] Gomez, A. et al. From jet fuel to electric power using a mesoscale, efficient Stirling cycle. *Proceedings of the Combustion Institute* 2006. Vol. 31: 3251-3260.

[6] The Energy Dimension of Climate Change and Energy and Climate Change, part IV, IEA/OECD Paris, 1997.

[7] Michel, J.B. and Michelfelder, S. and Payne, R. Survey on prediction procedures for the calculation of furnace performance. *Paper presented at the Propulsion and Energetics Panel 54th (B) Specialist's Meeting.* DFVLR, Cologne, Germany, October 3-5, 1979.

[8] Kouprianov, V.I. and Tanetsakunvatana, V. Optimization of excess air for the improvement of environmental performance of a 150 MW boiler fired with Thai lignite. *Applied Energy* 2003. Vol. 74: 445-453.

[9] Katsuki, M. and Hasegawa, T. The science and technology of combustion in highly preheated air. *Twenty-Seventh Symposium (International) on Combustion/The Combustion Institute* 1998. Pp. 3135-3146.

[10] Kim, W. and Do, H. and Mungal, M.G. and Cappelli, M.A. Investigation of NO production and flame structure in plasma enhanced premixed combustion. *Proceedings of the Combustion Institute* 2006. Vol. 31: 3319-3326.

[11] Lou, G. and Bao, A. and Nishihara, M. and Keshav, S. and Utkin, Y.G. Ignition of premixed hydrocarbon-air flows by repetitively pulsed, nanosecunded pulse duration plasma. *Proceedings of the Combustion Institute* 2006. Vol. 31: 3327-3334.

[12] Lin, H. Huang, Z. and Shangguan, W. and Peng, X. Temperature-programmed oxidation of diesel particulate matter in a hybrid catalysis plasma reactor. *Proceedings of the Combustion Institute* 2006. Vol. 31: 3335-3342.

[13] Chigier, N. A. The atomization and burning of liquid fuel sprays. *Progess in Energy and Combustion Science* 1976. Vol. 2:97-114.

[14] Chuvieco, E. and Cocero, D. and Aguado, I. and Palacios, E. and Gephys, J. Improving burning efficiency estimates through satellite assessment of fuel moisture content. *Journal of Geophysical Research* 2004. Vol. 109: D14S07.

[15] ZhengQi, L. and LongBin, Y. and Penghua, Q. Experimental study of the combustion efficiency and formation of NOx in an industrial pulverized coal combustor. *International Journal of Energy Research* 2004. Vol. 28: 511-520.

[16] El-Mahallawy, F. M. and Habib, M. A. Study of mixing of two coaxial swirling jets in a cold model furnace. *Flow, mixing and heat transfer in furnaces. 1st Conference on Mechanical Power Engineering* 1977. Vol. 2: 35-48.

[17] Moneib, H. A. Theoretical investigation of the effect of combustion air swirl on the characteristics of the central recirculation zone in furnaces. *Flow, mixing and heat transfer in furnaces. 1st Conference on Mechanical Power Engineering* 1977. Vol. 2: 81-92.

[18] Khalil, E. E. Numerical computation of turbulent swirling flames in axisymmetric combustors. *Flow, mixing and heat transfer in furnaces. 1st Conference on Mechanical Power Engineering* 1977. Vol. 2: 231-246.

[19] Ibrahim, M. A. and El-Mahallawy, F. M. Effect of relative angle between fuel and air jets. *Combustion and Flame* 1985. Vol. 60:141-146.

[20] El-Mahallawy, F. M. and Hassan, A. A. Effect of the exit section geometry and the furnace length on mixing and flow patterns in a cold model industrial furnace. *The First Conference of the Mechanical Power Engineering 1977.* Faculty of Engineering, Cairo University.

[21] El-Mahallawy, F. M. and Ghali, F. Y. Effect of burner geometry on the aerodynamic mixing pattern in a cold model furnace. *The Second Mechanical Power Engineering Conference* 1978. Ain Shams University.

[22] Bray, K. N. C. The challenge of turbulent combustion. *Proc. Symposium International Combustion* 1996. Vol. 26.

[23] Bilger, R. W. Turbulent Diffusion Flames. *Annual Review of Fluid Mechanics* 1989. Vol. 21: 101-135.

[24] Chen, J-Y. and Kollman, W. Pdf modeling of chemical nonequilibrium effects in turbulent non-premixed hydrocarbon flames. *Proceedings of the International Symposium of Combustion* 1988. Vol. 22: 645-653.

[25] Hawthorne, W. R. and Weddell, D. S. and Hotell, H. C. Mixing and combustion in turbulent gas jets. *Symp. Combust., Flame, and Explos. Phenom.,* 1949. Vol. 3: 267-288.

[26] Toor, H. L. Mass transfer in dilute turbulent and non-turbulent systems with rapid irreversible reaction and equal diffusivities. *AIChEJ* 1962. Vol. 8:70-78.

[27] Spalding, D. B. Mathmatische modelle turbulenter flammen. *VDI Ber.* 1970. Vol. 146:25-30.

[28] Bilger, R. W. The structure of diffusion flames. *Combust. Sci. Technol.* 1976. Vol. 13:155-170.

[29] Osgerby, I. T. Literature Review of Turbine Combustor modeling and emissions. *AIAA journal* 1974. Vol. 6:743.

[30] Khalil, E. E. and Spalding, D. B. and Whitelaw, J. H. The calculation of local flow properties in two-dimensional furnaces. *Int. Journal Heat Mass Transfer* 1975. Vol. 18:775.

[31] Hutchinson, D. and Khalil, E. E. and Whitelaw, J. H. The calculation of wall heat transferrate and pollutant formation in symmetric furnaces. *4th members conf. IFRF* 1976. Paper 13.

[32] Mizobuchi, Y. and Tachibana, S. and Shinio, J. and Ogawa, S. and Takeno, T. A numerical analysis of the structure of a turbulent hydrogen jet lifted flame. *Proceedings of the Combustion Institute* 2002. Vol. 29:2009-2015.

[33] Wegner, B. and Maltsev, A. and Schneider, C. and Sadiki, A. and Dreizler, a. and Janicka, J. Assessment of unsteady RANS in predicting swirl flows instability based on LES and experiments. *Heat Fluid Flow* 2004. Vol 25:528-536.

[34] Durbin, P. A. et al. *Eng. Turbul. Model. Exp.* 2002. Vol. 5: 3-16.

[35] Akselvoll, K. and Moin, P. Large-eddy simulation of turbulent confined coannular jets. *Fluid Mechanics* 1996. Vol. 315:387-411.

[36] Johnson, B. V. and Bennett, J. C. Statistical characteristics of velocity, concentration, mass transport, and momentum transport for coaxial jet mixing in a confined duct. *Eng. Gas Turbines and Power* 1984. Vol. 106:121-127.

[37] Dae, H. L. Scale effects on combustion phenomena in a microcombustor. *Nanoscale and microscale thermophysical engineering* 2003. Vol. 7: 235-251.

[38] Lowe, H. and Ehrfeld, W. and Hessel, V. and Richter, T. and Schiewe, J. Micromixing technology. *IMRET 4: 4rt Conf. on microreaction technology, AIChe Meeting* 2000. Atlanta, GA, 43-44.

[39] Liu, R. H. and Stremler, M.A. and Sharp, K.V. Passive mixing in a three-dimensional serpentine microchannel. *J. Microelectrical Systems* 2000. Vol. 9(2): 190-197.

[40] Ming-hsun, W. and Wang, Y. and Yang, V. and Yetter, R.A. Combustion in mesoscale vortex chambers. *Proceedings of the Combustion Institute* 2006. Vol. 31: 3235-3242.

[41] Miesse, C. M. and Masel, R.I. and Jensen, C.D. and Shannon, M.A. Submilimiter-scale combustion. *Aiche Journal* 2004. Vol. 50:3206-3214.

[42] Kyritsis, D. C. and Roychoudhury, S. and McEnally, C.S. Mesoscale combustion: a first step towards liquid fueled batteries. *Experimental Thermal and Fluid Science* 2004. Vol. 28: 763-770.

[43] Zel'dovich, Y. B. Theory of limit of quite flame propagation. *Zh. Eksp. Theor. Fiz,* 1941. Vol. 11: 159-168.

[44] Spalding, D. B. A theory of inflammability limits and flame quenching. *Proceedings of the Royal Society of London* 1957. Vol. A240: 83-100.

[45] Vican, J. and Gajdeczko, B.F. and Dryer, F.L. and Milius, I.A. Development of a microreactor as a thermal source for microelectromechanical systems power generation. *Proceedings of the Combustion Institute* 2003. Vol. 29: 909-916.

[46] Kyritsis, D. C. et al. Optimization of a catalytic combustor using electrosprayed liquid hydrocarbons for mesoscale power generation. *Combustion and flame* 2004. Vol. 139: 77-89.

[47] Maruta, K. Extinction limits of catalytic combustion in microchannels. *Proceedings of the Combustion Institute* 2003. Vol. 29: 957-963.

[48] Matta, L. M. Miniature excess enthalpy combustor for microscale power generation. *39th AIAA Aerospace Sciences Meeting & Exhibit* 2001. Reno, NV, U.S.A.

[49] Chen, M. and Buckmaster, J. Modelling of combustion and heat transfer in Swiss roll micro-scale combustors. *Combustion Theory and Modelling* 2004. Vol. 8:701-720.

[50] Oh, H. Effect of scale on the performance of heat-recirculating reactors. *4th International Energy Conversion Engineering Conference and Exhibit* 2006. San Diego, CA, U.S.A.

[51] Miesse, C. and Masel, R.I. and Short, M. and Shannon, M.A. Diffusion flame instabilities in a 0.75mm non-premixed microburner. *Proceedings of the Combustion Institute* 2005. Vol. 30:2499-2507.

[52] Matta, L. M. and Neumeier, Y. and Lemon, B. and Zinn, B.T. Characteristics of microscale diffusion flames. *Proceedings of the Combustion Institute* 2002. Vol. 29: 933-939.

[53] Norton, D. G. and Vlachos, D. G. Combustion characteristics and flame stability at the microscale: a CFD study of premixed methane/air mixtures. *Chemical Engineering Science* 2003. Vol. 58: 4871-4882.

[54] Domingo, P. and Vervisch, L. Triple flames and partially premixed combustion in autoignition of non-premixed turbulent mixtures. *Twenty-Sixth Symposium (International) on Combustion/ The Combustion Institute* 1996. Pp. 233-240.

[55] Edelman, R. B. and Harsha, P. T. Laminar and turbulent gas dynamics in combustors-current status. *Progess in Energy and Combustion Science* 1978. Vol. 4:1-62.

[56] Jones, W. P. and Whitelaw, J. H. Calculation methods for reacting turbulent flows: a review. *Combustion and Flame* 1982. Vol. 48:1-26.

[57] Smith, P. J. and Smoot, L. D. Turbulent gaseous combustion, part II: Theory and evaluation for local properties. *Combustion and Flame* 1981. Vol. 42:277-285.

[58] Pierce, C. D. and Moin, P. Progress-variable approach for large-eddy simulation of non-premixed turbulent combustion. *Journal of Fluid Mechanics* 2004. Vol. 504:73-97.

[59] Spadaccini, L. J. and Owen, F.K., and Bowman, C.T. Infulence of aerodynamic phenomena on pollutant formation in combustion (phase I. gaseous fuels) *U.S Environmental Protection agency Rep. EPA-600/2-76-247a.* 1976.

[60] Vanka, S. P. Calculation of axisymmetric, turbulent, confined diffusion flames. *AIAA journal* 1986. Vol. 24:462-469.

[61] Kim, YM and Chung, TJ. Finite-element analysis of turbulent diffusion flames. *AIAA Journal* 1989. Vol. 27:330-339.

[62] Lockwood, FC, El-Mahallawy FM and Spalding, DB. An experimental and theoretical investigation of turbulent mixing in a cylindrical furnace. *Combust. Flame* 1974, Vol. 23: 283-293.

[63] Sitzki, L. and Borer, K. and Schuster, E. Combustion in Microscale Heat-Recirculating Burners. *AIAA-2001-1087, 38th AiAA Space Sciences & Exhibit* 2001. Reno, NV, U.S.A.

[64] Ju, Y. and Minaev, S. Dynamics and Flammability Limit of Stretched Premixed Flames Stabilized by a Hot Wall. *Proceedings of the Combustion Institute* 2002. Vol. 29: 949-956.

[65] Xu, B. and Ju, Y. Studies of non-premixed flame streets in a mesoscale channel. *Proceedings of the combustion institute.* 2009. Vol. 1: 1373-1382.

[66] Vuthaluru, R. and Vuthaluru, H.B. Modelling of a wall fired furnace for different operating conditions using FLUENT. *Fuel Processing Technology 2006.* Vol. 87: 633-639.

[67] Coelho, P.J. and Peters N. Numerical Simulation of a Mild Combustion Burner. *Combustion and Flame 2001.* Vol. 124: 503-518.

[68] Jinsong H. Wu, M. and Kumar, K. Numerical simulation of the combustion of hydrogen-air mixture in micro-scaled chambers Part II: CFD analysis for a micro-combustor. *Chemical Engineering Science 2005.* Vol. 60: 3507-3515.

[69] Zhou. L.X. Wang, F. and Zhang, J. Simulation of swirling combustion and NO formation using USM turbulence-chemistry model. *Fuel 2003.* Vol. 82: 1579-1586.

[70] Lysenko, D.A. and Solomatnikov, A.A. Numerical modeling of turbulent heat exchange in the combustion chambers of gas-turbine plants with the use of the fluent package. *Journal of Engineering Physics and Thermophysics 2003.* Vol. 76: 888-891.

[71] Chorin, A.J. Numerical solution of navier-strokes equations. *Mathematics of Computation 1968.* Vol. 22:745-762.

[72] Barth, T.J. and Jespersen, D. The design and application of upwind schemes on unstructured meshes. Technical Report AIAA-89-0366. AIAA 27th Aerospace Sciences Meeting, Reno, Nevada, 1989.

[73] FLUENT Users Service Center. Reacting Flow Models in FLUENT. Introductory FLUENT Training. 2006.

[74] Pope, S.B. Computationally efficient implementation of combustion chemistry using in-situ adaptive tabulation. Combustion Theory and Modeling, 1:41-63, 1997

[75] Wilcox, D.C. Turbulence modeling for CFD. *DCW Industries, Inc., La Canada, California, 1998.*

[76] Lee, CS, and Park, SW, and Kwong, SI. An experimental study on the atomization and combustion characteristics of biodiesel-blended fuels. *Energy Fuels* 2005, 19(5): 2201-2208

[77] Thumann, A. *Guide to improving efficiency of combustion systems.* Fairmont Press, 1988; 119-123

[78] Baukal, CE, and Gershtein, VY, and Li, X. *Computational Fluid Dynamics in Industrial Combustion.* CRC Press, 2000.

[79] Lilley, D.G. Flowfield modelling in practical combustors: A Review. *Journal of Energy* 1979. Vol. 3, No. 4: 283-293

[80] Elgobashi, S. *Studies in the Prediction of Turbulent Diffusion Flames, Studies in Convection* (Vol. 2). B. E. Launder, Academic, New York, 1979, pp. 141-189

[81] Smith, P.J. and Smoot, L.D. Turbulent gaseous combustion, Part II: theory and evaluation for local properties. *Combustion and Flame* 1981, Vol. 42: 277-285

[82] Jones, W.P. and Whitelaw, J.H. Calculation methods for reacting turbulent flows, A Review. *Combustion and Flame* 1982, Vol. 48:1-26

[83] Vanka, S.P. Calculation of axisymmetric turbulent confined diffusion flames. *AIAA Journal* 1986, Vol. 24: 462-469.

[84] Warnatz, W, Maas, U and Dibble, RW. *Combustion: Physical and Chemical Fundamentals, Modeling and Simulation, Experiments, Pollutant Formation* (4rd ed). Springer, 2006; 209-210.

[85] Jin, P. and Gao, Y.L. and Liu, N. and Tan, J.B. and Jiang, K. Design and fabrication of alumina micro reciprocating engine.*Journal of physics: conference series* 2007. Vol. 48:1471-1475.

[86] Yang, W.M. and Chou, S.K. and Shu,C. and Li, Z.W. and Xue, H. Combustion in micro-cylinrical combustors with and without a backward facing step. *Applied Thermal Engineering* 2002. Vol 22:1777-1787.

[87]Li, J. and Chou, S.K. and Yang W.M and Li, Z.W. A numerical study on premixed micro-combustion of CH4-air mixture:Effects of combustor size, geometry and boundary conditions on flame temperature. *Chemical Engineering Journal.* 2009. Vol. 150:213-222.

[88] Lloyd, S.A. and Weinberg, F.J.,A burner for mixtures of very low heat content. Nature. 1974. Vol. 251: 47-49.

[89] Hasegawa, T., Tanaka, R., Niioka, T., *Proceedings of the International Joint Power Generation Conference*, Book No. G017072, ASME International 1997, EC-Vol. 5:259-266.

[90] Pfefferie, L.D. Pfefferie, W.C. Catalysis in Combustion. *Catal. Rev. Sci. Eng.* 1987. Vol. 29: 219-267.

[91] Kuo, K. *Principles of Combustion.* New York: 1986.

[92] Peterson, R. and Hatfield, J. A catalytically sustained microcombustors burning propane. *Micro-Electro-Mechanical Systems.* 2001. Vol. 3: 861-865.

[93] Sitzki, L. and Borer, K. and. Schuster, E. Combustion in microscale heat-recirculating burners. AIAA Paper 2010-1097. Presented at the 38th Aerospace Sciences Meeting, Reno, Nev., January 2001.

[94] Weinberg, F. Combustion temperatures: The future?. *Nature.* 1971. Vol. 233:239-241.

[95] Norton, D. G. and Vlachos, D.G. A CFD study of propane/air microflame stability. *Combustion and Flame* 2004. Vol. 138: 97-107.

[96] Daou, J. and Matalon, M. Influence of conductive heat-losses on the propagation of premixed flames in channels. *Combustion and Flame.* 2002. Vol. 128:321-329.

[97] Cui, C. Matalon, M. and Jackson, T. Pulsating mode of flame propagation in two-dimensional channels. *AIAA Journal.* 1966. Vol. 4:1284-1292.

[98] Leach, T. and Cadou, C. The role of structural heat exchange and heat loss in the design of efficient silicon micro-combustors. *Proceedings of the Combustion Institute.* 2005. Vol. 30:2437-2444.

[99] Chen, M. and Buckmaster, J. Modeling of combustion and heat transfer in "swiss roll" micro-scale combustors. *Combustion Theory and Modeling.* 2004. Vol. 8: 701-720.

[100] Ju, Y. and Choi, C. An analysis of sub-limit flame dynamics using opposite propagating flames in mesoscale channels. *Combustion and Flame.* 2003. Vol. 133; 483-493.

[101] Ono, S. & Wakuri, Y. An experimental study on the quenching of flame by narrow cylindrical passage. *Bulletin of JSME* 20 (147). 1977

[102] Lee, D.H., & Kwon, S. Heat transfer and quenching analysis of combustion in a micro combustion vessel. *Journal of Micromechanics and Micro engineering.*2002. Vol. 12:670.676.

[103] Kamali, R., Binesh, A.R., & Hossainpour, S. Numerical Simulation of Wall Treatment Effects on the Micro-Scale Combustion. *Proceedings of world academy of science, engineering and technology.* 2007. Vol. 26: 444-451.